TU WIEN

TECHNISCHE
UNIVERSITÄT
WIEN
Vienna University of Technology

Development and Evaluation of a Murine ECG Annotation Algorithm

D I P L O M A   T H E S I S

submitted in partial fulfillment of the requirements for the degree of

Diplom-Ingenieurin

in

Biomedical Engineering

by

Caroline Magg

Registration number 01225388

Muhrengasse 52/22-23

A-1100 Vienna

at the Institute of Electrodynamics, Microwave and Circuit Engineering
TU Wien

Supervisor: Univ.Lektor Dipl.-Ing. Dr.techn. Christopher Mayer
Univ.Lektor Dipl.-Ing. Dr.techn. Martin Bachler
Ao.Univ.Prof. Dipl.Ing. Dr.techn. Eugenijus Kaniusas

Vienna, 28th May 2018

Statutory Declaration

I hereby declare that I have written this Master Thesis independently, that I have completely specified the utilized sources and resources and that I have definitely marked all parts of the work - including tables and figures - which belong to other works or to the internet, literally or extracted, by referencing the source as borrowed.

Vienna, _____
             Date   Caroline Magg

Eidesstattliche Erklärung

Hiermit erkläre ich, dass die vorliegende Arbeit gemäß dem Code of Conduct, insbesondere ohne unzulässige Hilfe Dritter und ohne Benutzung anderer als der angegebenen Hilfsmittel, angefertigt wurde. Die aus anderen Quellen direkt oder indirekt übernommenen Daten und Konzepte sind unter Angabe der Quelle gekennzeichnet. Die Arbeit wurde bisher weder im In- noch im Ausland in gleicher oder in ähnlicher Form in anderen Prüfungsverfahren vorgelegt.

Wien, _____
             Datum   Caroline Magg

Acknowledgement

First of all I would like to express my gratitude to Christopher Mayer from the Austrian Institute of Technology (AIT) without whom this thesis would not have been possible. Then, I wish to thank Martin Bachler (AIT), he always had an open ear for my technical questions. Both provided me with their helpful input during all states of the thesis process for which I am very grateful. Moreover, I would like to thank the whole cardiovascular diagnostics group for making my days in the office most pleasant.

I would like to express my sincerest thanks to Professor Eugenijus Kaniusas for giving me the opportunity to write this thesis in cooperation with the AIT under his supervision.

A big thank you goes to my student colleagues and friends, who have accompanied me on this 6 year lasting journey. They made the time of my studies something special. And without their company and help, I would not be where I am today. A very special thank you to my boyfriend who was always by my side no matter what. I am really grateful it was him whom I met on my first day in front of the lecture hall.

Last but not least I would like to express my deepest gratitude to my parents. The past 6 years have not been easy, but they always believed in me, even when I did not. They supported me in every way possible and gave me the opportunity to find my own path.

Thank you!

Abstract

Automatically detected electrocardiogram (ECG) features are used to calculate risk parameters for patients with cardiovascular diseases. In this context, mice are often used for experiments in terms of heart disease models. The anatomy and physiology of humans are comparable to that of mice and gene manipulation for varying the function of proteins is possible. This way, certain cardiovascular disease patterns can be generated and treatments can be tested. Therefore, the analysis of murine ECG signals is a topic of great interest for preclinical research. In particular, automatic methods with little or no manual intervention are desirable. However, despite the high number of similarities between humans and mice, there are two major differences. On the one hand, the heart rates of mice are multiple times higher than human heart rates. And on the other hand, the different shapes of the action potentials and their consequences for the ECG morphology make it difficult to use human ECG signal analysis algorithms for murine data. The main differences occur in the QRS-offset representing the end of ventricular depolarization and the subsequent T-wave corresponding to the ventricular repolarization. In murine ECG signals, there is no ST-interval, but a deflection directly starting after the QRS-complex that precedes the T-wave. The feature is called J-wave and does not occur in this form for humans. Thus, algorithms for analysing human ECG signals provide wrong annotations for mice.

The aim of this master thesis was the implementation, evaluation, description, and application of an algorithm for automatic feature annotation of murine ECG signals. The algorithm is based on the AIT ECGsolver, which is used for the ECG analysis for human data. The problem of the different T-wave morphology is addressed by the implementation of a new feature detection for the QRS-offset and the T-wave features. There were three task in the algorithm pipeline which were solved by two different implemented methods. The performance of all 8 resulting algorithm versions and a slightly adapted version of the AIT ECGsolver was determined. The automatically annotated ECG features and the calculated ECG intervals were evaluated against manually annotated recordings. Moreover, the algorithm was applied to murine ECG signals from a preclinical study to investigate the influence of medical intervention of mice.

The developed murine algorithm performs better than the human algorithm. Both the detection rates and the differences from the detected feature to their target values provided by the manual annotations have been improved. A sensitivity up to 91.6 % and a positive prediction up to 94.18 % can be achieved by different

algorithm versions. However, there is still an overestimation of the QRS- and the QT-interval durations and most of the T-offsets are detected too late in the signal. In addition, it has been found that the detection of P-wave features offers potential for improvement. The finding of the medical treatment analysis was a decreasing heart rate after the intervention. Other consequences could not be found.

In this thesis, the focus was more on the annotations of the QRS-offset and the T-wave features due to the different T-wave characteristic. However, it turned out that the localisation of the P-wave features also shows potential for improvement, which can be addressed in future work. In addition, the algorithm should be further tested with data that shows a clearly recognisable negative T-wave.

Kurzfassung

Automatisch detektierte Elektrokardiogramm (EKG) Merkmale werden zur Berechnung von Risikoparametern für PatientInnen mit kardiovaskulären Krankheiten verwendet. In diesem Zusammenhang werden Mäuse häufig für Experimente verwendet. Die Anatomie und Physiologie von Menschen und Mäusen ist vergleichbar und die Möglichkeit einer Genmanipulation zur Veränderung von Proteinfunktionen ist gegeben. So können bestimmte kardiovaskuläre Krankheitsbilder erzeugt und Behandlungen getestet werden. Daher ist die Analyse von Mäuse-EKG-Signalen von großem Interesse für die präklinische Forschung. Vor allem eine automatische Methode mit wenig oder keinem manuellen Eingreifen ist wünschenswert. Allerdings gibt es trotz der vielen Gleichheiten zwischen Mensch und Maus zwei wesentliche Unterschiede. Einerseits ist die Herzrate von Mäusen um ein Vielfaches höher als bei Menschen. Andererseits machen es die unterschiedlichen Aktionpotentialformen und ihre Auswirkung auf die EKG Form schwierig, Algorithmen zur menschlichen EKG Analyse auf Mäuse EKGs anzuwenden. Der Hauptunterschied liegt im QRS-Offset, das Ende der ventrikulären Depolarisation, und in der T-Welle, der ventrikulären Repolarisation. Bei Mäuse EKGs gibt es kein ST-Intervall, sondern eine Ausprägung direkt nach dem QRS-Komplex, die der T-Welle vorausgeht. Dieses Merkmal wird J-Welle genannt und kommt in dieser Form bei Menschen nicht vor. Daher liefern menschliche EKG-Signal-Analyse Algorithmen falsche Ergebnisse bei Mäusen.

Das Ziel dieser Diplomarbeit war die Implementierung, Evaluierung, Beschreibung und Anwendung eines Algorithmus für die automatische Merkmalserkennung bei Mäuse EKG Signalen. Der Algorithmus basiert auf dem AIT ECGsolver, der für die Analyse von menschlichen EKG Daten verwendet wird. Das Problem der unterschiedlichen T-Wellen Form wird durch eine neue Merkmalssuche für den QRS-Offset und die T-Wellen Merkmale behoben. Es gibt drei Schritte im Algorithmus, die durch zwei unterschiedlich implementierten Methoden gelöst werden. Die Leistung der 8 resultierenden Versionen und des leicht adaptierten menschlichen Analysealgorithmus wurden ermittelt. Die automatisch annotierten EKG Merkmale und die berechneten EKG Intervalle wurden mit manuellen Annotationen verglichen. Außerdem wurde der Algorithmus auf Mäuse-Daten aus einer preklinischen Studie angewendet, um die Auswirkung von medikamentöser Behandlung zu untersuchen.

Der entwickelte Algorithmus liefert bessere Ergebnisse als der menschliche. Sowohl die Detektionsrate als auch die Differenzen zwischen den detektierten Merk-

malen und den Sollwerten konnte verringert werden. Eine Sensitivität von bis zu 91.6 % und ein positiver Vorhersagewert von bis zu 94.18 % können für verschiedene Versionen erreicht werden. Allerdings gibt es immer noch eine Überschätzung des QRS- und des QT-Intervalls und viele der T-offsets werden zu spät detektiert. Außerdem wurde festgestellt, dass die Erkennung der P-Wellen Merkmale noch Potential für Verbesserung aufweist. Das Ergebnis der Verabreichung eines Medikamentes war eine gesenkte Herzrate. Weitere Auswirkungen konnten nicht festgestellt werden.

In dieser Arbeit lag der Schwerpunkt mehr auf den Annotationen des QRS-Offsets und den T-Wellen-Features aufgrund der unterschiedlichen T-Wellen-Eigenschaften. Es stellte sich jedoch heraus, dass die Lokalisierung der P-Wellen Merkmale auch Potential zur Verbesserung aufweist, auf das in zukünftigen Arbeiten eingegangen werden kann. Außerdem sollte der Algorithmus noch weiter getestet werden mit Daten, die eine klar erkennbare negative T-Welle aufweisen.

Contents

Contents

Abbreviations and Symbols

Note: Variables used within limited context are described at the relevant section and are not listed here.

AP	action potential
au	arbitrary unit
AV	atrioventricular
ECG	electrocardiogram
FN	false negative
FP	false positive
FVB	Friend leukaemia Virus B
HR	heart rate
HRV	heart rate variability
IQR	interquartile range
KChIP2	Potassium Channel Interaction Protein 2
Pp	positive prediction
PQ	PQ-interval; time interval between P-offset and Q-onset
PR	PR-interval; see PQ
QRS	QRS-complex; time interval between Q-onset and S-offset
QT	QT-interval; time interval between Q-onset and T-offset
QT$_C$	QT$_C$-interval; heart rate corrected QT-interval
RR	RR-interval; time interval between two R-peaks
SA	sinoatrial
SCA	sickle cell anaemia
SD	standard deviation
Se	sensitivity

ST	ST-interval; time interval between S-offset and T-onset
TN	true negative
TP	true positive
TRA	trapezium's area
u	(membrane) voltage
U$_\mathbf{R}$	resting membrane potential
V	voltage
VAP	ventricular action potential
VEGF-B	Vascular Endothelial Growth Factor B
w	moving window width
α	level of significance
ϕ	potential

Introduction | 1

The introductory chapter explains the motivation and the goal of this thesis. Furthermore, an overview of the structure of the work is given.

1.1. Motivation

Automatically detected features of the Electrocardiogram (ECG) are used to calculate risk parameters for patients with heart diseases. ECG intervals, such as the QT-interval, are used to detect and observe cardiac diseases. The analysis of ECG signals and automatic determination of ECG parameters and features are a topic of great interest for clinical and preclinical research, especially automatic procedures with little to none manual intervention. The majority of preclinical studies on murine ECG signals uses manually annotated recordings.

Mice have many similarities with human anatomy and physiology, including electrocardiographic parallels. Thus, it is possible to translate results from mice models to humans. Furthermore, the possibility of gene manipulation to influence the function of proteins related to cardiac diseases and action potential generation exists for mice. Thus, genetically modified mice models are widely used for experiments concerning heart diseases.

Besides the similarities, one major difference between human and murine ECG signals is the heart rate. Heart rates of mice vary from 180 to 600 beats per minute [1]. They are multiple times higher than human heart rates, which range from 56 to 101 beats per minute [2]. Furthermore, electrocardiographic differences in morphology make it difficult to use human ECG signal analysis algorithms for murine data. For both species, the P-wave representing arterial depolarization and the QRS-complex representing ventricular depolarization are clearly recognizable in the ECG signal. The main difference in the morphology occurs in the QRS-offset and the T-wave features. There is no ST-interval in murine ECG signals. The subsequent wave to the QRS-complex is called J-wave. It starts right where the QRS-offset is located. The J-wave is followed by the T-wave. Depending on the measured lead, the T-wave in humans and in mice is positive or negative [3].

As a result of the differences, algorithms for analysing human ECG signals provide wrong annotations for mice. Especially for the QRS-offset and the T-wave, the

development of a specialised algorithm for the automatic detection of ECG features such as R-peak, QRS-onset and -offset, T-wave and P-wave in ECG signals of mice is relevant for medical applications and especially preclinical research.

1.2. Aim of the Thesis

The aim of this master thesis is the implementation, description, evaluation and application of an algorithm for automatic feature annotation of murine ECG signals based on the AIT ECGsolver, an algorithm for human ECG signals developed by Bachler et al. [4]. Relevant ECG intervals such as the QT interval should be calculated automatically based on the annotations.
The automatically annotated ECG features and calculated ECG intervals are evaluated against manually labelled annotations. In this way, the performance of the algorithm is determined. Moreover, the algorithm is applied to murine ECG signals from a preclinical study to investigate the influence of medical treatment on mice.

1.3. Structure of the Thesis

This thesis is structured into six chapters. After the introductory part, Chapter 2 is dedicated to provide the necessary background knowledge. The anatomy and physiology of the human and the mouse heart, general information about ECG signals, the state of the art methods for ECG analysis and some selected applications are presented. Chapter 3 describes the used data and the manual annotations. Furthermore, it introduces the used ECG analysis methods as well as the statistical methods for the evaluation. A detailed description of the implemented algorithm for the analysis of murine ECG data is given in Chapter 4. The results from the comparison between the manual and automatic annotations are presented in Chapter 5 together with results from the comparison before and after medical treatment of the mice. Chapter 6 provides the analysis and interpretation of the findings in Chapter 5 and an outlook for future investigations.

Background |2

In the following section, the anatomy and physiology of the human and murine heart are described. Furthermore, the origin, lead placements and components of the ECG are explained. In the last subsection, an overview of the state of the art and applications of murine ECG analysis algorithms is given.

2.1. Heart

Differences in the anatomical structure and the functionality of a mammalian heart exist, but are subtle [5]. Therefore, the human and mouse heart are explained at the same time with remarks on the main characteristics and dissimilarities. If not stated otherwise, the description of the human heart and general statements are based on the book *Biomedical Signals and Sensors I* by Kaniusas [6].

2.1.1. Anatomy

The heart of both species consists of a left and right side separated by a muscular wall, called the septum. Each side has two compartments, the atrium and the ventricle. The atria and ventricles are separated by atrioventricular valves. They are called tricuspid valve on the right side and mitral valve on the left side. The semilunar valves are the interconnection between the ventricles and the attached blood vessels. The valve between the right ventricle and the pulmonary artery is called pulmonary valve. The aortic valve regulates the blood flow between the left ventricle and the aorta. The inner tissue layer of the heart is called endocardium, the outer layer epicardium. Figure 2.1 and Figure 2.2 show a schematic representation of the human and murine heart and the connected blood vessels.

The blood circulation driven by the heart can be subdivided into the pulmonary and systemic circulation. The pulmonary circulation consists of the right part of the heart including the right atrium, the tricuspid valve, the right ventricle, the pulmonary valve and arteries, the capillaries and the veins in the pulmonary system. Its purpose is the transport of blood with low oxygen and high carbon dioxide concentration to the lungs for oxygenation. The left side of the heart pumps oxygenated blood through the systemic circulation, which includes the left atrium, the mitral valve, the left ventricle, the aortic valve, and the systemic arteries, the capillaries and the veins.
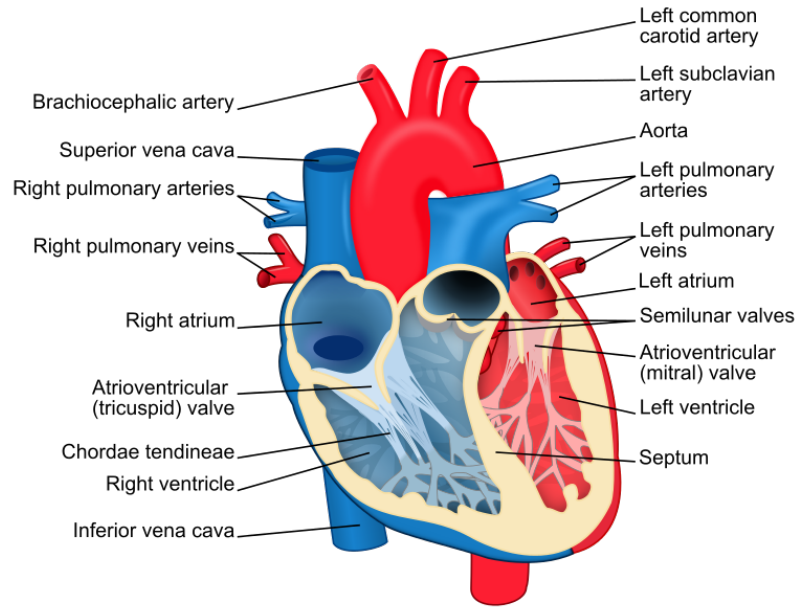
Figure 2.1.: Schematic representation and description of the human heart and the connected blood vessels [7].
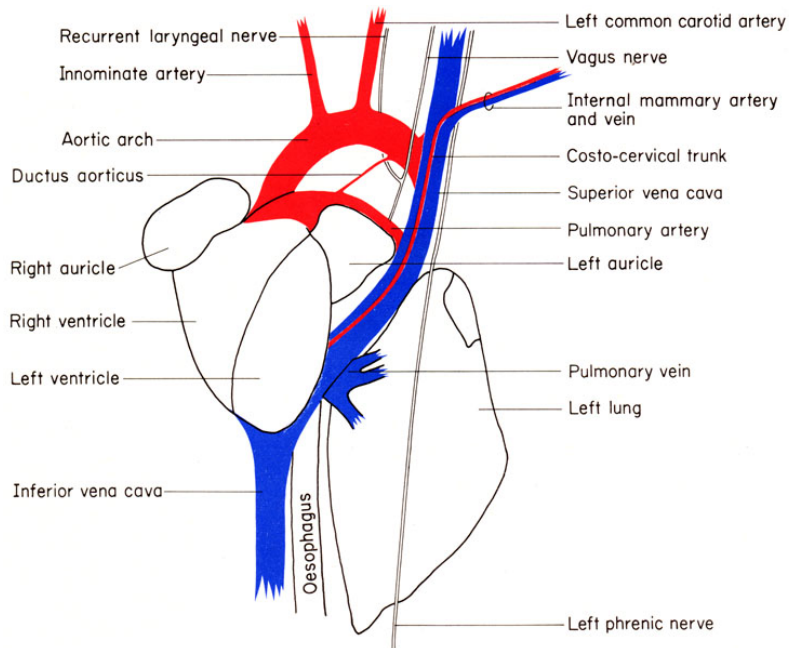

Figure 2.2.: Schematic representation and description of the murine heart and the connected blood vessels (auricle means atrium) [8].

The muscular structure of the heart is formed by two distinct cardiac muscles, called myocardia. Both, atria and ventricles, are each built by one myocardium leading to a functional separation. Furthermore ,the fibrous skeleton ensures the electrical separation. Only special conducting tissue can electrically connect the atrium and the ventricle.

The valves are composed of connective nonmuscular tissue. Pressure differences govern their opening and closing. The structure of the valves and the connection via tendious cords to the papillary muscles within the ventricles are responsible for the unidirectional blood flow through the heart.

The main components of the electrical conduction system are called sinoatrial node (SA node), atrioventricular node (AV node) and Bundle of His. All three can act as pacemaker for the heart at different rates. The primary pacemaker is the sinoatrial node. In humans, this collection of specialized cardiac muscle cells, is located in the right atrium. In mice, the location is not in the atrium, but in the Superior Vena Cava above the junction with the atrium [5]. The SA node spontaneously generates action potentials, which spread through cells into the right and left atrium. The AV node is the only conducting part between atria and ventricles. It is in the region of the interatrial septum. The Bundle of His transmits the action potential further through the fibrous skeleton to the apex of the heart. Two branches along the interventricular septum are connected to the ventricle walls through so called Purkinje fibers. The composition of the connection from the AV node to the bundle branches seems to be maintained for small mammals [5].

2.1.2. Physiology

The function of the heart is a composition of the mechanical pumping and the electrical activation. In this section, the chronology of one heartbeat is given without going into detail regarding the electrical conduction pathway (see Section 2.2.2).

Deoxygenated blood with low oxygen amount and high carbon dioxide enters the right atrium via the Superior Vena Cava. The left atrium is filled with oxygenated blood after the oxygen exchange in the lungs. The blood flows into the atrium through the pulmonary vein. Both atrioventricular valves are closed. The SA node initiates a heartbeat by generating an action potential which spreads through the atrial myocardium. This stimulates the right and left atria to contract. Due to the contraction, the atrial pressure exceeds the ventricular pressure, resulting in the opening of the atrioventricular valves. Since the ventricular myocardium is relaxed and the semilunar valves closed, the deoxygenated blood enters the right ventricle and the oxygenated blood the left ventricle. The action potential propagates to the AV node. A short time delay gives the atria time to eject the blood

into the ventricles. Then, the action potential is transmitted via the Bundle of His to the Purkinje fibers in the ventricular walls. The contraction of both ventricles increases the ventricular pressures. The semilunar valves open at the time the ventricular pressure exceeds the pressure of the following arteries. Thus, the blood is pressed from the heart into the arterial vessels. The ventricular pressure does not decrease until the ventricular heart muscle begins to relax. The semilunar valves close because of decreasing pressure in the ventricles. It is a mechanism to avoid blood backflow into the ventricles. Both atria and ventricles are relaxed. The valves are closed and both atria are filled with blood. The system is ready for the next action potential created by the SA node.

The heart beat can be divided into two time intervals - systole and diastole. Systole, or more precisely ventricular systole, is the time when both ventricles contract, atrioventricular valves are closed, semilunar valves are open. Blood enters into the arterial vessels and atria. The time period between closure of aortic and mitral valve is called ventricular diastole, or simply diastole. The blood flows through open atrioventricular valves into relaxed ventricles.

2.2. Electrocardiogram

The electrocardiogram is classified as electrical biosignal [6]. It represents the electrical excitation of the myocardia and thus is an important signal for the heart function. The general mechanism of the cell activation through an action potential, the standard lead placements, the origin and its corresponding components of the ECG are described in the following subsections.

2.2.1. Action Potential

This subsection is based on the explanation about action potential in the books *Biomedical Signals and Sensors I* by Kaniusas [6] and *Angewandte Biophysik* by Pfützner [9].

An action potential (AP) is a signal transporting physiological information within the body and is triggered by temporal ionic flow across the membrane of excitable cells, such as muscle and nerve cells. The intra- and extracellular areas of cell membranes are filled with ions. The concentration of potassium K^+ and anions is higher inside, sodium Na^+ and chloride Cl^- are more common outside. Although other ions are involved as well, these ions have a significant concentration and role in the AP generation. Since the electric charges between the intra- and extracellular space are unbalanced, a membrane voltage u occurs. Normally the membrane potential is in a resting stage of $U_R = -70$ mV. The equilibrium is maintained by flux through resting state ion channels. Local stimulation, such as artificial excitations or outward local currents, yields increasing local u (see Figure 2.3). This may

be the origin of an AP, if the depolarization of the membrane exceeds a threshold of about -50 mV. According to an all-or-nothing-law, an AP is only triggered when the threshold is reached. After the AP introduction, the ongoing depolarization causes more and more voltage-gated Na^+ channels to open, which in return increase the depolarization and the membrane voltage. Within the subthreshold level, only resting state channels of K^+ and Cl^- ions are active. Voltage-gated K^+ channels react with a delay and reach their peak in conductance way after Na^+ channels. Towards the end of the depolarization, voltage-gated Na^+ channels become temporal inactive. The influx of positive Na^+ ions is compensated by the K^+ efflux. After reaching the maximum of $u = 40$ mV, the voltage starts to decrease and repolarization starts. It is mainly controlled by voltage-gated K^+ channels. The outflow of K^+ and inflow of Cl^- ions overcompensate the inflow of Na^+ during depolarization and lead to hyperpolarization. The voltage u even drops below the resting state U_R until K^+ conductance reaches its resting level. Voltage u returns to the level of U_R and the local AP is over.
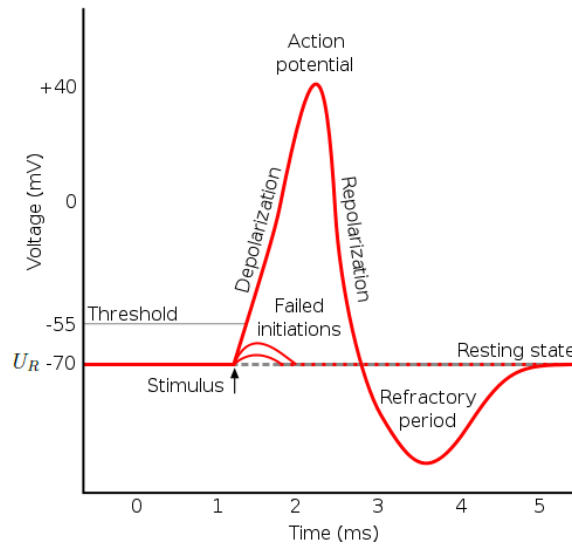

Figure 2.3.: Schematic representation of the potential differences during an action potential. Image is adapted from [10].

As mentioned before, outward local currents work as depolarization stimuli and can trigger an AP. They are caused by the increased flow of positive Na^+ ions during local depolarization and negatively charged membrane potential in adjacent areas. This imbalance leads to the equalizing ionic current along inner and outer membrane surface. The affected membrane part introduces another AP after reaching the voltage threshold, which can be the origin of another AP. This mechanism is responsible for the propagation of APs through axons. The refractory period of the voltage-gated ion channels protects against overlaps of APs and backpropagation. As a result, the spread in one direction is guaranteed.

2.2.2. ECG origin

In the previous section, a general explanation of the generation and propagation of an action potential was given. This knowledge is now applied to describe the origin of an ECG. The section is based on the book Bioelectromagnetism by Malmivuo and Plonsey [11].

Action potentials propagate through the heart via myocardic muscle cells. For resting cells, the extracellular space is positively charged, for activated cells, it is negatively charged. The charges in intracellular space are not considered. The differences in the extracellular space generate a dipole, which is orientated from negatively to positively charged areas. At a given time point, activation (depolarization) and relaxation (repolarization) generate many of these dipoles, differing in magnitude and direction. Each dipole can be represented by an electrical vector. Summing up all individual vectors, results in the mean electrical vector. Resulting potential differences can be recorded by placing electrodes on the body surface. However, potential differences only occur at the boundary between activated (depolarized) and relaxed (repolarized) heart regions and not at fully excited or relaxed areas. Thus, the recurring waves and segments of the ECG are determined by the propagation of depolarization and repolarization and their sign depends on the spatial spread direction.

The depolarization of one cell leads to the excitation of the adjoining cells. The resulting wave front propagates through the heart. The resulting dipole is oriented in the direction of the depolarization propagation (from negatively to positively charged extracellular space). Repolarization occurs as soon as the AP is over. Since it is not triggered by surrounding cells, but dependent on the AP duration, it is strictly spoken not a propagation phenomenon. However, the movement of the boundary between still depolarized and repolarized areas is defined as propagation. The AP duration depends on the heart region and is not the same for all cells. For both humans and mice, the duration is shorter in epicardium than endocardium. Thus, the repolarization phase moves from epicardium to endocardium. However, since the propagation direction of the inward repolarization phase is opposite to the outward depolarization wave, the sign of the resulting waves is equal.

The exact shape of the resulting waveform and its polarity depend on the placement of the electrodes, which is discussed in Section 2.2.3. Furthermore, the propagation pattern of depolarization and repolarization, which differs between species, has a great influence. Section 2.2.4 is dedicated to target these differences and their consequences.

2.2.3. Lead placement

There are several possible ways to position the recording electrodes on the body surface. In this section, the measurement points of the standard 6-lead and 12-lead ECG are briefly explained.

For humans, the Einthoven leads I, II, III are measured using electrodes on the right arm (R), the left arm (L) and the left foot (F) (see Figure 2.4 A). The voltages V at the three standard limb leads are given by $V_I = \phi_L - \phi_R$ for lead I, $V_{II} = \phi_F - \phi_R$ for lead II, $V_{III} = \phi_F - \phi_L$ for lead III, with potential ϕ at the corresponding electrodes. The leads are bipolar and lie in the frontal plane. Goldberg augmented leads aVR, aVL, aVF are also lying in the frontal plane and are measured at the same points. However, they are unipolar. The potentials are measured between one limb electrode and the average of the remaining limb electrodes (see Figure 2.4 C). The equations are given by $V_{aVR} = \phi_R - \frac{\phi_L + \phi_F}{2}$, $V_{aVL} = \phi_L - \frac{\phi_R + \phi_F}{2}$ and $V_{aVF} = \phi_F - \frac{\phi_L + \phi_R}{2}$. Together, Einthoven and Goldberg leads define the standard six lead ECG in humans. [11]

In mice, the three limb electrodes are usually placed in the left and right armpit and the left groin [12] (see Figure 2.4 B). Thus, an ECG with six leads can be derived analogous to the human ECG. The schematic drawing of a human and murine standard six lead ECG is shown in Figure 2.4 D,E.

The standard 12-lead ECG consists of the three Einthoven leads, the three Goldberg leads and the Wilson leads V_1 - V_6. The unipolar chest leads by Wilson V_1 - V_6 are placed close to the heart on the left chest (see Figure 2.5). The six leads are lying in the horizontal plane. Thus, the 12-lead ECG provides a 3D representation of the electrical heart vector.
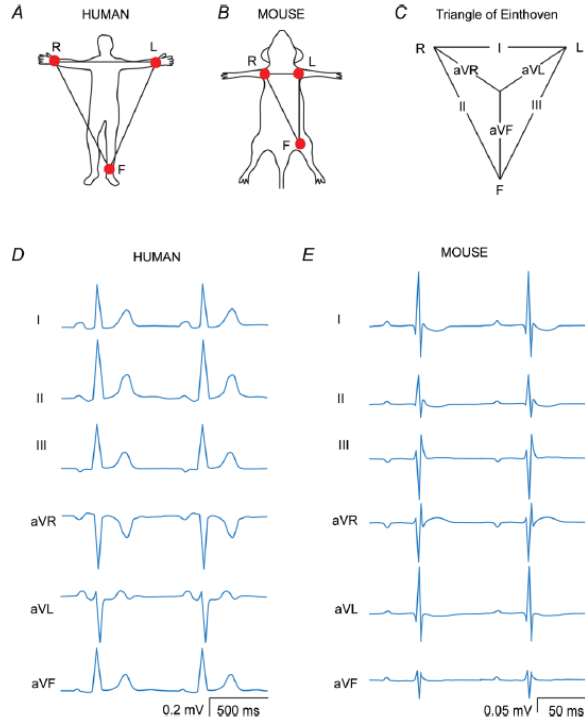

Figure 2.4.: Schematic illustration of the lead placements in human (A) and mouse (B) and the Einthoven's triangle (C). Schematic standard six lead ECG signals of human (D) and mouse (E). Image is taken from [12].
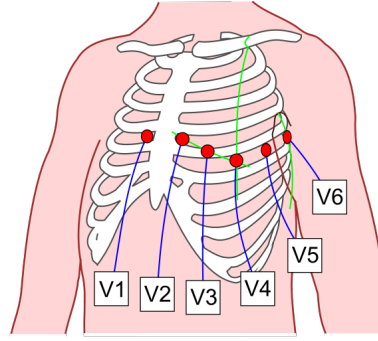
Figure 2.5.: Schematic illustration of the lead placements for Wilson leads V_1 - V_6 close to the heart on the left chest. Image is taken from [13].

Another way of placing the leads are the orthogonal Frank leads X, Y, and Z. The placement of the corresponding 7 electrodes can be seen in Figure 2.6. The electrodes A, C, E, I, M are located on the horizontal level, electrode F is placed on the left leg and electrode H on the back of the neck. The potential difference V_X is the right-to-left component derived by the electrodes A, C and I. By using the electrodes on the horizontal level A, C, E, I and M, the front-to-back component V_Z can be determined. The head-to-foot component V_Y is derived by the neck electrode H, the leg electrode F and the horizontal back electrode M.
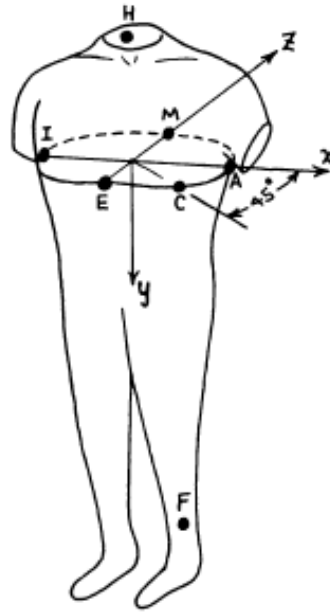

Figure 2.6.: Schematic illustration of the lead placements for Frank leads X, Y, and Z. Seven electrodes (A, C, E, I, M, H, F) are used to derive the orthogonal leads. Image is taken from [14].

2.2.4. ECG components

Atria activation and relaxation hardly differs between human and mouse. However, the situation is rather different for activation and repolarization of ventricles as can be seen in Table 2.1. Different shapes of ventricular action potentials (VAP) cause clear dissimilarities between the two species. They manifest themselves in the surface ECG morphology and have been extensively studied by, among others, Danik et al. [15], Liu et al. [16], Kaese and Verheule [2], Boukens et al. [12, 17] and Speerschneider and Thomsen [3]. Their results, along with those of Durrer et al. [18] about the activation patterns for human hearts, are discussed below.
The schematic representation of the ECG signal and its features is given in Figure 2.7. The human ECG signal is shown in Figure 2.7a, the murine ECG representation is shown in Figure 2.7b. Table 2.1 provides an overview of the definition of ECG components and the corresponding physiological source.

According to [3,17] the **isoelectric line** (also called the baseline) for mouse ECGs is defined as the segment between the end of T-wave and the onset of the next P-wave.

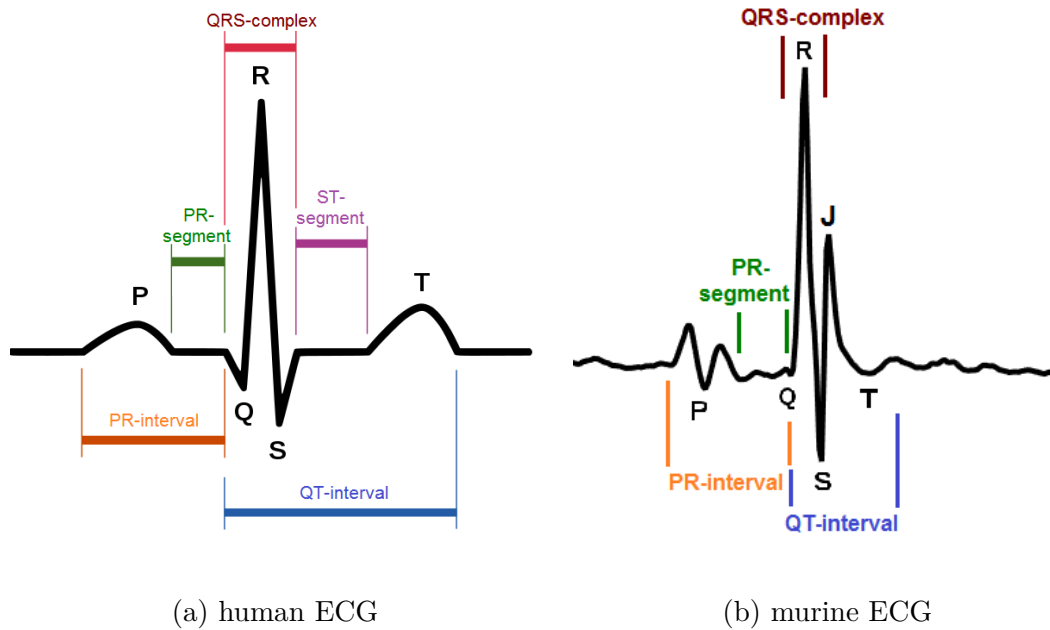(a) human ECG   (b) murine ECG

Figure 2.7.: Schematic representation of a human (a) and murine (b) ECG signal and its features. Image (a) is modified from [19]. Image (b) was creating using the data described in Section 3.1.

Component	Definition	Source	
		Human	Mouse
P-wave	baseline intersection marks start and end	depolarization of both atria	
PR-interval	from start of P-wave to start of Q-wave	the electrical impulse travels from atria to ventricles	
QRS-complex	from start of Q-wave to end of S-wave	depolarization of both ventricles	
ST-segment	from end of S-wave to start of T-wave	ventricles are nearly uniformly excited	no segment on level of baseline exists (see J-wave)
J-wave	from end of Q-wave to start of T-wave	not existing (see ST-segment)	early ventricular repolarization
T-wave	baseline intersection marks start and end	repolarization of both ventricles	
QT-interval	start QRS-complex to end of T-wave	complete ventricular activation and relaxation, generation of ventricular beat	not exactly clear, complete activation and parts of relaxation

Table 2.1.: An overview of ECG components, their definitions, and their physiological source in humans and mice.

P-wave

In mice, the initial activation of atria takes place near the location of the SA node and spreads over left and right atrium, as in humans [2]. It is not clear if mice have the largest conduction pathway, called Bachmann's bundle, between the two atria [2]. However, the spread of activation is similar in humans. The atrial depolarization towards the apex is called P-wave. The maximum of the P-wave is reached when half of the atria are depolarized [6].

PR-interval

In murine ECG signals, a small deflection follows the P-wave. It was proposed by Boukens et al. [12], that the deflection either represents the atrial repolarization or emerges when leads L and R are positioned in a way that atria are not in the middle. During the isoelectric part of the PR-interval (also called the PR-segment), the atrial myocytes are fully depolarized. The AV node and bundle of His conducts the impulse to the ventricles [2]. In humans, atrial repolarization happens during the QRS-complex. Thus, it is not explicitly visible in the ECG signal. Depending on the literature, the PR-interval is also called the PQ-interval.

QRS-complex

The similar activation pattern of the heart ends after the atrial activation. In humans, ventricular depolarization starts in the interventricular septum on the left ventricular side and then spread subsequently into the right ventricle [18]. The activation runs from apex to base [18]. The epicardial ventricular depolarization in mice starts either by clearly defined breakthroughs in the right ventricle followed by propagation into the left ventricular part or in the left ventricular apex with shortly following breakthroughs in the right ventricle [2]. In both cases, the endocardium is earlier activated than the epicardium [16]. In mice, the interventricular septum is excited in the opposite direction as in humans, from base to apex [2]. Even if the spread of the ventricular depolarization differs between the two species, it corresponds for both to the QRS-complex with similar shapes.

ST-segment and J-wave

In 1968, Goldbarg and his colleagues were the first to describe and analyse the murine ECG in [20]. They published the first detailed study of different electrocardiographic variables and the repolarization mechanism of mice. They already documented the problem of not well-defined QT-intervals and were certain that adding the J-wave to the QRS-complex duration would overestimate the complete activation time.

Liu et al. [16] were the first to study the temporal and spatial distribution of the ventricular depolarization and repolarization in vivo by means of monophasic VAPs. The different shapes of VAPs and their consequences on the surface ECG morphology have been extensively studied by Boukens et al. [12,17]. They isolated the AP of ventricular myocytes of humans and mice and used them to determine the body surface ECG under normal conditions in silico. Their results are illustrated in Figure 2.8. The left side of the figure shows the result for the human heart, the right part corresponds to the mouse heart. The electrocardiogram in part A is displayed without P-wave. The VAP for earliest ventricular activation is represented by the continuous line. The dashed line represents the latest activation.

The ST-segment in humans is the phase when both ventricles are fully activated. It is caused by the plateau phase in the VAP, which separates the depolarization represented by the QRS-complex and repolarization [17]. After the upstroke in the mouse, the VAP follows a fast downstroke and a plateau with lower voltage than in humans. The different shape in VAP occurs in response to the different magnitudes of ionic currents [16]. The lack of a distinct plateau phase leads to an overlap of the depolarization and repolarization waveform in the ECG. A significant part of the repolarization happens even before the entire activation has been completed. It starts already during the QRS-complex. According to Boukens et al. [17], the end of the QRS-complex correlates with the end of ventricular activation measured by optical mapping technique only in leads III and aVF. The rapid

initial repolarization is the source of the J-wave in murine ECG signals. Thus, there is no distinct ST-segment on the level of the isoelectric line and the J-wave follows immediately after the S-wave (see Figure 2.8 A). Lowering the voltage level of the plateau in the VAP produces only a QRS-complex with smaller amplitude, but no J-wave [17]. Thus, the low plateau level is not the reason for the appearance of the J-wave.
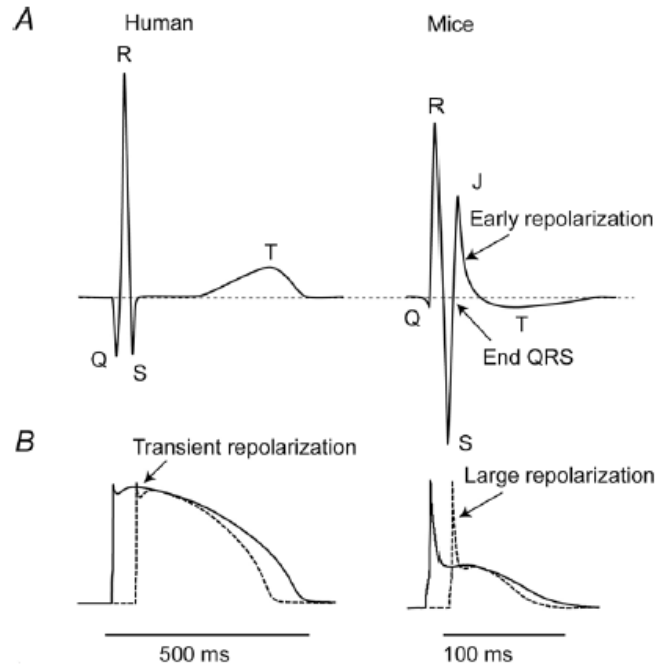

Figure 2.8.: Relationship between ECG without P-wave (A) and the action potential in isolated ventricular myocytes (B) in humans (left) and mice (right). In (B), the continuous line represents earliest ventricular activation, the dashed line represents latest activation. Image is adapted from [12].

T-wave

For both species, the T-wave indicates the ventricular repolarization. Nevertheless, there are some major differences. Since the ST-segment in humans is a clear boundary for depolarization and repolarization, the T-wave is a distinct deflection. The last activation moment is detected in the left and right ventricular base [18]. Boukens et al. [17] stated that the last activated part in a mouse heart is the right ventricular base, because the activation in the left ventricle is faster than in the right ventricle. The origin of the murine T-wave is the difference in ventricular repolarization between the left and right part. The exact direction of the repolarization gradient is from the right ventricular base to the right ventricular apex.

The sequence of relaxation is the opposite of activation [16]. The epicardium is relaxed earlier than the endocardium and the repolarization goes from apex to base [2]. As mentioned in [15], the low amplitude of the T-wave can be explained by the weak electrical forces generated by the slow gradual time course for relaxation. According to Speerschneider and Thomsen [3], the T-wave has negative sign for leads I, II, aVL, aVF. For lead II and aVR, it is a positive deflection.

QT-interval

J- and T-wave both belong to the repolarization of the ventricle in mice. The end of right ventricular repolarization correspond to the J-wave offset [17]. The T-wave offset coincide with the left ventricular repolarization [17]. However, neither the QJ- nor the QT-interval correspond to the complete ventricular depolarization and repolarization [3, 12, 15, 17]. Danik et al. [15] even reported that they could not clearly define the QT-interval for most of their signals. It is recommended by Boukens et al. [17] that the ventricular repolarization in mice is measured by optical mapping or monophasic AP to get exact results, because the body surface ECG is not sufficient. For humans, the QT-interval reflects the complete depolarization and repolarization phase of ventricles [6].

The QT-interval in humans depends on the heart rate. Thus, it can be corrected according to Bazett [21] or other formulas [22]:

$$QT_\mathrm{C} = \frac{QT}{\sqrt{RR}}. \tag{2.1}$$

Mitchell et al. [23] modified Bazett's formula (2.1) for the use in mice. They developed a formula for heart rate-corrected QT-intervals based on their ECG recordings of conscious FVB (Friend Virus B) mice. The approximate average duration of an RR-interval in this strain of 100 ms was used as a normalisation factor for the RR-intervals. The QT-intervals are plotted against the normalised RR-intervals. Fitting the data to a linear curve by a linear least squared regression analysis lead to a slope of 0.44. This means the QT-interval is approximately proportional to the square root of the normalized RR-interval. The correction formula derived by Mitchell et al. [23] is Bazett's formula applied to the normalised RR-interval:

$$QT_\mathrm{C} = \frac{QT}{\sqrt{(RR/100)}}. \tag{2.2}$$

However, according to [3, 12], a heart rate correction should not be done in anaesthetised mice. It would lead to erroneous corrections and introduce a systematic error in the measurement. Anaesthetics can change cardiac repolarization. Speerschneider and Thomsen [3] used isoflurance as anaesthetic and documented a reduced heart rate and QT-interval prolongation. Setting QT_C in relation to RR does not yield to a horizontal linear relationship. They concluded that the

duration of repolarization did not depend on the heart rate in anaesthetized mice. Boukens et al. [12] suggested the application of a disease-specific heart rate correction.

2.2.5. Electrophysiological parameters

An overview of some selected parameters of general physiology and cardiac electrophysiology are provided in Table 2.2. The data is taken from [2]. The most obvious differences are the lower body mass and heart weight of mice. This corresponds to a faster contraction rate and results in a higher heart rate than in humans. However, not only the RR-interval is shortened, but also the PR-, QRS-and QT-interval.

	Human	Mouse
Body mass (kg)	58-85	0.015-0.043
Heart weight (g)	261-366	0.12-0.17
Heart rate (beats/min)	56-101	500-724
RR interval(ms)	500-1070	80-120
PR interval (ms)	120-200	30-56
QRS duration (ms)	84-110	9-30
QT (ms)	385	29-109
QT_C (ms)	398-430	30-124

Table 2.2.: Quantitative comparison of selected parameters concerning general physiology and cardiac electrophysiology in humans and mice. Values are taken from [2].

The variations in the mouse data due to differences in strains of mice and different applied anesthesia can be seen in Table 2.3. Mouse ECG intervals of 9 different studies, chronologically ordered, are qualitatively compared.

Most of the mice strains used in the studies are laboratory mice of the species Mus Musculus (house mouse). They are named according to their genotypes. One of the most commonly used inbred strains is the C57 black, from which the substrains C57Bl/6J and C57Bl/10 of the Jackson Laboratory are derived [24,25]. The albino strain FVB(/NJ) is also widely used. The full name is Friend Virus B (NIH Jackson) due to a sensitivity to Friend leukemia virus B [26]. The Swiss Webster mice are an albino outbred strain from the Rockefeller Institute [27]. The genetic differences between the strains also cause anatomical and physiological differences. The heart weight alone varies between 150 in FVB mice and 180 mg in Swiss mice according to Doevendans et al. [5] and between 120 and 170 mg according to Kaese et al. [2], who considered five different sources.

The heart rates of Table 2.3 are in the same range, if the values are compared independently of the mouse strain, but only based on the anesthesia used in the study.

Author & Year	Mouse strain	n	Anesth.	Heart rate	PR	QRS	QT
O'Bryant et al. (1949) [28]	Mus Musculus	40	None	635 ± 9	$*$	$*$	$*$
Lombard (1952) [29]	White Mouse	10	Barbital	376 ± 49	43	$22 \pm 2 \dagger$	$*$
Richards et al. (1953) [30]	Newborn	10	None	286 ± 57	60 ± 3	10 ± 0	80 ± 18
	Adult	10	None	632 ± 51	38 ± 100	10 ± 4	35 ± 5
Giordano and Nigro (1957) [31]	White Mouse	20	Barbital	$320 - 640$	$30 - 40$	$10 - 30$	$20 - 40$
Goldbarg et al. (1968) [20]	C57BL/10	18	Ether	322 ± 99	46 ± 4	12 ± 2	83 ± 24
	SEC/1	15	Ether	354 ± 66	39 ± 5	12 ± 3	83 ± 21
	F_1 1005/L	18	Ether	340 ± 71	41 ± 5	12 ± 2	96 ± 12
Mitchel et al. (1998) [23]	FVB	5	None$^\blacktriangle$	616 ± 77	$*$	$*$	54.9 ± 4
	FVB	6	Ketamine, Xylazine	226	$*$	$*$	99
Danik et al. (2000) [15]	Swiss Webster	13	Pentobarital sodium	121 ± 21	$*$	$*$	22 ± 2
Boukens et al. (2013) [17]	FVB/N, wild-type, 129P2 Scn5a1798insd	16	Isoflurane	406 ± 15	33.2 ± 1.8	8.4 ± 0.4	66 ± 4.4
Merentie et al. (2015) [32]	C57Bl/6J young	73	Isoflurane	420 ± 50	43.6 ± 3.2	10.8 ± 1.2	48.3 ± 5.7
	C57Bl/6J middle aged	34	Isoflurane	468 ± 37	50.3 ± 16.5	10.8 ± 0.9	48.0 ± 4.0
	C57Bl/6J old	40	Isoflurane	475 ± 64	59.6 ± 23.9	11.3 ± 1.4	46.3 ± 5.8

Table 2.3.: Quantitative comparison of murine ECG intervals. This table is inspired by [20] and [1].
$*$ Not assessed. $\dagger$With T-wave. $\blacktriangle$ Telemetry

2.3. State of the Art of ECG Analysis in Mice

This sections purpose is to give an overview of the state of the art methods for ECG-analysis, especially for murine data. The first part is about analysis algorithms and methods for feature detection, whereas the second part is focused on selected applications.

2.3.1. ECG analysis algorithm

Many analysis methods and programs for human ECGs have been developed in the last decades. An overview and comparison of the most common methods for QRS-complex detection can be found in Köhler et al. [33]. The described approaches include signal derivatives, digital filters, wavelets and neural networks. After performing the QRS-complex detection, various methods to determine onset, offset, and peak of the P- and T-wave can be applied. One of the common methods for the T-offset detection is using a threshold on the first derivative. This method has been used by Laguna et al. [34] and McLaughlin et al. [35], among others. McLaughlin and his colleges compared this approach with other methods such as using a threshold for the T-wave amplitude and determining the intersection with the isoelectric level [35]. A description of the detection based on a threshold for the first derivative was also given by Vazques-Seisdedos et al. [36]. They developed an alternative approach based on the calculation of a trapezium's area. For the detection of the T-wave peak, Christov and Simova [37] used special "wings" functions, which can be applied regardless of the T-wave polarity. Many methods to determine T-wave features can be adapted and also used for P-wave detection. The described list of approaches is far from complete. However, some of the mentioned methods are used for the developed algorithm and therefore described in more detail in Section 4.2.

In addition to methods for individual features, there are also software packages and programs that can annotate all common ECG features, such as the AIT ECG-solver developed by Bachler et al. [4]. It is an automatic ECG analysis algorithm for online and offline detection of the R-peak, the QRS-complex, the P- and T-wave features. A detailed algorithm description will be given in Section 4.2 as it is the basis for the murine algorithm. A verification against PhysioNet databases resulted in a sensitivity of 98.2 % and a positive predictive value of 98.7 %.

Due to the differences in human and murine ECGs, there are not many automatic analysis algorithms for mice. As a result, manual annotations by clinical experts often are used to evaluate the murine ECG signal.

Chu et al. [38] developed a non-invasive ECG recording system for conscious mice in 2001 (Mouse Specifics, Inc. [39]). The ECG recording device called ECGenie works without anaesthesia, surgical device implantation or attached wires. Instead, three conductive paw-sized electrodes on a recording platform, on which the conscious mouse can be placed, are used. The corresponding analysis algorithm

called EzCG (previously e-MOUSE) determines the R-peak and the heart rate by means of a peak detection algorithm. The 1st and 2nd derivatives together with "if-then" queries are used to annotate the QRS-onset and -offset and the P-peak. The T-wave is determined, with the biphasic a part included. The feature detections are plotted for visual confirmation. Finally, the mean ECG interval durations are calculated as well as the QT_C-interval by Mitchell et al. [23].

In 2010, Galetin et al. [40] provided a guideline to use the PhysioToolkit for murine ECG analysis. The PhysioToolkit is an open source software developed by the Massachusetts Institute of Technology and available at physionet.org under GNU General Public License. It is designed for signal processing and analysis in humans with its main application in heart rate variability (HRV) analysis. Galetin et al. described a way to manipulate the source code and the analysis pipeline to deal with the increased heart rate of murine ECGs. Furthermore, they tested different settings of the median filter for noise reduction and achieved up to 99.7 % accuracy. According to Galetin et al., the PhysioToolkit is very flexible and can be adapted for other species as well. However, the program application is limited to HRV analysis. Other features, such as the P- and T-wave, are not annotated. Five years later, Merentie et al. [32] developed a software specialized in mouse ECG analysis. The program implemented in Matlab pays attention to the special features of ECG signals from mice. Kubios HRV, the automatic QRS-detection algorithm by Tarvainen et al. [41], is used for the R-peak annotation. The detection of the ECG waves onset and offset is performed on an averaged wave epoch by the first derivative threshold method described in [36]. However, the algorithm does not work fully automatic, since all annotations were visually confirmed by specialists and corrected if necessary. Therefore, no statement can be made about the accuracy of the program. Nonetheless, the adjusted Kubios HRV was used by Naumenko et al. [42] for their studies in 2017.

2.3.2. Applications

There are numerous applications of ECG analysis. This also applies to the data of mice. A few selected applications are presented in this subsection.

The specialized mouse ECG analysis algorithm by Merentie et al. [32] was used to study the changes due to aging and the effects of selected drugs on C57Bl/6j mice. The ECG parameters of three groups with different ages were compared. Typical for middle-aged (14 months) and older (20-24 months) mice is an increase in heart rate, P-wave and PQ-interval duration as well as a widening of the J-wave. The QRS-complex width shows no major changes, only the R-wave amplitude is reduced. The effects of pharmacological treatment with drugs affecting the conduction system, such as atropine, beta blocker metoprolol, and calcium-channel blocker verapamil, are similar to those of humans. After the administration of atropine, the heart rate increases and the PQ-interval duration decreases. A decreased heart rate and longer PQ-intervals are recorded after the treatment with

metoprolol and verapamil. However, verapamil causes a slighter reduction of the heart rate and a stronger increase in the PQ-interval duration.

Chu et al. [38] presented their findings in strain and gender differences in adult mice ECG signals. Depending on the mouse strain, the heart rate is slightly increased or decreased in female mice compared to male mice for C57BL/6 mice and FVB/N mice, respectively. The ECG recording device and algorithm was also used by other researches for their studies, such as Xing et al. [43]. They investigated the genetic influence on ECG-interval durations and the heart rate in aging mice. The ECG features of 8 male and 8 female representatives of 28 inbred strains were recorded at three different ages. The findings revealed significant age-related variations in the PR-interval, the QRS-complex, and the heart rate among strains. However, the changes of ECG parameters not only depend on the age and the race of the mouse, but also on its gender.

However, not only mouse-specific research issues, such as the comparison between different age groups, mouse strains, and gender are studied. Already mentioned was the study of the effects of pharmacological treatment with medication influencing the cardiac activity. Additionally, modifications in the physiology, such as the expression of genes and pathological changes, and their effects on the ECG signal are examined.

The algorithm by Merentie et al. [32] was also used by Naumenko et al. [42] to study the effects of the Vascular Endothelial Growth Factor B (VEGF-B), which influences the myocardial metabolism, growth, and the heart's stress response. The changes in the electrical properties of the cardiac muscle cells also affect the ECG signal. Especially the amplitudes of the R- and S-waves decrease and the duration of ventricular depolarization and early repolarization is prolonged.

Gottlieb et al. [44] investigated the role of KChIP2 (Potassium Channel Interaction Protein 2) in the circadian rhythm in the QT-interval of mice. KChIP2 is an important subunit for the ventricular repolarization and is claimed to play a role in ventricular arrhythmias, sudden cardiac deaths, and the circadian rhythm in repolarization duration. Thus, the hypothesis was that there is no circadian rhythm in the QT-interval in the absence of KChIP2. However, their findings revealed that missing KChIP2 expression does not cause the cardiac rhythm in QT-interval to vanish, since it is preserved in KCHIP2-deficient mice.

ECGenie, the non-invasive recording system by Chu et al. [38], was also used by Bakeer et al. [45], who were dealing with the physiology of sickle cell anaemia (SCA) mice. SCA is a blood disorder caused by a point mutation in the β-globin gene. The consequence is a mutation of the oxygen-carrying protein haemoglobin S in red blood cells, which leads to many unexplained sudden deaths and a higher morbidity. The researchers around Bakeer used cardiac imaging, ECG recording, cardiac histopathology, and molecular analysis to investigate the cardiac dysfunction in Berkeley SCA mouse models. Their electrocardiographic findings revealed a prolongation of the QT_C- and the QRS-interval. However, the ECG differences occurred before the functional changes, suggesting that there is no causation.

Data and Methods | 3

This section is dedicated to give a description of the used data and an overview of the manual annotations. Furthermore, the methods of human ECG analysis, which are used and adapted in the murine ECG analysis algorithm, are described together with statistical methods for the evaluation.

3.1. Data

The used dataset is provided by the clinical partner LMU, University Clinic Munich. It consists of 26 ECG recordings with Frank leads X, Y, and Z (see Section 2.2.3), which were acquired with LabChart [46] at a sampling rate of 1000 Hz. The recordings were taken from 13 laboratory mice under isoflurane 1.5% anesthesia, 2 recordings per animal. The first recording was taken before the medical intervention with Atenolol 5mg/kg and the second recording afterwards.

For the algorithm development process, the dataset has been divided into 2 subsets. The development subset consists of the first 14 recordings (7 mice) and was used for planning the detection criterion and testing feasibility of the algorithm. The remaining 12 recordings (6 mice) were used as control subset to verify the independence of the algorithm from the development subset and to test its correctness.

3.2. Manual Annotations

The manual annotations are used as target values for the evaluation of the automatic murine ECG analysis algorithm. The AIT MurineECGAnnotator (MEGA), a Matlab based annotation software, was used to annotate the ECG features manually. After labelling the onset and offset manually, the peak of the corresponding wave is annotated automatically.

The procedure of the manual annotation for one lead is illustrated in Figure 3.1. The basis for the target value was provided by a medical partner at LMU. Overall, he annotated about 465 heart beats with at least one heart beat in each lead (except lead Z in one file which is excluded from the evaluation). Based on this template (Figure 3.1 A), approximately 10 seconds in each lead were annotated by 4 different non-clinical experts (Figure 3.1 B). The intervals were choosen individually, either split in two intervals of 5 seconds or in one 10 seconds lasting interval.

3. Data and Methods

Each interval contains at least one annotation of the medical expert (Figure 3.1 C).
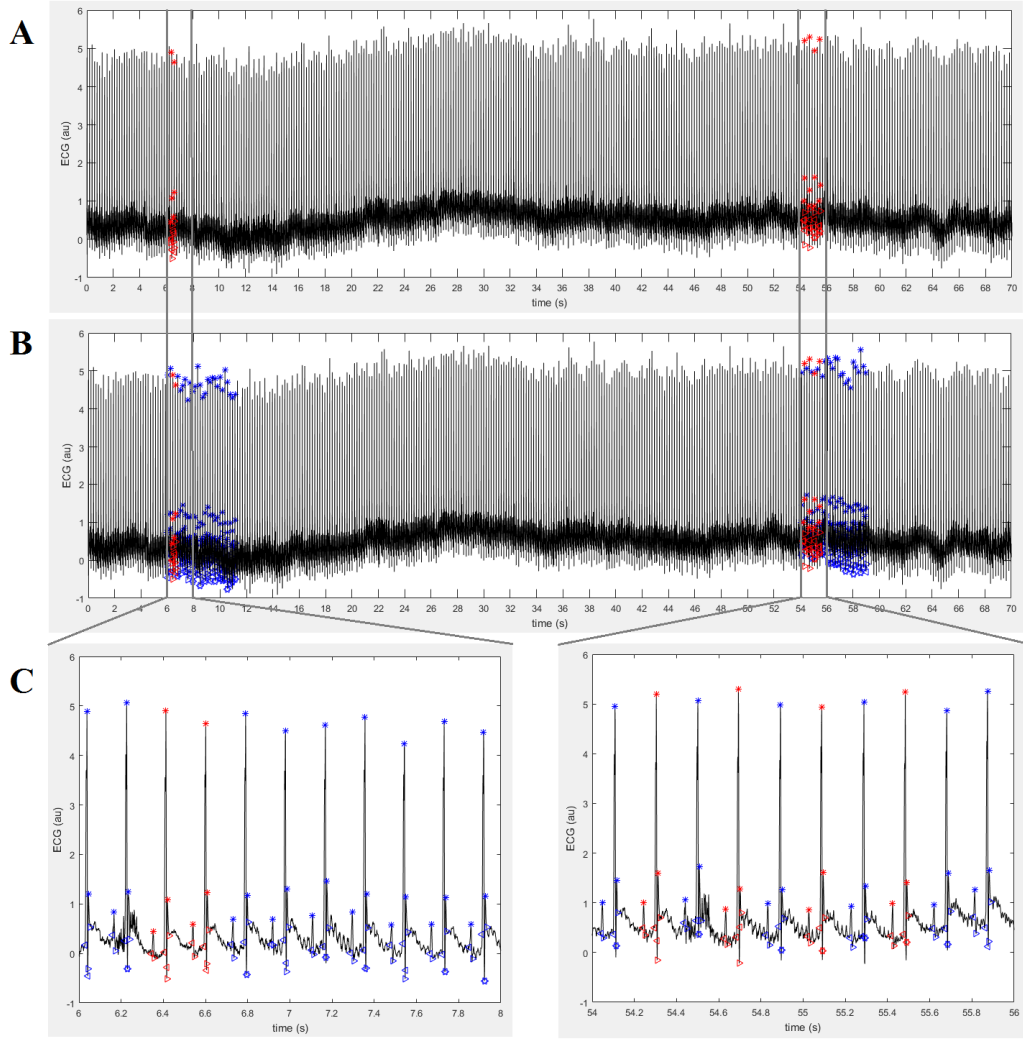
Figure 3.1.: Illustration of the manual annotation procedure. A medical expert labelled the features of some individually chosen heart beats in every ECG recording (A, red labels). Based on this template, 4 non-clinical experts annotated approximately 10 seconds in each lead (B, blue labels), either split into two 5 seconds or one 10 seconds lasting interval. Each interval contains at least one annotation of the medical expert (C).

3.3. Methods for ECG Signal Processing

In this section, different methods used in the process of ECG annotation are presented, especially with focus on those methods, which are used for the murine ECG analysis. At the beginning, methods for clustering are explained. Then, an overview of the processing algorithm AIT ECGsolver, which acts as basis for the developed algorithm, is given and an alternative method to determine the T-offset is presented. The implementation of the developed algorithm was performed in Matlab R2015b.

3.3.1. Clustering

There exist various methods to partition a given data set into clusters. The goal of all methods is to gather similar objects in a cluster. For that, both the intra-cluster similarity and the inter-cluster dissimilarity should be as high as possible. All methods make use of a distance measure. An overview of some distance measures is given in Table 3.1. The most commonly used is the Euclidean distance or the squared Euclidean distance. But there are others as well, such as the Mahalanobis distance, the City block distance (L_1 distance), the Minkowsky distance, and the correlation distance, which are all implemented in Matlab [47].

Distance	Definition
Euclidean distance	$d(x,y) = \sqrt{\sum_{j=1}^{n}(x_{\mathrm{j}} - y_{\mathrm{j}})^2}$
Mahalanobis distance	$d(x,y) = \sqrt{(x-y)^T \cdot Cov(x,y) \cdot (x-y)}$
City block distance	$d(x,y) = \sum_{j=1}^{n} \lvert x_{\mathrm{j}} - y_{\mathrm{j}} \rvert$
Minkowsky distance	$d(x,y) = \sqrt[p]{\sum_{j=1}^{n} \lvert x_{\mathrm{j}} - y_{\mathrm{j}} \rvert^p}$
Correlation distance	$d(x,y) = 1 - \dfrac{(x-\overline{x})(y-\overline{y})}{\sqrt{(x-\overline{x})\cdot(x-\overline{x})^T}\sqrt{(y-\overline{y})\cdot(y-\overline{y})^T}}$ with $\overline{x} = \frac{1}{n}\sum_{j=1}^{n} x_{\mathrm{j}}$ and $\overline{y} = \frac{1}{n}\sum_{j=1}^{n} y_{\mathrm{j}}$

Table 3.1.: An overview of selected distance measures implemented in Matlab for two vectors $x = (x_1, \ldots, x_n)$ and $y = (y_1, \ldots, y_n)$.

kMeans algorithm

An easy and often used clustering algorithm is the kMeans algorithm [48], which is already implemented in Matlab [49]. The default distance measure is the squared

Euclidean metric. The partition method divides a given data set into k clusters in such a way that the distance between two objects of the same cluster is as short as possible and the distance between two objects of different clusters is as large as possible. This is done by iteratively calculating the cluster centroids (centres) and the distance between the objects and the centroids. The objects are assigned to the centroids, to which the distance is minimal. Then the new centroids are calculated by taking the mean value of all assigned objects. This is done until the centroids do not change anymore or a certain termination criterion is fulfilled.

There are different methods for choosing the initial values for the cluster centroids. The standard kMeans Algorithm by Lloyd [48] uses randomly chosen initial values for the cluster centroids. Since their choice can influence and even alter the result, Arthur and Vassilvitskii [50] proposed a specific way of choosing the seeding points. According to them, the so called kMeans++ algorithm improves the speed and the accuracy of the performance.

Apart from the dependency of the initial centroids, the disadvantages of the kMeans algorithm are the need of a predefined given number of clusters k and the sensitivity to outliers since the mean value is used for the centroid calculation.

Hierarchical clustering

A second method for partitioning, which is implemented in Matlab [51] as well, is the hierarchical clustering. The fundamental principle of this method is to create a cluster tree, also called dendrogram. Therefore, two single data objects which are close to each other are linked and a new object is formed. The so formed clusters are further linked to larger ones. In this way, a binary and hierarchical tree is formed, until all objects are linked to one large cluster. [52]

The real partitioning takes place when the dendrogram is cut into clusters. This can be done either at an arbitrary point to ensure a fixed number of clusters or by taking natural grouping into account. The natural grouping is measured by the inconsistency coefficient, which sets the height of the currently observed link in relation to the height of neighbouring links at lower levels. It is calculated by the difference between the currently observed link height and the mean link height, normalized by the standard deviation. High inconsistency coefficients indicate the linkage of two cluster, which are far apart. Low inconsistency coefficients indicate close clusters. The dendrogram can be partitioned by a threshold for the inconsistency coefficients. This flexibility of the final cluster number is a major advantage of the hierarchical clustering. However, the method is not able to recover from misclassification. [53]

3.3.2. AIT ECGsolver

The AIT ECGsolver is an automatic human ECG signal processing algorithm introduced by Bachler et al. [4] in 2013. It is the basis for the murine ECG analysis algorithm developed in this work and therefore explained in more detail.

An overview is given in Figure 3.2, which serves as guideline for the following explanation.
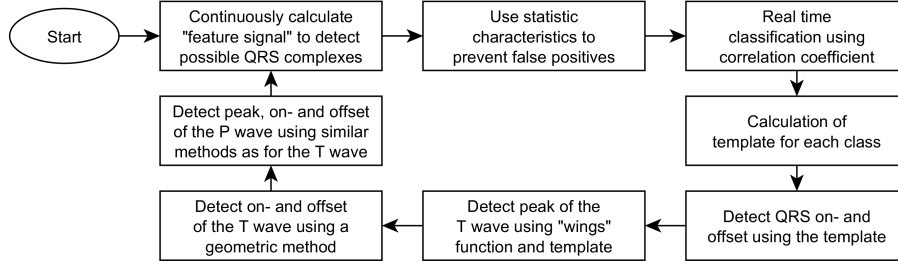
Figure 3.2.: Overview of the processing algorithm AIT ECGsolver. Image taken from [4].

R-peaks

Due to the usually clearly recognizable morphology of the R-peak, a combination of amplitude and first derivative of the signal is compared to a certain threshold. For that, a "feature signal" is continuously calculated in the following way:

- Calculate the first derivative D_t of the signal S_t:

$$D_t = S_t - S_{t-1}. \tag{3.1}$$

- Calculate the amplitude SA_t of S_t and DA_t of D_t within a moving window with $w = 60$ ms:

$$SA_t = max(S_{(t-w)...t}) - min(S_{(t-w)...t}) \tag{3.2}$$
$$DA_t = max(D_{(t-w)...t}) - min(D_{(t-w)...t}). \tag{3.3}$$

- Calculate C_t as a combination of SA_t and DA_t:

$$C_t = SA_t^2 \cdot DA_t \tag{3.4}$$

- Derive the feature signal FS_t within a moving window with $w = 100$ ms:

$$FS_t = max(C_{(t-w)...t}). \tag{3.5}$$

- The threshold is the mean value of the last 2 seconds of FS_t:

$$Th_t = \frac{1}{w} \cdot \sum_{k=t-w}^{t} FS_k. \tag{3.6}$$

If the feature signal exceeds the threshold $FS_t > Th_t$, than the signal part is a possible QRS complex. Statistic characteristics are used to avoid the detection of artefacts.

If all criteria are met, the R-peak is located at the maximum with the highest amplitude to its neighbouring minima.

3. Data and Methods

Template calculation

The R-peaks are classified and assigned to the cluster with the highest correlation. The representative object of each cluster is the template, which is built by averaging the signal parts around the R-peaks within this cluster. The templates reduce the noise in the signal and are used for the detection of all subsequent ECG features.

The method is similar to a kMeans clustering, which is used for the offline version of the algorithm. Although, it should be mentioned that the kMeans algorithm used in the AIT ECGsolver is slightly modified concerning the initial values to make the clustering result reproducible and independent of the initial cluster centroids. For the online version, the procedure is adapted to build the clusters in real time. A newly detected R-peak is compared to the clusters of the already detected R-peaks and classified according to its correlation.

QRS on- and offset

The QRS on- and offset are the preceding and the succeeding points of the R-peak. They are detected using the amplitude and the first derivative of the signal. The QRS-onset is annotated in an interval of 150 ms before the R-peak and with a moving window $w = 30$ ms as follows:

- Calculate amplitude TA_t of the template T_t and TDA_t of its first derivative $T'_t = T_t - T_{t-1}$ within the moving window w:

$$TA_t = max(T_{(t-w)...t}) - min(T_{(t-w)...t}) \tag{3.7}$$
$$TDA_t = max(T'_{(t-w)...t}) - min(T'_{(t-w)...t}) \tag{3.8}$$

- Calculate threshold for TA_t and TDA_t with specified constants c_1 and c_2:

$$TT = c_1 \cdot (max(TA_t) - min(TA_t)) + min(TA_t) \tag{3.9}$$
$$TD = c_2 \cdot (max(TDA_t) - min(TDA_t)) + min(TDA_t) \tag{3.10}$$

- The QRS-onset is annotated at the point nearest to the R-peak, where $TA_t < TT$ and $TDA_t < TD$ is fulfilled.

The annotation of the QRS-offset is performed similar, except for a larger interval after the R-peak and a moving window w twice as long.

T-wave features

The T-peak is the next feature in the ECG signal which is annotated after the QRS-offset. It is detected by using a method introduced by Christov and Simova [37], which is independent of the T-wave polarity and uses special "wings"

functions. Between the last detected QRS-offset and the template end, the "wings" function is calculated with $w = 40$ ms in the following way:

$$W1_\mathrm{t} = T_\mathrm{t-w} - T_\mathrm{t}$$
$$W2_\mathrm{t} = T_\mathrm{t} - T_\mathrm{t+w} \qquad (3.11)$$
$$W_\mathrm{t} = W1_\mathrm{t} \cdot W2_\mathrm{t}$$

Examples for "wings" functions of a positive (A) and a negative (B) T-wave are illustrated in Figure 3.3. In both cases, it can be seen, that the peak of the T-wave corresponds to the minimum of the "wings" function. Thus, the minimum's location is used as starting point for the search in the original signal for a local minimum or maximum, depending on the polarity.
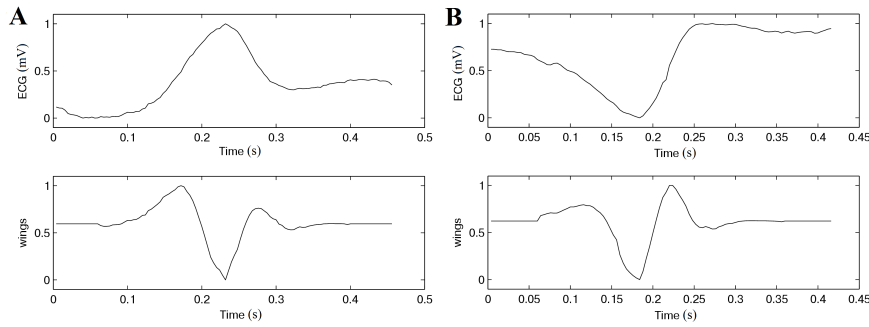
Figure 3.3.: Top: Human T-waves with different polarities: (A) positive T-wave, (B) negative T-wave. Bottom: Their corresponding "wings" function. Image is taken from [4].

A geometric method, which presupposed the annotation of the T-peak and the QRS-offset, is used for T-onset and T-offset detection. It is illustrated in Figure 3.4 for the T-onset detection. For the signal, the connection line g between QRS-offset and T-wave is calculated as well as the longest line n, which is perpendicular to g and intersects g and the signal (see Figure 3.4 A). The intersection point of n with the signal is the location of the wave onset. The calculation of n can be simplified by subtracting g from the signal and finding its minimum (see Figure 3.4 B). The T-offset detection uses the geometric method with a straight line g connecting the T-peak and the end of the template.

P-wave features

The P-wave and the T-wave have a similar morphology. The two main dissimilarities are the lower amplitudes and the strictly positive polarity. Therefore, a slightly adapted "wings" function calculation is used for the P-peak annotation and the geometric method with adjusted observation intervals for the onset and offset detection of the P-wave.
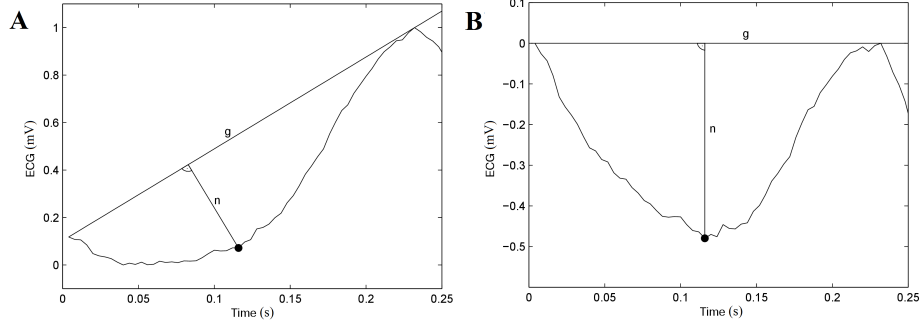
Figure 3.4.: Geometric method to detect the location of the T-onset in a human ECG signal. (A) Original signal with connecting line g between QRS-offset and T-peak and the longest line n perpendicular to g which intersects g and the signal. (B) Simplification by subtracting g from the signal and finding the minimum. Image is taken from [4].

3.3.3. Trapezium Area (TRA) method

The Trapezium's Area (TRA) method, to detect the T-wave end point location of monophasic T-waves, was introduced by Vazquez-Seisdedos et al. [36] in 2011. They proposed their new algorithm as an alternative to the commonly used approach based on thresholding the first derivative. They claim that the TRA method is more robust under noisy conditions and achieves a better accuracy and repeatability than the standard method.

The requirement for the T-wave end detection by the TRA method is the successful detection of the R-peak and the T-peak. It works for both monophasic T-wave polarities, positive and negative, and can be adapted to other wave morphologies, such as biphasic.

As can be seen in Figure 3.5, the approach is based on the calculation of the trapezium's area spanned by three fixed vertices and one moving vertex. The point with the highest absolute derivative after the T-peak is named $(x_\mathrm{m}, y_\mathrm{m})$. The reference point $(x_\mathrm{r}, y_\mathrm{r})$ is beyond the T-offset on the TP isoelectric segment. Between these two points, the vertex $(x_\mathrm{i}, y_\mathrm{i})$ is moving along the signal. At each position of the mobile vertex, the trapezium's area A is calculated:

$$A = 0.5 \cdot (y_\mathrm{m} - y_\mathrm{i}) \cdot (2x_\mathrm{r} - x_\mathrm{i} - x_\mathrm{m}). \tag{3.12}$$

The maximum area is produced for the mobile vertex located at the offset of the T-wave. Thus, the x_i corresponding to the maximum area is identified as the T-wave end point.
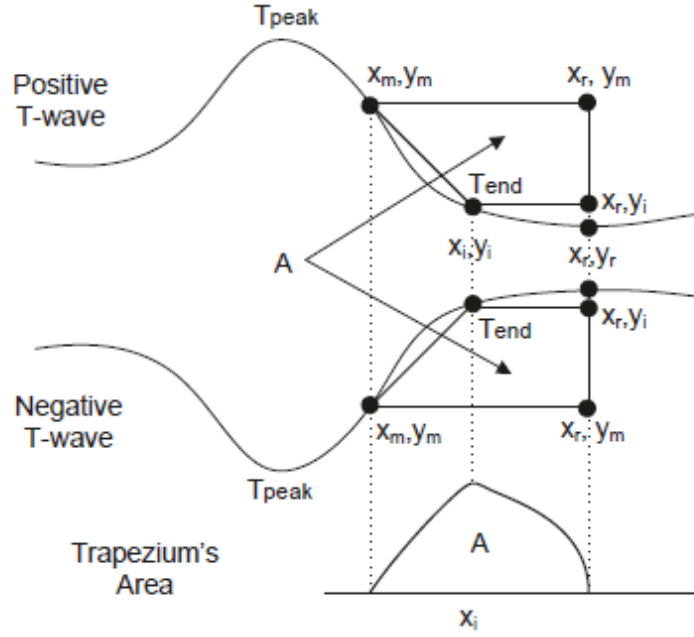
Figure 3.5.: Graphical illustration of T-offset detection with TRA method for monophasic T-waves. The trapezium's area is maximal for the mobile vertex located at the T-wave end point. Image is taken from [36].

3.4. Statistical Methods

The following subsections provide an overview of the used statistical methods and tools to evaluate the murine algorithm results. First, the parameter calculation for the detection rate is explained. Then, the boxplot is described, followed by the Bland-Altman plot. Finally, an overview of the used statistical tests is given.

3.4.1. Detection rate

For two classes of data, the quantitative evaluation between actual and target values includes the identification of the true positive (TP), true negative (TN), false positive (FP) and false negative (FN) predictions. The values can be formulated by means of the 2x2 confusion matrix, also called contingency table, as shown in Table 3.2. The TP and TN correspond to the correct classifications as positive or negative. Is the actual classification negative, but the prediction is positive, then it is counted as FP. It is the type I error of a test, where the result is wrongly positive. A negative prediction, which should be positive according to the ground truth, is counted as FN. The FN is the type II error, where the test wrongly gives a negative decision, although it should have been positive.

	predicted			
		positive	negative	total
actual	positive	TP	FN	pos. ground truth
	negative	FP	TN	neg. ground truth
	total	pos. classified	neg. classified	number of all samples

Table 3.2.: Confusion matrix for a dataset with two classes to evaluate the values for TP, FN, FP, TN.

The values are used to determine two detection rate parameters for the classification. The sensitivity (Se) is the true positive rate:

$$Se = \frac{TP}{TP + FN} \tag{3.13}$$

The positive prediction (Pp) is the precision:

$$Pp = \frac{TP}{TP + FP} \tag{3.14}$$

The sensitivity measures which proportion of actually positive classification is also tested positive. The precision is a measure for how many of the positive classified samples are actually positive.

3.4.2. Boxplot

Normally distributed data is displayed as mean $\pm$ standard deviation (SD). Data which is not normally distributed is displayed as median and interquartile range (IQR). The median of values $(x_i)_{i=1,...,N}$ is defined as the middle element of the (ascending) sorted values and is also called second quartile. The difference between the third (Q_3) and the first (Q_1) quartile is defined as IQR and contains 50 % of the data. The other half of the data is above Q_3 and below Q_1, 25 % on each side. The median and the IQR can be visualised by means of a boxplot. It is a graphical visualisation of data distributions. The data within the IQR range are displayed as a box. Above Q_3 and below Q_1, the box is extended by so called whiskers, which have a length of $1.5 \cdot$ IQR. Outliers are plotted as individual data points. The boxplot of a randomly generated data set is shown in Figure 3.6.
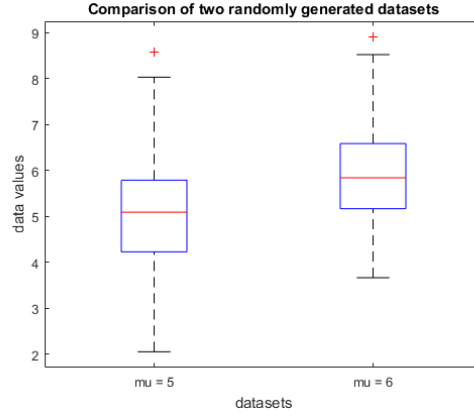
Figure 3.6.: Example for a boxplot based on two randomly generated data sets. The IQR, which is 50 % of the data, is displayed in the blue box. The red line in the box marks the median. The whiskers have a length of $1.5 \cdot$ IQR and outliers are plotted as individual red data points.

3.4.3. Bland-Altman plot

The difference plot introduced by Bland and Altman [54] compares the differences between two methods, such as the results produced by an automatic algorithm and manual labelling. Bland-Altman plots are used to determine the occurrence of systematic errors and trends in the differences. The average of both methods are plotted on the x-axis, the differences on the y-axis:

$$x = \frac{automatic + manual}{2} \tag{3.15}$$

$$y = automatic - manual \tag{3.16}$$

In addition to the data, the arithmetic mean μ of the differences and the boundary of $\mu \pm 1.96\ SD$ are shown by means of dashed lines. Examples for Bland-Altman plots for randomly generated data are shown in Figure 3.7. The data points are normally distributed and rounded to integers. Creating the Bland-Altman plot from values separated by an equidistant gap, the data points build clusters. Due to their overlap, the interpretation becomes more difficult (see Figure 3.7 A). This problem can be solved by adding a small independent random value to all the data points (called jittering). The data points are better visible due to the small disturbance (see Figure 3.7 B).

A good method is characterised by having a mean close to 0 for the differences to the actual values. Furthermore, there should be no correlation between differences and averages, which is called a trend, and the deviation of the mean should be constant and small over the entire range.
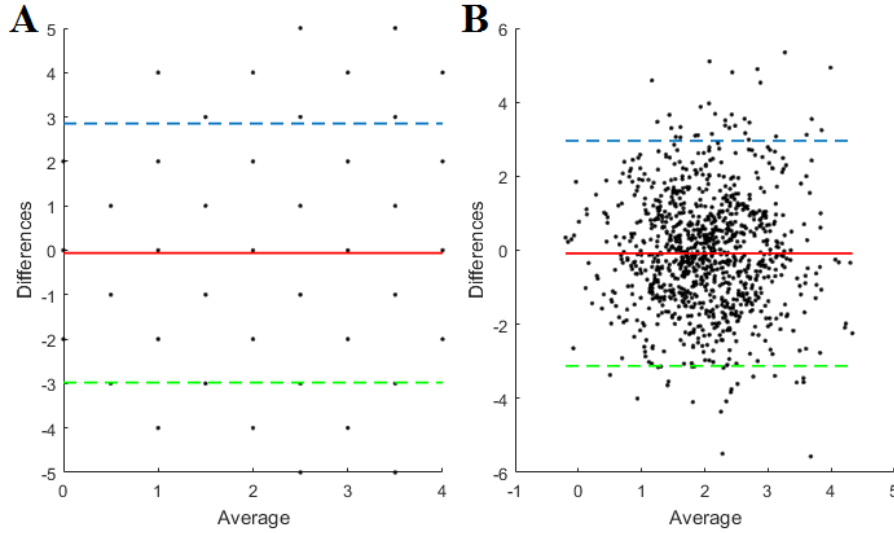
Figure 3.7.: Examples for Bland-Altman plots based on randomly generated data, which is normally distributed. The differences of the data points are plotted against their average with (B) and without (A) jittering. The mean μ (red line) and the boundary of $\mu \pm 1.96\ SD$ (green and blue line) are shown.

3.4.4. Statistical tests

To compare two paired datasets, the paired t-test is used. The requirements for using the test are normal distribution and equal variances for the differences of the data values. The Kolmogorov-Smirnov test is used to test for normal distribution. The equality of variances is tested with a two-sample F-test. Since the requirements are fulfilled for the resulting data in Section 5, no other statistical test have to be used.

The null hypothesis testing for a statistical tests is done with the p-value. It is the probability of receiving a same or more extreme result as in the sample data, under the condition that the null hypothesis is valid. A small p-value corresponds to a high significance. Therefore, the null hypothesis of the statistical test can be rejected, if the p-value is below a predefined level of significance α. If not stated otherwise, α is set to 5% in the Sections 5 and 6. For a p-value below 0.001, the result is considered as highly significant.

Murine ECG analysis algorithm | 4

This chapter provides a detailed description of the algorithm implemented in Matlab for the automatic detection of the ECG components for murine data. The explanation is divided into the signal preprocessing and the feature detection part.

An overview of the algorithm is given in Figure 4.1. The algorithm for human ECG analysis by Bachler et al. [4], which is described in Section 3.3.2, is referred to as "human algorithm".

The first step in the workflow is the signal preprocessing, which is described in more detail in subsection 4.1. The signal is then divided into parts of 5 minutes to stabilise the template generation. The R-peak is clearly recognisable in the ECG signal, due to its high amplitude and steep slope. Thus, the R-peak is the first feature to be detected by the human algorithm. The information about the R-peak's location is used to determine the onset of the QRS-complex again by the human algorithm. Due to the different morphology of a murine ECG signal compared to a human one concerning the J-wave and the T-wave, the QRS-offset and the T-wave features cannot be identified correctly by the human algorithm. Therefore, a new detection algorithm for these features was implemented specialised for mouse ECGs. The developed algorithm and the handling of the J-wave and the T-wave are described in Section 4.2. Afterwards, the P-wave features are detected by means of the annotations of the R-peaks, QRS-onsets, and T-offsets by the human algorithm. The last step in the ECG analysis workflow, which is performed on the whole ECG signal, is the calculation of the ECG intervals PR-, RR-, QRS-, QT-interval and the heart rate corrected QT-interval by Mitchell et al. [23].
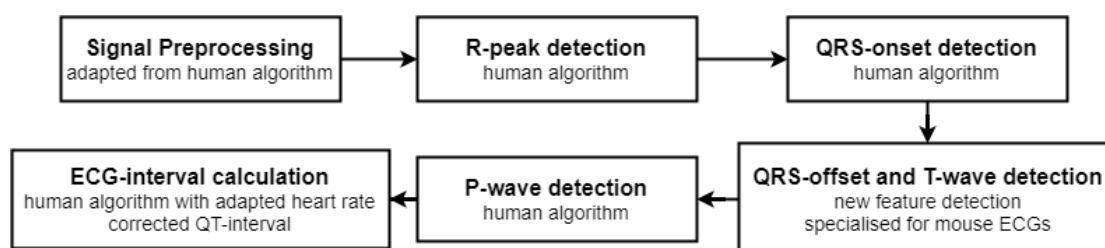
Figure 4.1.: Overview of the processing algorithm for murine ECG signals.

4.1. Signal Preprocessing

Before the ECG features are detected, the signal has to be processed with different filters to reduce artefacts and noise. Furthermore, the sampling rate has to be adjusted when using a human ECG analysis algorithm, due to the different heart rates between humans and mice.

4.1.1. Sampling Rate

The original sampling rate of the recorded murine ECG signals was 1000 Hz. Since the human algorithm was designed to handle ECG signals with human heart rates, many feature annotations are missing or wrong (see Figure 4.2 A). To overcome this problem, the sampling rate used by the algorithm is divided by factor 4.
As already mentioned, the heart rate of mice vary from 180 to 600 beats per minute (bpm) according to [1]. The division leads to heart rates corresponding to humans (45 to 150 bpm). These are values, which can be handled by the used parts of the human algorithm without further adjustments (see Figure 4.2 B). Opposed to Figure 4.2 A, the R-peaks are detected correctly.
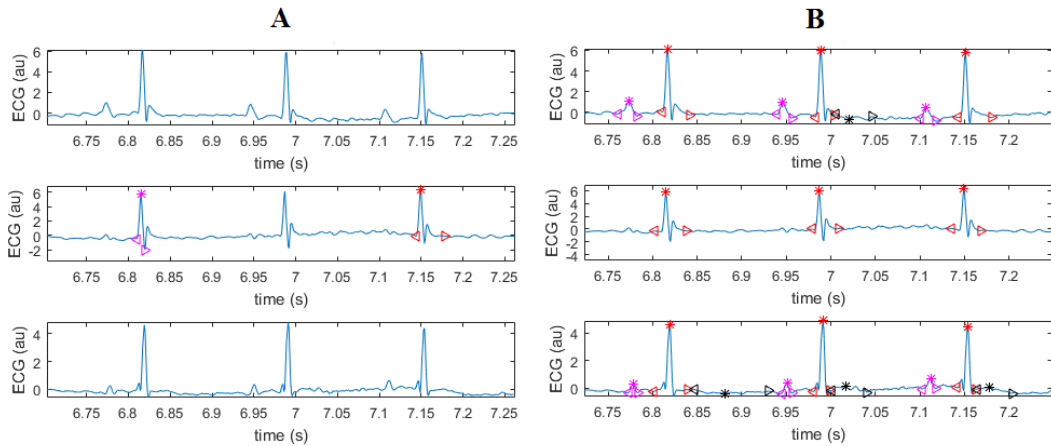
Figure 4.2.: Murine ECG signal analysed by human algorithm without sampling rate correction (A) and with sampling rate divided by factor 4 (B). Red labels correspond to QRS-complex, magenta labels to P-wave features, and black labels to T-wave features.

4.1.2. Filtering

A highpass filter is applied to the murine ECG signal to reduce respiration artefacts. A Butterworth bandpass filter is used for the R-peak detection only. For the other features, the filter is not applied, since sharp edges, which are necessary for accurate feature recognition, are over-smoothed.

4.2. Feature detection

The successful R-peak localisation is a requirement for the detection of the J- and the T-wave. As the workflow in Figure 4.1 shows, the QRS-onset detection is performed before the search for the QRS-offset and the T-wave features as well. This is not necessary and their order could be inverted, since the QRS-offset and the T-wave detection is independent of the QRS-onset location.

As explained in the section about the ECG components, Section 2.2.4, the T-wave morphology differs between humans and mice. Unfortunately, not all signal parts show the behaviour illustrated in Figure 2.7b with a clear distinguishable negative T-wave following the J-wave. An overview of the different existing ECG morphologies of the data set can be found in Appendix A.1. It should be mentioned that although the murine T-wave can have a positive or a negative shape, as stated in Speerschneider and Thomsen [3], the T-wave of the used data set is always negative. Thus, the J-wave is assumed to be positive and the T-wave to be negative for the development of the analysis algorithm. However, since the implemented methods can theoretically handle both monophasic behaviours (positive and negative T-wave), only minor adaptions in the algorithm would be necessary.

Due to the sometimes missing distinguishable T-waves in the ECG signal on the one hand and the missing discrimination between J- and T-wave in the manual annotations of the clinical expert on the other hand, the features of the J- and the T-wave are not annotated separately. The two waves are considered as one combined wave, which is referred to as T-wave in the following. Therefore, the definition of the T-wave features is different to Boukens et al. [17], and Speerschneider and Thomsen [3]. A visualisation of the T-wave feature definition in this thesis is shown in Figure 4.3. The important part of the T-wave is the wave offset, since it is used for the calculation of the QT-interval, which serves as ECG parameter. Depending on the existence of a clearly recognisable T-wave, there are two different definitions of the T-offset. If a negative deflection exists, the point, where the signal returns to the isoelectric line, is identified as the T-offset (see Figure 4.3 A). If the negative part is missing, the offset of the actual J-wave is taken (see Figure 4.3 B). The T-onset is identified as the actual J-onset, which is defined as the point in the middle of the upward slope between the S-wave and the actual J-peak. This point also coincide with the QRS-offset, due to the lack of an ST-segment. The actual J-peak is defined as the T-peak, since it is more prominent than the actual T-peak with its often lower amplitude. The peak is the least important feature for the ECG analysis.
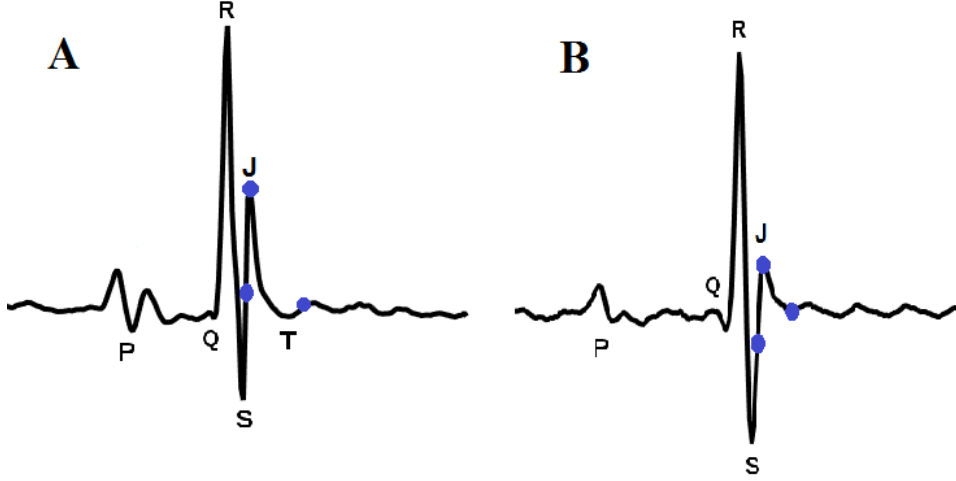
Figure 4.3.: Definition of the T-wave features (marked with blue dots) in the murine algorithm illustrated in two different cluster templates. The T-onset and T-peak are defined as the actual J-onset and the actual J-peak, respectively. The T-offset is either identified as the actual J-offset (A) or the actual T-offset (B), depending on the existence of a clear negative deflected T-wave.

The workflow of the murine algorithm is illustrated in Figure 4.4 and will be explained in detail in the following subsections. Generally, it can be divided into the analysis of a created cluster template and the analysis for each heart beat in the original signal, where the corresponding cluster information is used as reference point.

The 5 minutes long signal is further divided into parts of 10 seconds. This signal division results in a lower number of considered heart beats, which allows a more accurate clustering. To avoid missing annotations at the beginning or the end of a heart beat due to a lack of signal information, the signal after the previous and before the following R-peak are added to the 10 seconds. Both the template and the original signal analysis are performed for these signal sections.
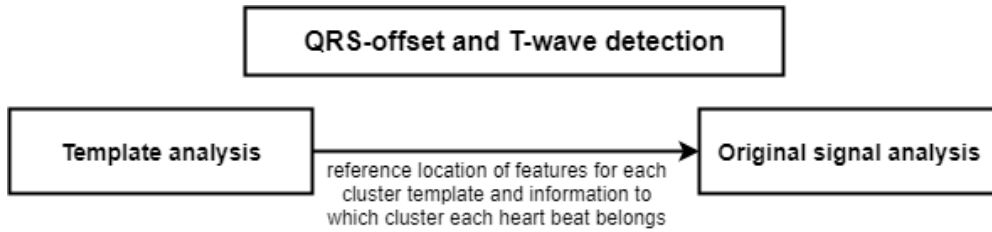
Figure 4.4.: Overview of the new feature detection for murine ECG signals.

4.2.1. Template analysis

The first step in the detection of the QRS-offset and the T-wave features is the creation and analysis of a template. The usage of a template for the identification of ECG features was also used in the human algorithm, since a template contains less noise than the original signal (see Section 3.3.2). As visualised in the workflow of the template analysis in Figure 4.5, three steps were solved by different methods, namely the clustering and the detection of the T-peak and the T-offset.
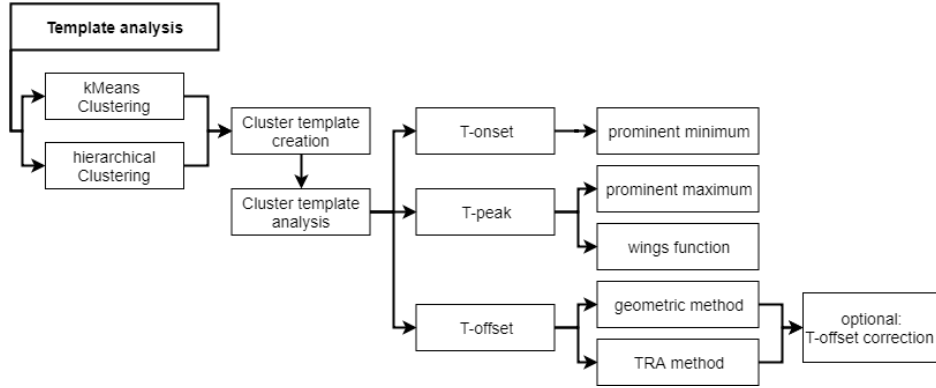
Figure 4.5.: Overview of the workflow for the template analysis.

Clustering

The clustering was one of three tasks, which was solved by different methods to compare their results. Independent of the clustering procedure, the signal information used by the method is limited to 100 ms before and after the R-peaks to ensure the classification according to the shape of the QRS-complex.

The kMeans clustering from the offline human algorithm was taken as first method. The predefined number of clusters was set to 3, the same as for human ECGs. If a certain number of different ECG morphologies is expected, then a fixed number of clusters makes sense. Since this is not the case for the murine ECG analysis, another option is to use a method with a variable cluster number. Thus, the hierarchical clustering was implemented as second clustering method. As described in Section 3.3.1, Matlab provides preimplemented functions for hierarchical clustering. The inconsistency coefficient of each linkage in the dendrogram is calculated. Depending on their quantity, the threshold for cutting the tree into clusters is determined. If there are more than three different inconsistency coefficients, the threshold is chosen just below the second highest value. If there are less, a value just below the highest coefficient is chosen. This decision rule should ensure the building of clusters with a strong enough natural linkage.

Cluster template creation

The procedure of generating the cluster templates is illustrated in Figure 4.6. Based on the cluster assignment of each heart beat in the observed signal part (see Figure 4.6 A), the cluster templates are created (see Figure 4.6 B). A template is calculated by the median of the cluster member's ECG signal (see Figure 4.6 C). Since the information before the R-peaks is irrelevant for the T-wave detection, only the signal parts after the R-peaks are stored as template. For each cluster template, reference points for the QRS-offset and the features of the T-wave are determined, which will be explained in the following subsections.
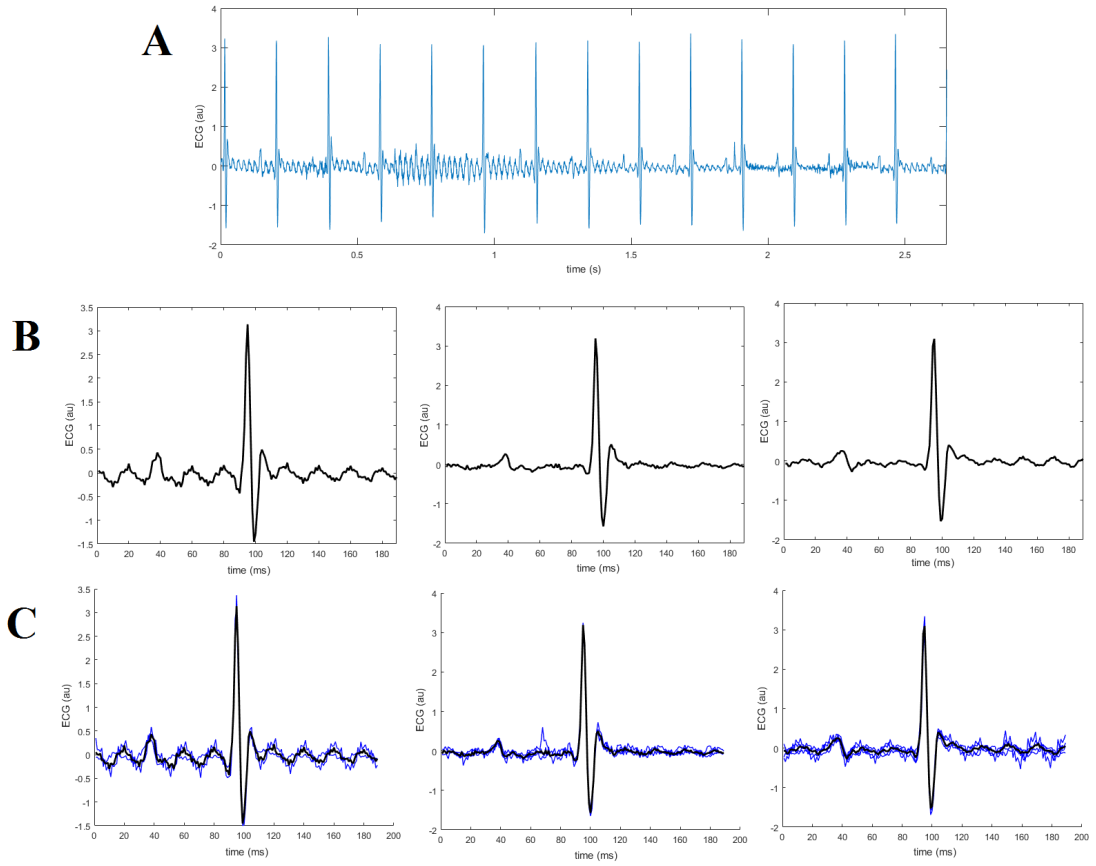
Figure 4.6.: Illustration of the cluster template creation. The heart beats of the observed signal part (A) are grouped into 3 clusters by the kMeans algorithm. Each cluster template (B) consists of the median signal of its cluster members (C).

Cluster template analysis - T-onset

The QRS-offset and the T-onset can be treated simultaneously due to their equivalence. An overview of the steps is given in Figure 4.7. The signal part after the R-peak is examined for a distinctive minimum. The prominence of the minimum, which is the local amplitude with respect to the surrounding extrema, is used as decision feature. A minimum is defined as prominent, if it has the highest prominence and the next highest prominence does not exceed 80% of it. If such a minimum exists, it serves as reference point for the T-onset and the QRS-offset in the template. If the search for a distinctive minimum or the detection of the other features fails, only the QRS-offset is determined by means of the TRA method.
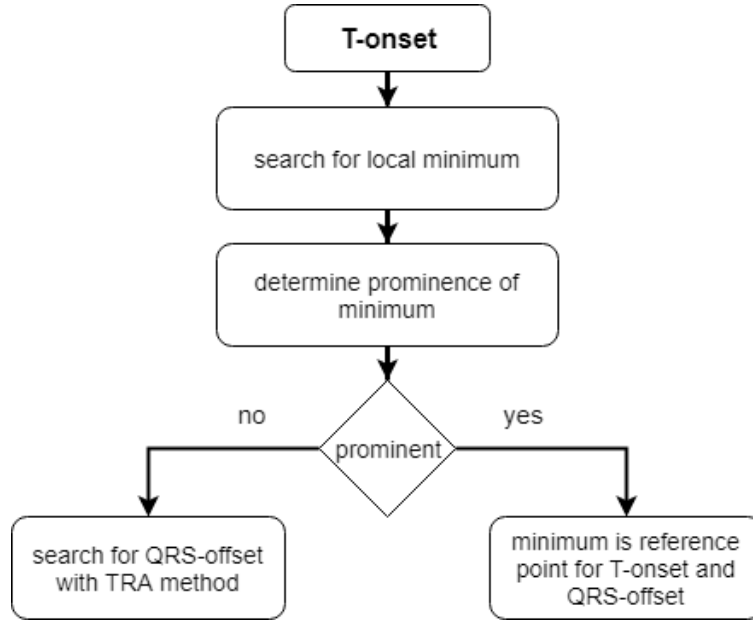
Figure 4.7.: Overview of the search for the T-onset and QRS-offset reference point in the template. The steps are performed for each cluster.

Cluster template analysis - T-peak

The search interval for the T-peak is defined as a 100 ms window after the T-onset reference point. For a missing T-onset, the search for the T-peak is not started. Two different methods are implemented for the feature detection as can be seen in Figure 4.8. The first way of checking for T-peaks is using "wings" functions described by the Equations 3.11 in Section 3.3.2.
The only difference to the human algorithm is the adaptation of the moving window width w from the originally 40 ms to 10 ms. This modification guarantees a more sensitive representation of $W1_t$ and $W2_t$. Otherwise important information would be ignored.
The second possibility uses a similar approach as in the search for the T-onset.

4. Murine ECG analysis algorithm

The search interval is checked for a prominent maximum, which is again defined by the highest prominence. This time, the ratio between second highest prominence and highest prominence must not exceed 90%.
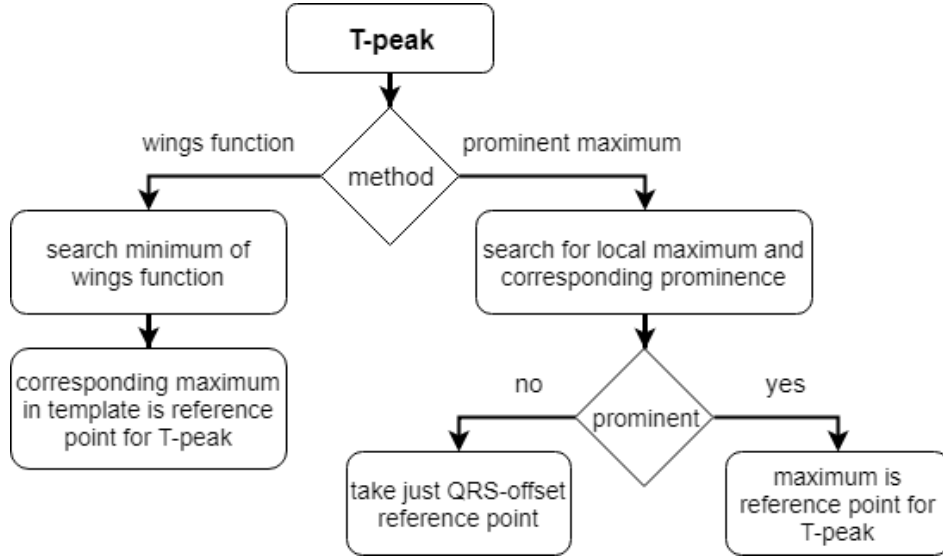
Figure 4.8.: Overview of the search for the T-peak reference point in the template. The steps are performed for each cluster, for which a T-onset is detected.

Cluster template analysis - T-offset

Not only the T-peak annotation can be performed by two different methods. Also for the determination of the offset of the T-wave, two different procedures are implemented (see Figure 4.9). The first possibility is the geometric method described in Section 3.3.2. It is applied to the signal beginning with the T-peak until the template end.

The TRA method, which is described in Section 3.3.3, is the second option to locate the T-offset. The used signal information is limited to the signal part from the T-onset to the template end. The point with the highest derivative x_m is expected at one of the next declining slopes after the T-peak. Since oscillations of the signal between T-wave and P-wave can influence the location of this point and falsely move the offset search to later parts of the signal, the search interval for x_m is restricted to the first half of the signal starting with the T-peak. The reference point x_r beyond the T-offset on the isoelectric segment is identified as the template end. After specifying the vertices of the trapezium, its area is calculated according to Equation 3.12. In contrast to the graphical illustration in Figure 3.5, the area can have more than one maximum. The T-offset reference point is defined as the first local maximum.
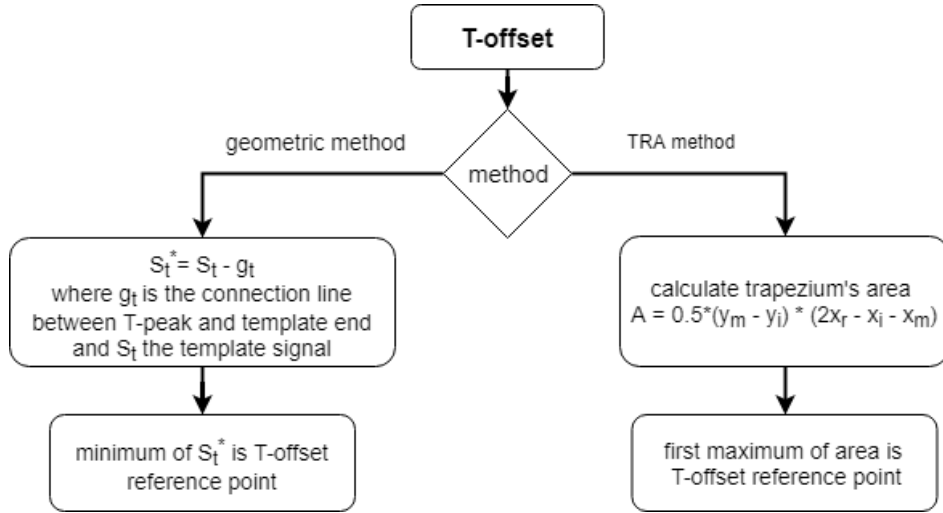
Figure 4.9.: Overview of the search for the T-offset reference point in the template. The steps are performed for each cluster, for which T-onset and -peak are detected.

Regardless of the used procedure, the TRA method is applied and extended to identify the clear distinct negative T-wave deflection. Further properties of the trapezium's area are used to determine a biphasic T-wave morphology. An overview of the T-offset correction is given in Figure 4.10. Three cases, how the signal and the corresponding trapezium's area can look like, are distinguished. In two of them, the T-offset will not be changed.

- **Signal oscillation - no correction**
  The first case is that the biphasic behaviour cannot be detected accurately, because the signal is oscillating after the TRA-detected T-offset. The oscillation is reflected in the corresponding area by more than one prominent maximum. Prominent for the correction step means that the prominence of the maximum exceeds a predefined threshold. To avoid a shifted feature detection, the T-offset is not changed in this case (see Figure 4.11).

- **No negative deflection - no correction**
  In the second case the number of prominent area maxima is limited to one, which means the signal is likely to decline after the T-peak. If the T-offset is located above the baseline or the signal does not show an upward slope after the TRA-detected T-offset, the reference point stays unchanged again (see Figure 4.12).

- **Negative deflection - T-offset correction**
  In the third case there also exist at most one prominent maximum. However, the signal shows the characteristic negative deflection of an actual T-wave.

The T-offset is located in a negative valley, if the baseline exceeds the T-offset and the signal is ascending again afterwards. Upward slopes are reflected in the trapezium's area by a decrease. Thus, if the area falls below a certain threshold, there is a negative deflection after the T-peak. A normalisation of the signal, with the R-peak mapped to 1 and the template end to 0, allows a predefined and fixed threshold. The minimum of the trapezium's area after the previously TRA-detected T-offset is identified as the end of the negative deflection. The corresponding point in the template signal is labelled as corrected T-offset (see Figure 4.13).

This TRA-based correction step for the negative T-wave part is applied independently of the selected T-offset determination method and can also be switched off. Then, the reference point for the T-offset is only based on either the geometric method or the basic TRA method.
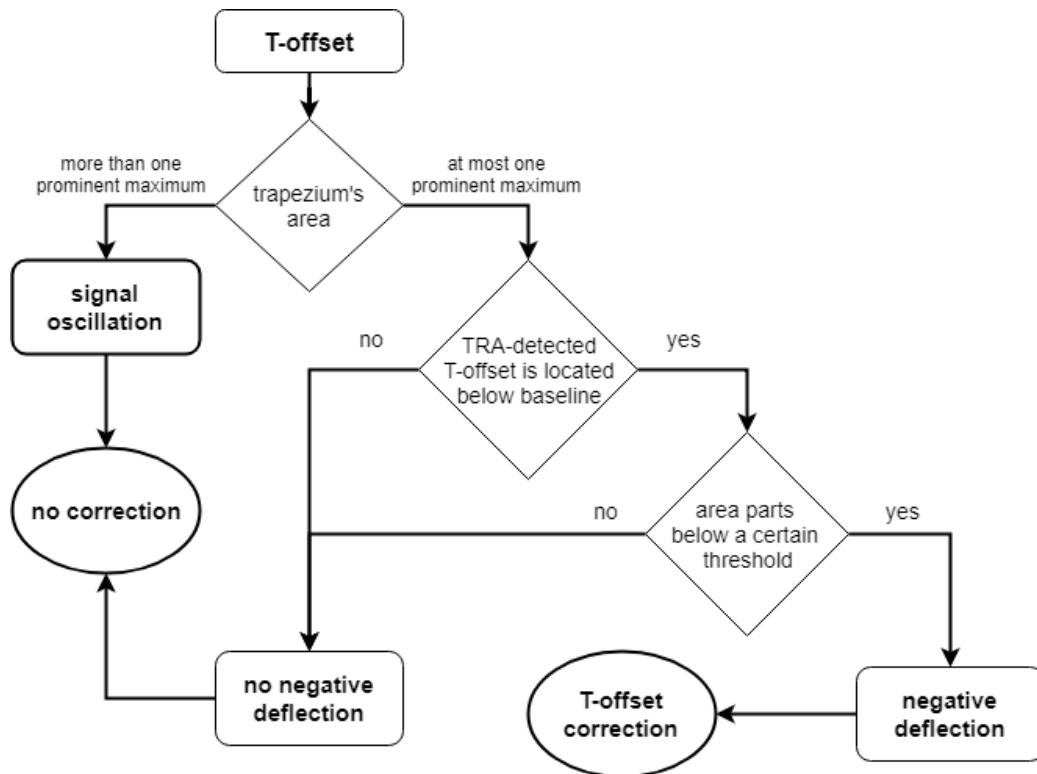
Figure 4.10.: Overview of the T-offset correction step based on the TRA method. This step is optional and can be switched off.
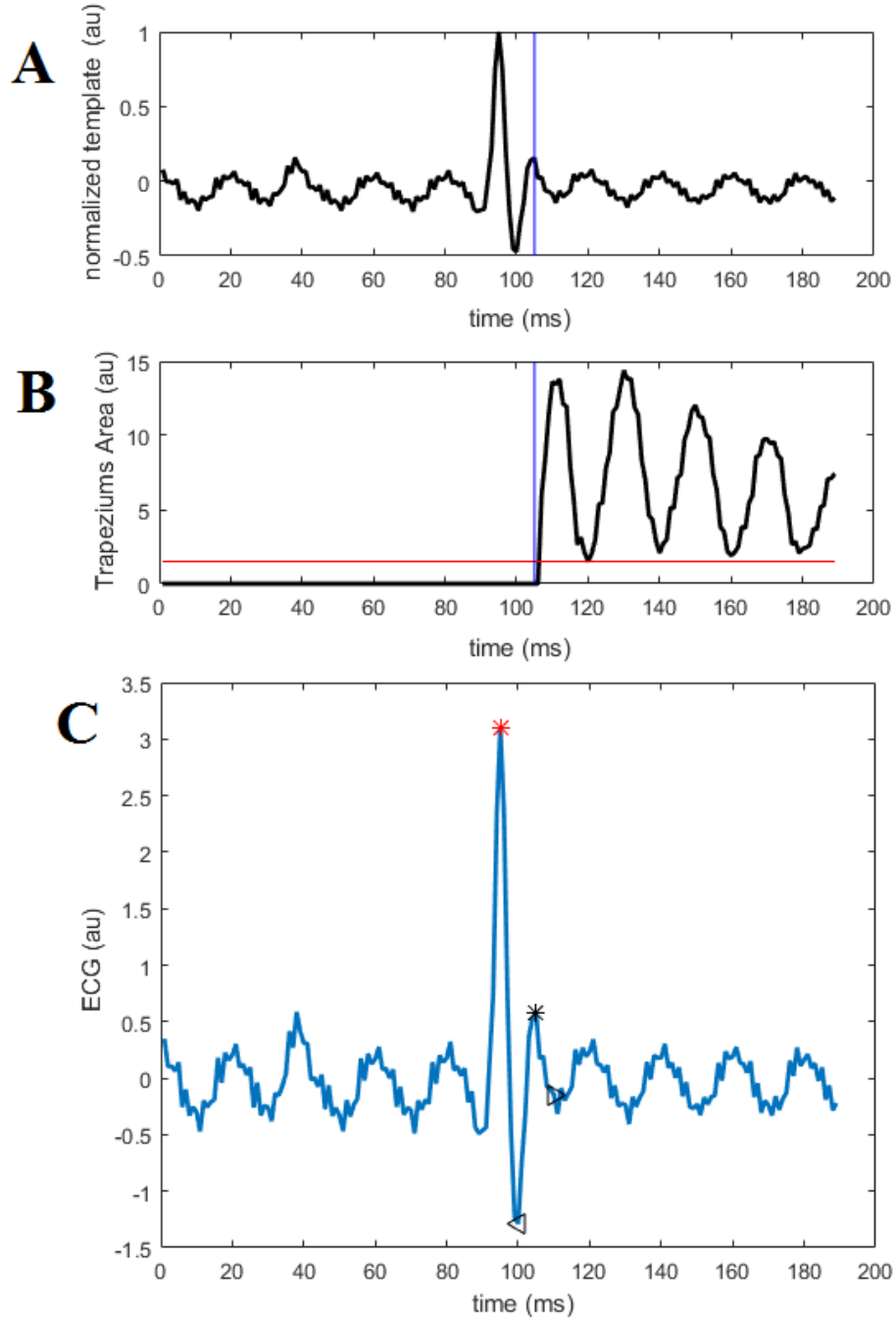
Figure 4.11.: Illustration of an oscillating signal and the corresponding trapezium's area. The cluster template with an oscillating signal after the T-peak (A). The trapezium's area with the threshold (red horizontal line) and the starting point for the area calculation x_m (blue vertical line) (B). The corresponding reference points for the annotations of R-peak (red) and the T-wave features (black) (C).
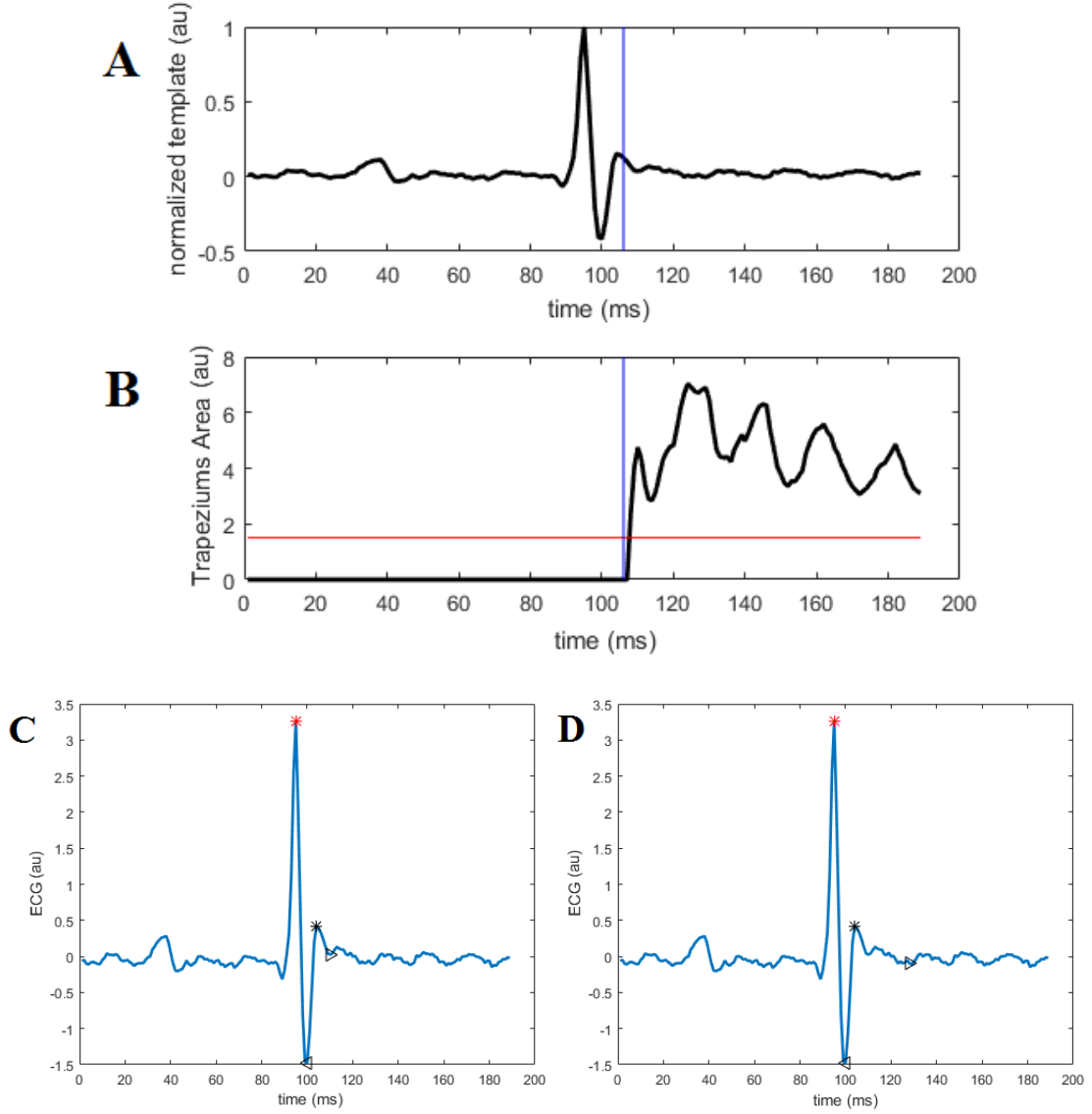
Figure 4.12.: Illustration of a signal without a negative T-wave deflection and the corresponding trapezium's area. Cluster template without a clear negative T-wave deflection (A). Trapezium's area with the threshold (red horizontal line) and the starting point for the area calculation x_m (blue vertical line) (B). Corresponding reference points for the annotations of R-peak (red) and the T-wave features (black) identified by means of the TRA method (C) and the geometric method (D).
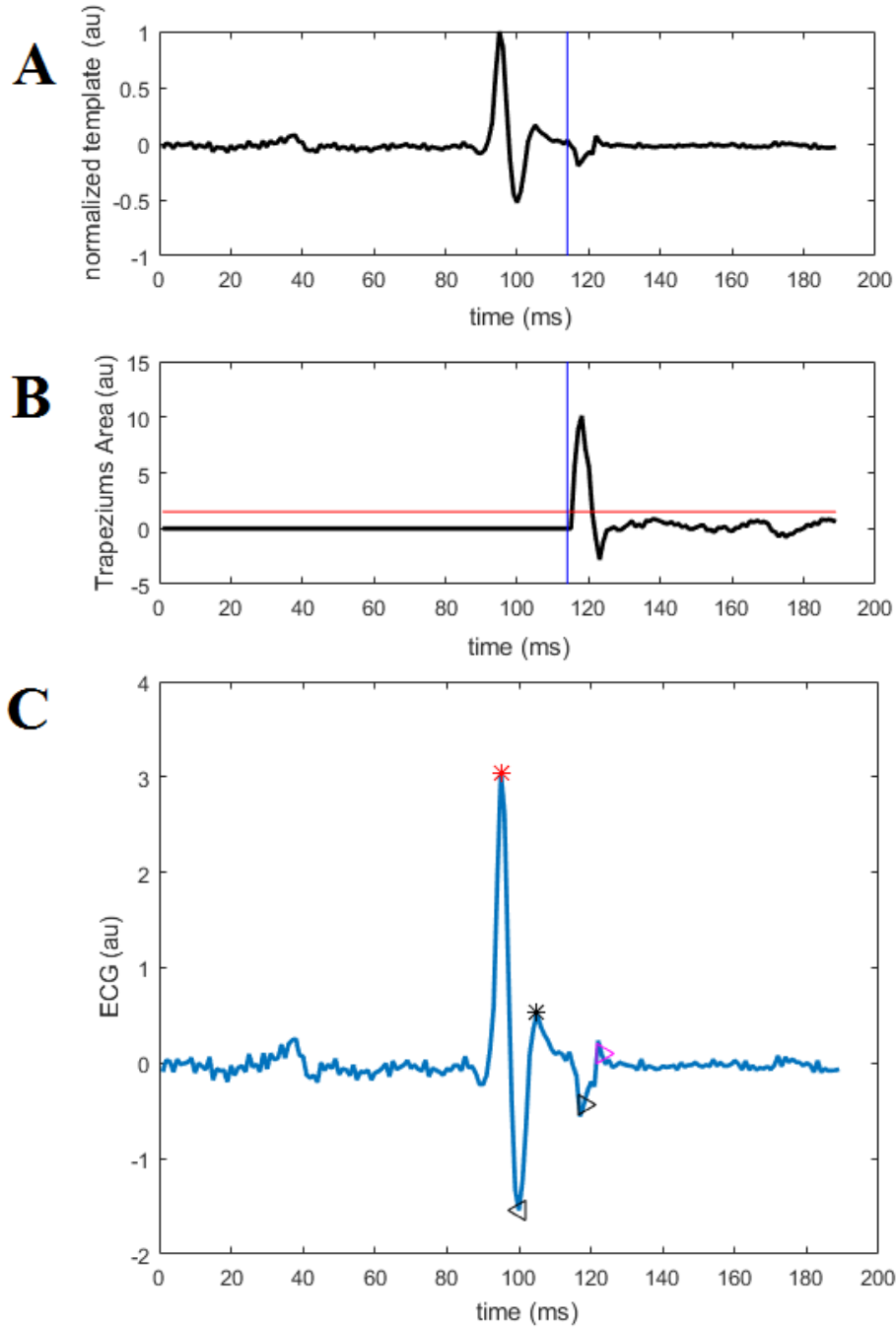
Figure 4.13.: Illustration of a signal with a negative T-wave deflection and the corresponding trapezium's area. The cluster template with a clear negative T-wave deflection (A). The trapezium's area with the threshold (red horizontal line) and the starting point for the area calculation x_m (blue vertical line) (B). The corresponding reference points for the annotations of R-peak (red) and the T-wave features (black) (C). The T-offset is annotated twice, the first label corresponds to the actual J-wave endpoint (black), the second annotation is the corrected T-offset (magenta).

4.2.2. Original signal analysis

The clusters and the corresponding reference points are used for the analysis of each heart beat in the original signal. Depending on the features, some decision rules for the exact location are applied. An overview of the original signal analysis is given in Figure 4.14 and will be explained in the following subsection.
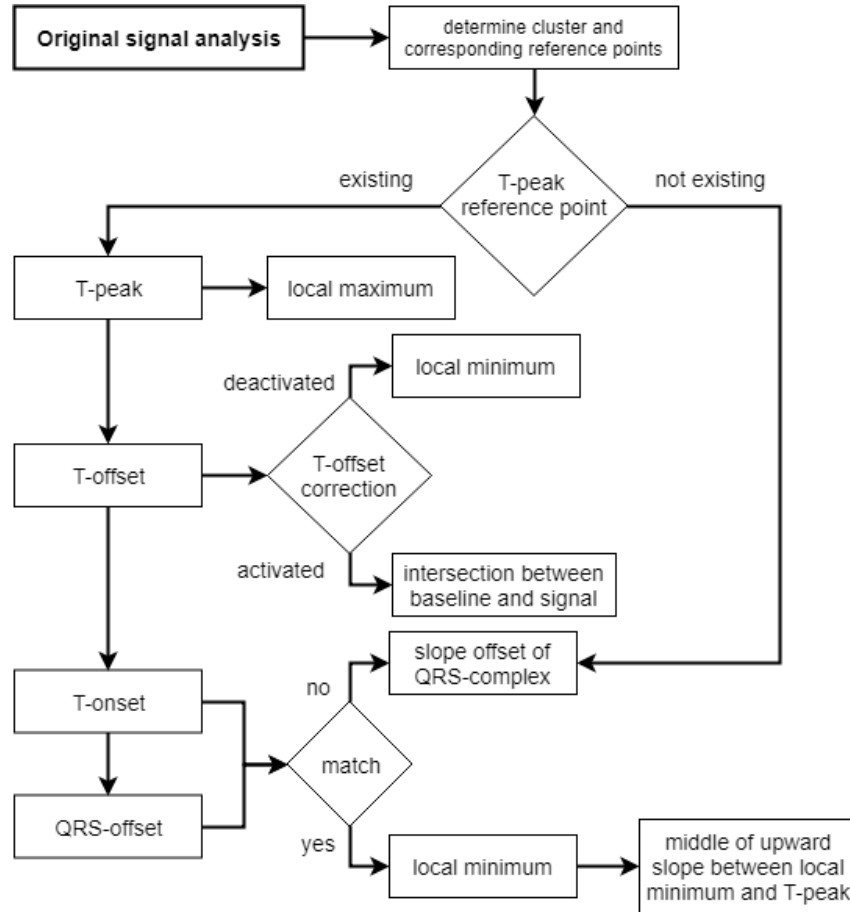
Figure 4.14.: Overview of the workflow for the analysis in the original signal for each heartbeat.

The first feature, which is detected, is the T-peak. Its location is used for the determination of the remaining features. Only if the order of all features makes sense, they are stored. If this is not the case or no reference point for the T-peak exists, it is tried to annotate at least the QRS-offset as the slope offset of the QRS-complex determined by the TRA method.

T-peak

The exact location of the T-peak in the original signal is identified as the local maximum around the reference point given by the cluster template T-peak.

T-offset

The detection of the T-offset depends on the T-wave morphology and the activation of the T-offset correction step. For a T-wave with negative deflection after the actual J-wave and an active T-offset correction, the intersection of the original signal with the baseline is calculated. In this context, the baseline is defined as median of the signal between the actual J-offset to the end of the heart beat signal. The intersection after the previously TRA-detected T-offset at the end of the negative T-wave deflection is identified as the corrected T-offset. Otherwise, the closest local minimum of the reference point determined by either the geometric method or the basic TRA method is annotated as T-offset.

T-onset

The T-onset is located in the middle of the upward slope between the minimum following the QRS-complex and the T-peak. First, the search for the closest local minimum around its cluster reference point locates the negative deflection after the QRS-complex. Then, there are two ways of getting the exact location in the upward slope. The first way is defining the middle point of the upward slope between the local minimum and the T-peak as T-onset. Another possible option is the calculation of the intersection point of the baseline with the original signal, which is not implemented.

QRS-offset

There are two possibilities for the reference point of the QRS-offset. It can coincide with the cluster T-onset, then the location of QRS-offset and T-onset matches. Or it can be determined by searching the slope offset of the QRS-complex, then the closest local minimum is identified as QRS-offset. This is also the case, if no other reference point was found in the cluster template. Then, only the QRS-offset is annotated in the new feature detection.

Results | 5

Chapter 5 contains the results of the verification for all 26 ECG signals and the comparison of ECG data before and after medical treatment. The ECG feature annotations and the calculated ECG intervals produced by the different versions of the automatic ECG analysis algorithm are compared to the manual annotations, which are explained in Section 3.2. The applied statistical methods are introduced in Section 3.4.

As mentioned in Section 4.2, there are three task which are solved by two different implemented methods. Building all possible combinations results in $2^3 = 8$ different algorithm versions. They are indicated by a three-digit code which is explained in Table 5.1. The first digit is 0 for using the kMeans clustering and 1 for using the hierarchical clustering. The second digit is 0 for using the prominent maximum approach to determine the T-peak and 1 for applying the wings function method. The third digit is 0 for the geometric T-offset determination and 1 for the T-offset annotation by means of the TRA method. The option of T-offset correction in the murine algorithm is turned off (see Section 6.1.3).

	1st digit		2nd digit		3rd digit	
Task:	Clustering		T-peak determination		T-offset determination	
Code:	0	1	0	1	0	1
Method:	kMeans	hierarchical clustering	prominent maximum	wings function	geometric	TRA

Table 5.1.: The three-digit code for the 8 different versions of the algorithm. Each digit (0 or 1) represents a task in the algorithm pipeline.

The annotations generated by an algorithm are called "automatic". For the human algorithm they are referred to as "human", for the murine algorithm as "mouse" or "murine" annotations. The manually labelled annotations are referred to as "manual" annotations.

5.1. Automatic vs manual results

The manual results are compared to the detections produced by the automatic murine ECG analysis algorithm and the human ECG analysis algorithm based on

the AIT ECGSolver [4]. To allow a comparison to the murine results, the sampling rate correction step described in Section 4.1.1 and the same filtering methods described in Section 4.1.2 are performed before using the human algorithm.

First, the annotations of the ECG features R-peak, QRS-onset, QRS-offset, T-peak, T-onset, T-offset, P-peak, P-onset and P-offset are studied. Then, the calculated ECG intervals, i.e. the RR-interval, the PQ-interval, the QRS-interval, the QT-intervals, and the QT_C-interval, are analysed.

5.1.1. ECG feature annotations

In this section, the results produced by the human algorithm and the 8 different versions of the murine algorithm are considered separately. First the human annotations are compared to the manual labelling, followed by the comparison between murine and manual annotations.

An automatic annotation is counted as correct (TP), if it exists together with its manual counterpart in the corresponding heart beat. In this comparison, no consideration is given to how far apart they are from each other. FP annotations are classified by a missing labelling in the manual annotations and an existing one in the automatic set. The class of FN is characterised by a missing automatic and an existing manual annotation. There are two reasons for preferring this all-or-none principle for the TP definition over using only automatic annotations, which are within a predefined interval around their target values. On the one hand, all automatic annotations should be analysed, since they are the final result of the algorithm. And on the other hand, it allows an unaltered analysis of the differences between the actual and the target annotations. The arbitrary definition of an interval boundary for correct annotations would influence the statistical parameters and decrease the actual values for the differences. Therefore, not only the sensitivity and positive prediction values are used to analyse the algorithm performance, but also the differences are an important parameter.

Human algorithm

The values for TP, FP, FN, sensitivity and positive predictive for the human algorithm are displayed in Table 5.2 for each ECG feature and in total. Furthermore, the table contains the median difference and the corresponding IQR in ms for each feature. The sensitivity for R-peak, QRS-onset and QRS-offset is 98.52 %, the positive prediction is 97.86 % for R-peak and QRS-onset and 97.8 % for QRS-offset. The average values for the T-features for sensitivity and positive prediction are 55.86 % and 95.94 %, for the P-features they are 72.8 % and 82.17 %. The values for the differences reveal a delay of 14 to 60 ms for the QRS-offset and the T-feature annotations. For the R-peak, the QRS-onset and the P-features, the median is in the range of -2 to 0 ms and the IQR is at most [-4,1]. The differences between the human algorithm and the manual annotations for each feature are shown in a boxplot in Figure 5.1.

Features	TP	FP	FN	Se [%]	Pp [%]	Differences (ms)
all features	24817	2101	16691	59.79	92.19	
R-peak	4796	105	72	98.52	97.86	0 [0,0]
QRS-onset	4796	105	72	98.52	97.86	-2 [-4,0]
QRS-offset	4793	108	72	98.52	97.8	14 [9,17]
T-peak	1458	101	3352	30.31	93.52	38 [28,52]
T-onset	1059	24	3750	22.02	97.78	26 [19,34]
T-offset	1458	101	3353	30.31	93.52	60 [48,75]
P-peak	2153	519	2006	51.77	80.58	0 [0,0]
P-onset	2153	519	2006	51.77	80.58	0 [-2,1]
P-offset	2151	519	2008	51.72	80.56	-1 [-3,1]

Table 5.2.: Performance values of all ECG features detected by the human algorithm compared to the manual annotations.
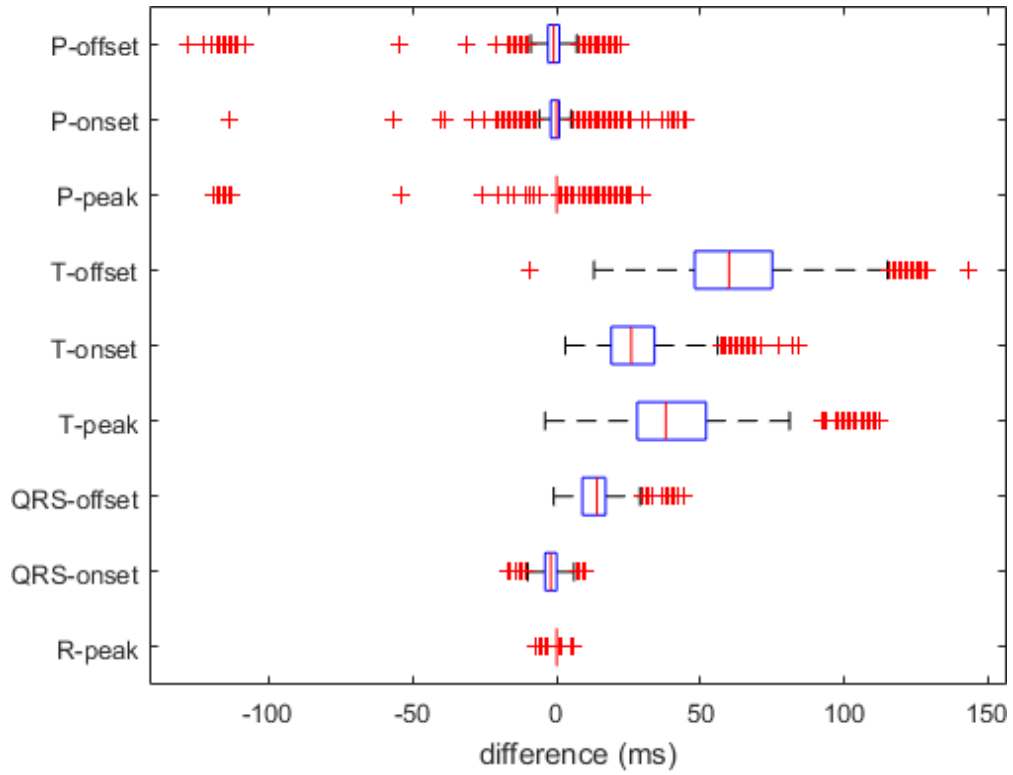
Figure 5.1.: Boxplot of the differences (ms) between the annotations determined by the human algorithm and the manual annotations for all ECG features.

5. Results

Murine algorithm

The 8 different existing murine algorithm versions are compared in Table 5.3 considering the overall values for TP, FP, FN, sensitivity and positive prediction. The version 110 has the highest sensitivity with 96.1 %, followed by version 111 with 95.94 %, version 010 with 95.65 % and version 011 95.61 %. The remaining versions have a sensitivity below 95.5 %. Comparing the positive prediction values, version 000 is the best with 94.18 %, followed by version 100 with 94.08 % and 010 with 94.07 %. The other versions have values below 94.0 %.

Versions	TP	FP	FN	Se [%]	Pp [%]
000	39534	2442	1974	95.24	94.18
001	39486	2888	2022	95.13	93.18
010	39704	2502	1804	95.65	94.07
011	39686	2972	1822	95.61	93.03
100	39576	2490	1932	95.35	94.08
101	39615	2901	1893	95.44	93.18
110	39890	2634	1618	96.1	93.81
111	39821	2994	1687	95.94	93.01

Table 5.3.: Comparison of sensitivity and precision between the results of the 8 different murine versions and the manual annotations for all features.

Taking a closer look at the values for the single features reveals the composition of the total values (see Tables 5.4 and 5.5, Appendix 5.3). The values for the R-peak and the QRS-onset are the same for all automatic algorithms. Thus, they are only shown once in Table 5.2. The values for the QRS-offset are at least in the same range. The differences to the target values are decreased by the murine algorithm from 14 ms for the human algorithm to 0 ms. In the most cases, the number of FN annotations is higher for features of the T-wave than for the P-wave. For the FP values, the relation is reversed with a higher contribution of the P-features to the overall FP number. For most of the versions using the geometric T-offset detection method (3rd digit is 0), the values for sensitivity and positive prediction for the P-features are higher than for their TRA-using counterpart (3rd digit is 1). Since the remaining values are the same, the versions with the geometric method have overall higher values for those two parameters. The only exception is the version pair 100 and 101. For these two, the sensitivity of the P-features is higher for version 101. However, the differences in the T-offset annotations are lower for versions using the TRA-method, which is reflected in the boxplot of the T-offset differences for all version in Figure 5.2 A. A small difference can also be recognised for the P-onset differences (see Figure 5.2 B). Apart from the two features, no other significant differences between the versions can be recognised.
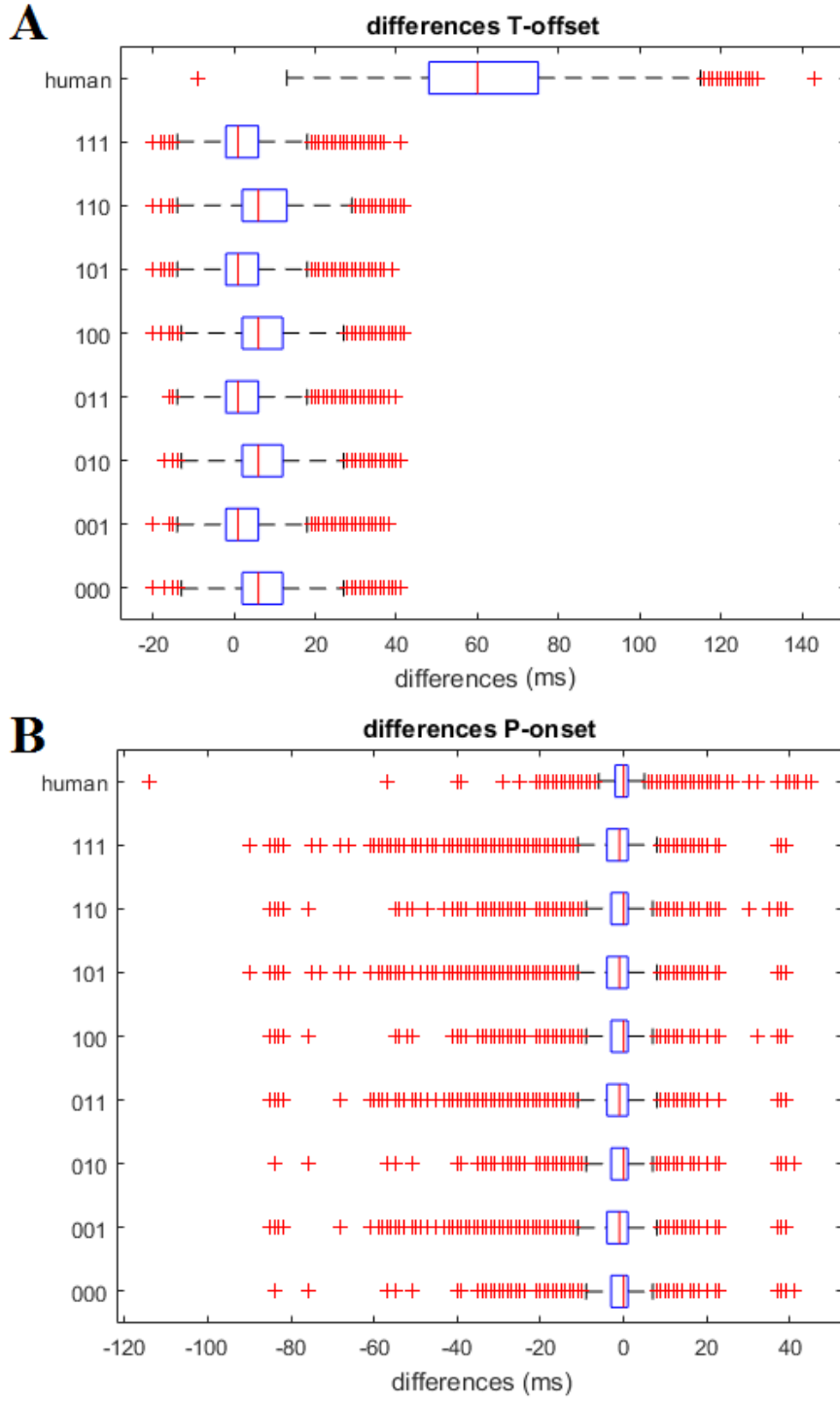
Figure 5.2.: Boxplot of the T-offset (A) and P-onset (B) differences (ms) between predicted locations and their target values for all versions including the human algorithm.

5. Results

The following Tables 5.4 and 5.5 contain the performance values of each feature for the algorithm versions 100 and 101. Version 101 was chosen as example, because it is the default setting of the algorithm, as will be explained in Section 6.1.5. The second example, Version 100, represents the counterpart of version 101 regarding the T-offset detection method. As mentioned earlier, the main difference between the two methods is the T-offset difference. The median difference for version 100 is 6 ms, for version 101 it is 1 ms. The information about all the versions can be found in the Appendix A.2.1. There are also boxplots for each version that represent the differences between the predicted and the target values.

The detected features of version 100 and 101 compared to the manual annotations are shown in Figure 5.3 A and B. In 5.4, the human and the manual annotations are shown together for the same example.

Features	TP	FP	FN	Se [%]	Pp [%]	Differences (ms)
QRS-offset	4793	108	72	98.52	97.8	0 [0,1]
T-peak	4485	127	325	93.24	97.25	0 [0,0]
T-onset	4484	128	325	93.24	97.22	0 [-1,1]
T-offset	4486	126	325	93.24	97.27	6 [2,12]
P-peak	3912	597	247	94.06	86.76	0 [0,0]
P-onset	3911	597	248	94.04	86.76	0 [-3,1]
P-offset	3912	597	247	94.06	86.76	-1 [-4,0]

Table 5.4.: Performance values of all ECG features detected by the murine algorithm version 100 compared to the manual annotations.

Features	TP	FP	FN	Se [%]	Pp [%]	Differences (ms)
QRS-offset	4793	108	72	98.52	97.8	0 [0,1]
T-peak	4485	127	325	93.24	97.25	0 [0,0]
T-onset	4484	128	325	93.24	97.22	0 [-1,1]
T-offset	4486	126	325	93.24	97.27	1 [-2,6]
P-peak	3925	734	234	94.37	84.25	0 [0,0]
P-onset	3924	734	235	94.35	84.24	-1 [-4,1]
P-offset	3925	734	234	94.37	84.25	-1 [-4,0]

Table 5.5.: Performance values of all ECG features detected by the murine algorithm version 101 compared to the manual annotations.

54
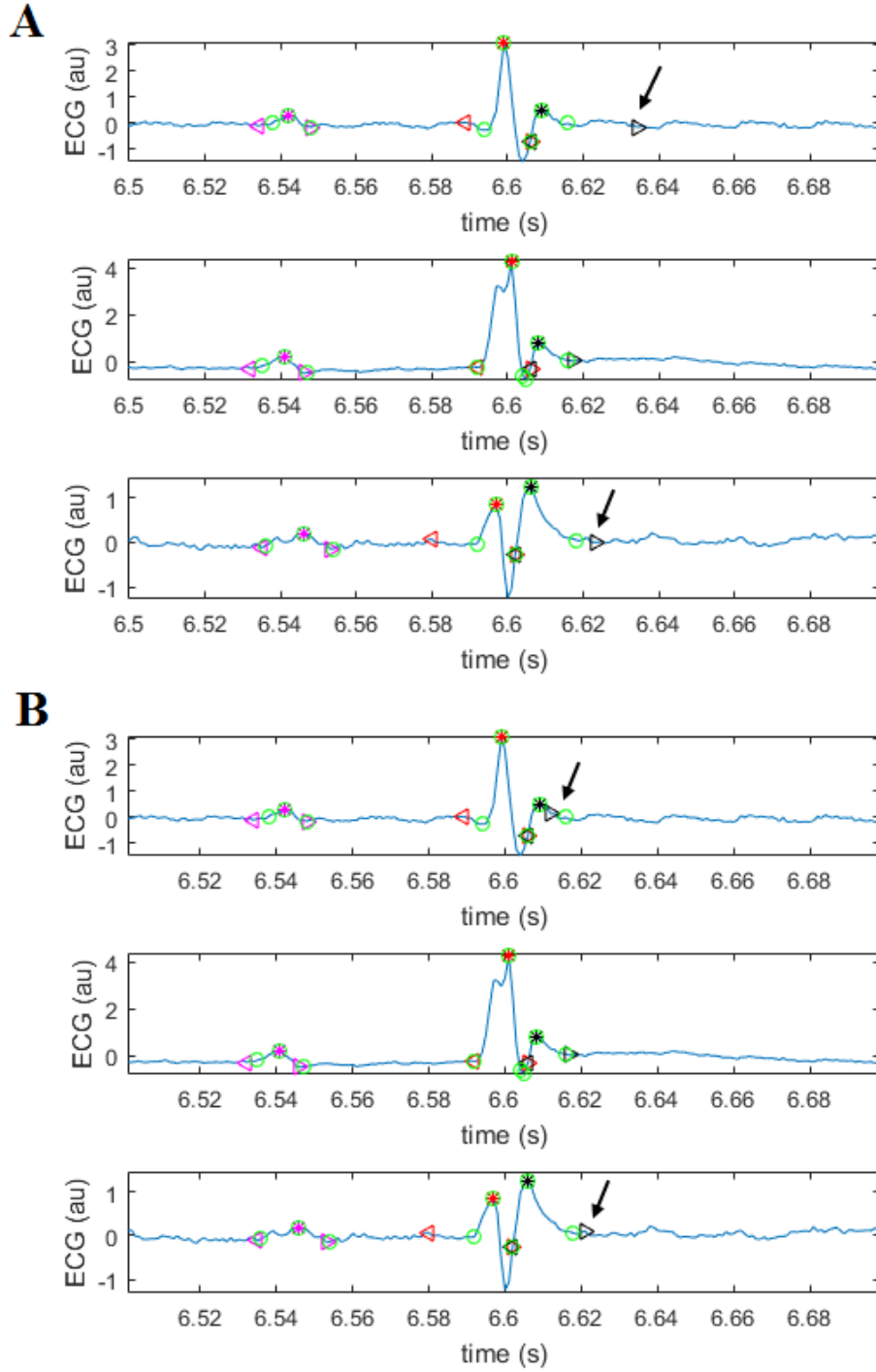
Figure 5.3.: Murine ECG signal analysed by the murine algorithm version 100 (A) and version 101 (B). Red coloured labels correspond to QRS-complex, magenta to P-wave features, and black to T-wave features. The asterisk stands for wave peaks, the right- and left-pointing triangles for beginning and endpoint. The green circles mark the actual locations according to the manual labelling. The main differences are marked with black arrows.
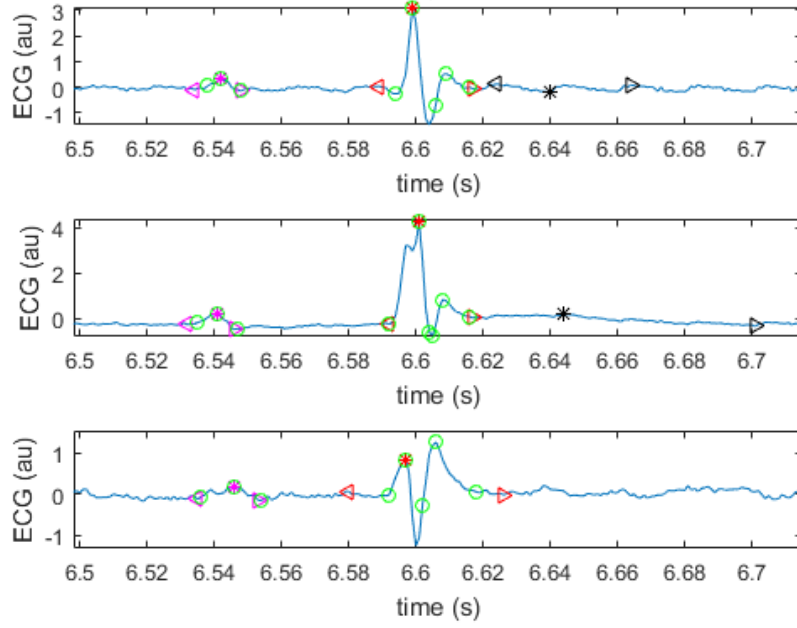
Figure 5.4.: Murine ECG signal analysed by the human algorithm. Red coloured labels correspond to QRS-complex, magenta to P-wave features, and black to T-wave features. The asterisk stands for wave peaks, the right- and left-pointing triangles for beginning and endpoint. The green circles mark the actual locations according to the manual labelling.

5.1.2. ECG intervals

The ECG intervals are calculated automatically based on the ECG feature annotations. The RR-, the PQ-, the QRS-, the QT-intervals, and the QT_C-intervals are determined by the same calculation algorithm independent of the annotation extraction. It should be mentioned that the duration of the computed RR-interval is limited to the interval between 100 and 330 ms, which corresponds to a heart rate between 180 and 600 bpm. For the QT_C-interval, the heart rate corrected formula by Mitchell [23] is used.

The median and the IQR for all calculated ECG interval durations based on the manual and all automatic algorithms are listed in Table 5.6. The ECG interval durations based on the annotations produced by the manual labelling and the automatic algorithm versions human, 101 and 100 are shown in the boxplots in Figure 5.5. The boxplots containing all versions are provided in the Appendix A.2.2. Due to the identical R-peak detection in all the automatic algorithms, the Bland-Altman plot for the RR-interval is only plotted for the human algorithm in

Figure 5.6. The Bland-Altman plots for the QRS-, the PQ-, and the QT-interval of human, version 100 and version 101 are given in the Figures 5.8 - 5.9.

The median duration for the manual RR-interval is 162 ms, for the QRS-complex 11 ms and for the PQ-interval 41 ms. For the QT-interval the median value of the duration is 21 ms, for the heart rate corrected QT_C-interval it is 16.6 ms.

For the automatic algorithms, the RR-intervals do not show any differences to the manual results. This can also be observed in the corresponding boxplot (see Figure 5.5 A) and in the Bland-Altman plot, where the data points are located within a compact band around 0 ms (see Figure 5.6). The PQ-interval is also assessed quite good. The medians of all versions are the same, just the IQRs differ by a maximum of 3 ms. The point cloud in the Bland-Altman plots (see Figure 5.7) is centered around 0 ms. The QRS- and the QT-interval are generally overestimated, independent of the automatic algorithm version. The Bland-Altman plots of both intervals show also a trend towards overestimation for larger interval averages (see Figures 5.8 and 5.9). However, it is noticeable that the QT-interval is generally overestimated more than the QRS-interval. In the plots for the QT-interval, the differences between the two murine versions are recognisable. The point cloud for version 100 is shifted towards the positive difference values more than for version 101. Furthermore, the data points of version 100 show a second smaller cluster in the right upper corner. This qualitative behaviour can also be observed for other pairs of versions, which differ only in the T-offset detection method. Thus, the overestimation of the QT- and also the QT_C-interval is worse for versions with the geometric T-offset detection. The comparison to the human algorithm shows an improvement in the overestimation for both the QRS- and the QT-interval.

Version	RR (ms)	QRS (ms)	PQ (ms)	QT (ms)	QT_C (ms)
manual	162 [151,179]	11 [9,12]	41 [39,45]	21 [19,24]	16.6 [15,18.5]
000	162 [151,179]	13 [11,17]	41 [37,47]	30 [25,38]	23.2 [19.5,28.5]
001	162 [151,179]	13 [11,17]	41 [37,47]	25 [21,31]	19.6 [16.3,23.4]
010	162 [151,179]	13 [11,17]	41 [37,47]	30 [25,38]	23.2 [19.6,29]
011	162 [151,179]	13 [11,17]	41 [37,47]	25 [21,31]	19.6 [16.4,23.5]
100	162 [151,179]	13 [11,17]	41 [37,47]	30 [25,38]	23.2 [19.6,28.6]
101	162 [151,179]	13 [11,17]	41 [37,47]	25 [21,30]	19.5 [16.3,23.1]
110	162 [151,179]	13 [11,17]	41 [37,47]	30 [25,39]	23.3 [19.7,29.1]
111	162 [151,179]	13 [11,17]	41 [37,47]	25 [21,30]	19.5 [16.3,23.3]
human	162 [151,179]	26 [22,30]	41 [36,47]	82 [69,99]	65.4 [56.7,78.2]

Table 5.6.: Comparison of the ECG interval durations [ms] based on the annotations produced by all the automatic algorithms and the manual labelling.
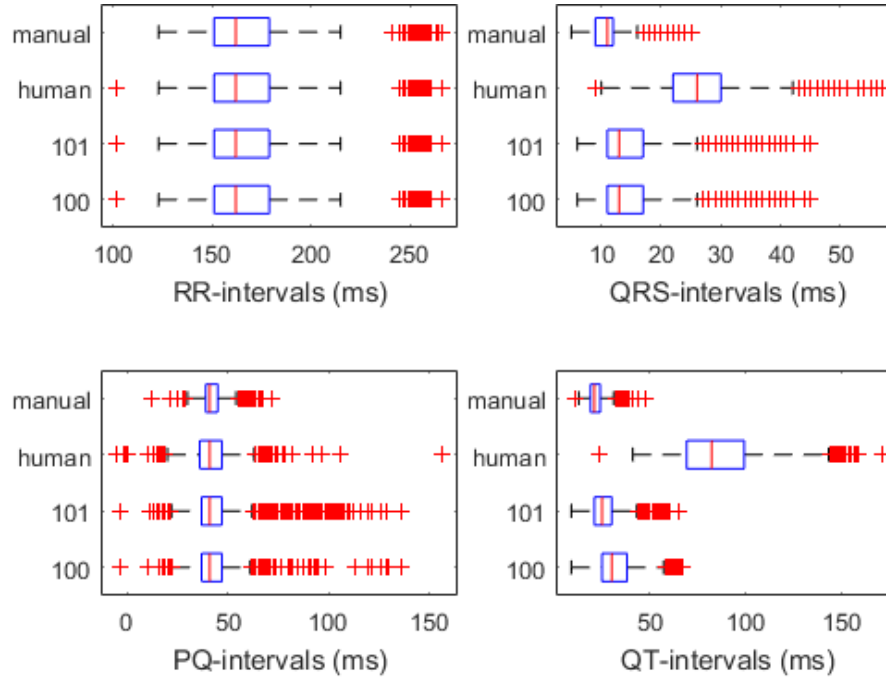
Figure 5.5.: Boxplots of the ECG interval durations (ms) based on the annotations produced by the manual labelling and the automatic algorithm versions human, 101 and 100.
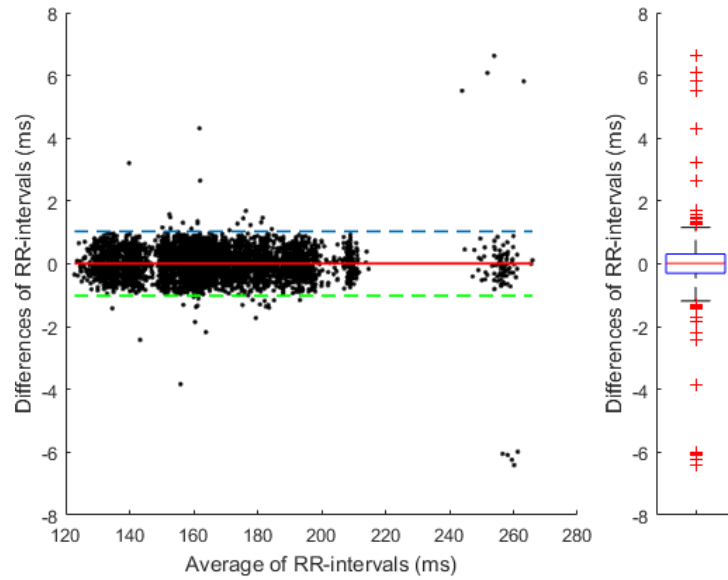
Figure 5.6.: Bland-Altman plot and boxplot of the PQ-interval differences (ms) for the algorithm version human. The plots for the other murine algorithm versions look the same.
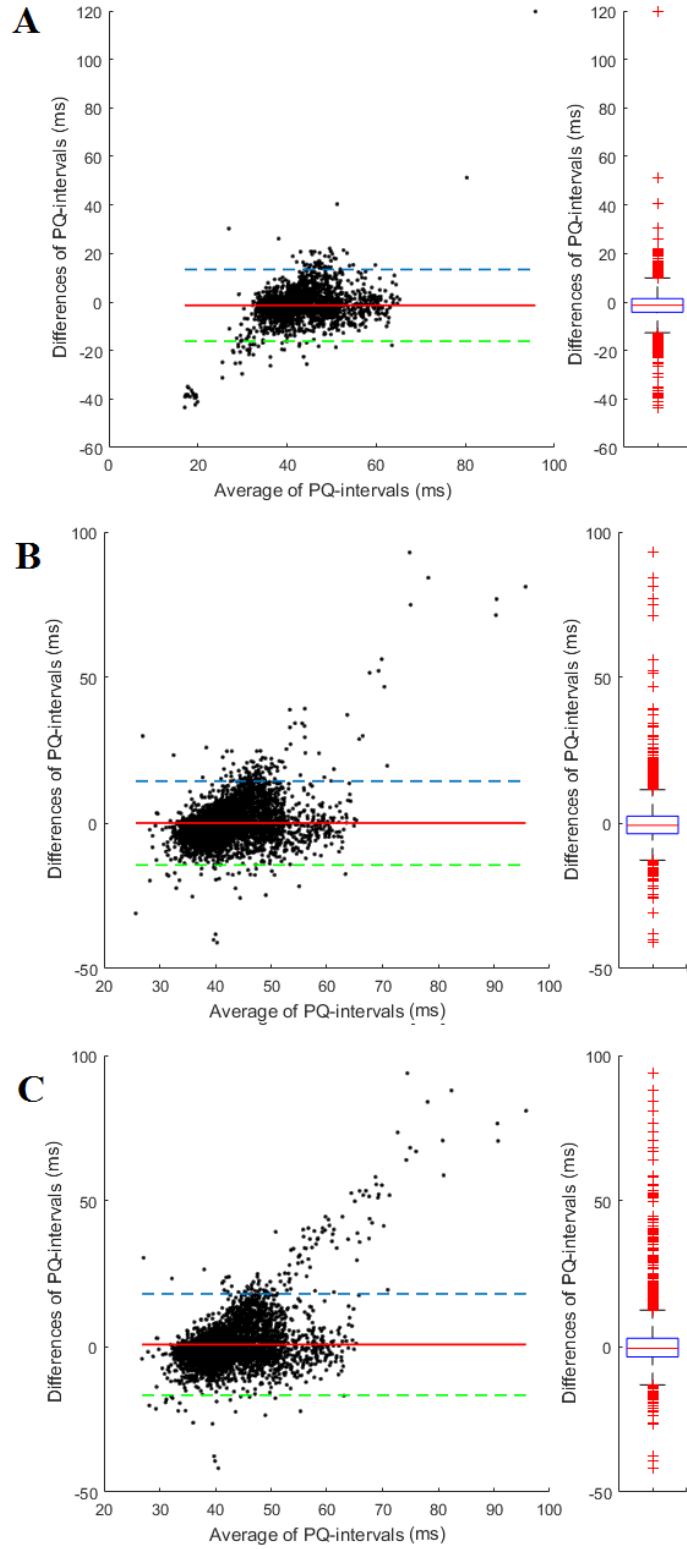
Figure 5.7.: Bland-Altman plot and boxplot of the PQ-interval differences (ms) for the algorithm versions human (A), 100 (B) and 101 (C).
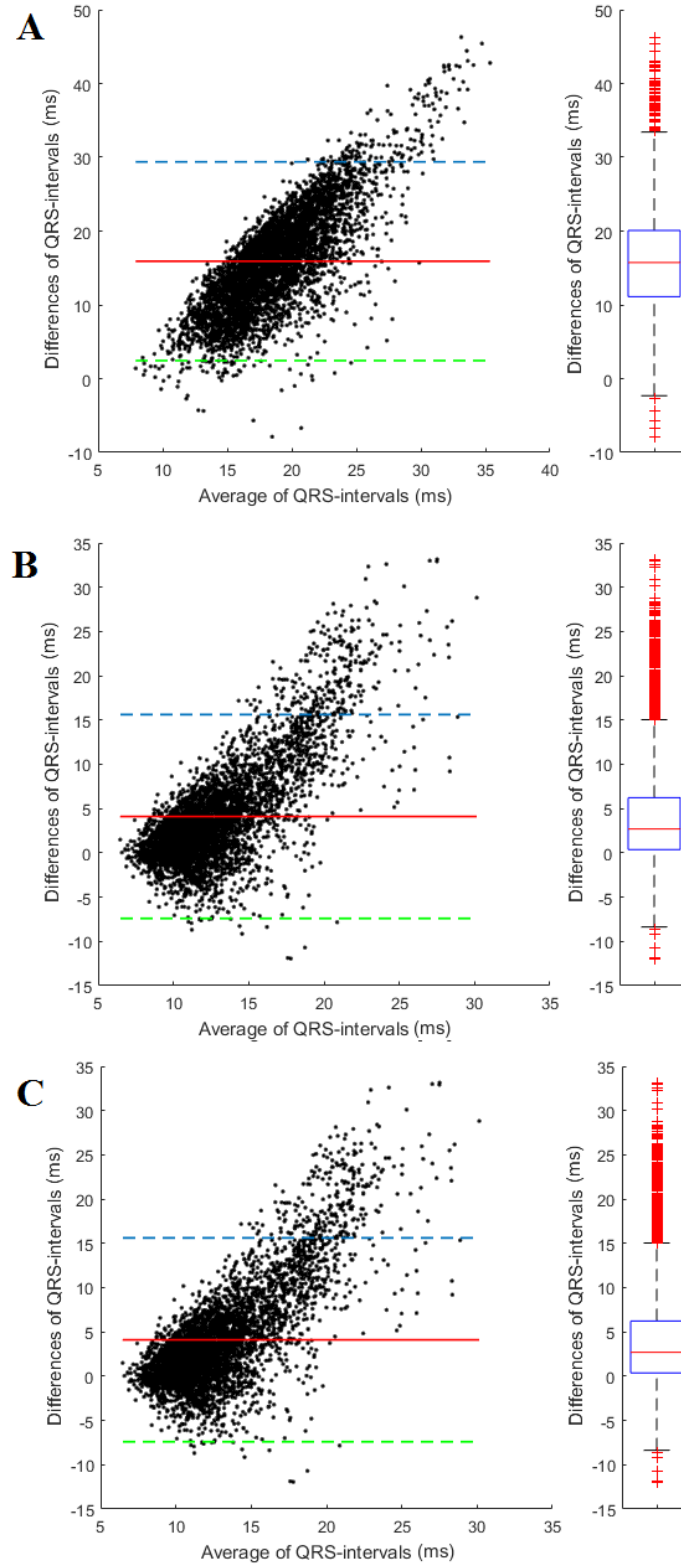
Figure 5.8.: Bland-Altman plot and boxplot of the QRS-interval differences (ms) for the algorithm versions human (A), 100 (B) and 101 (C).
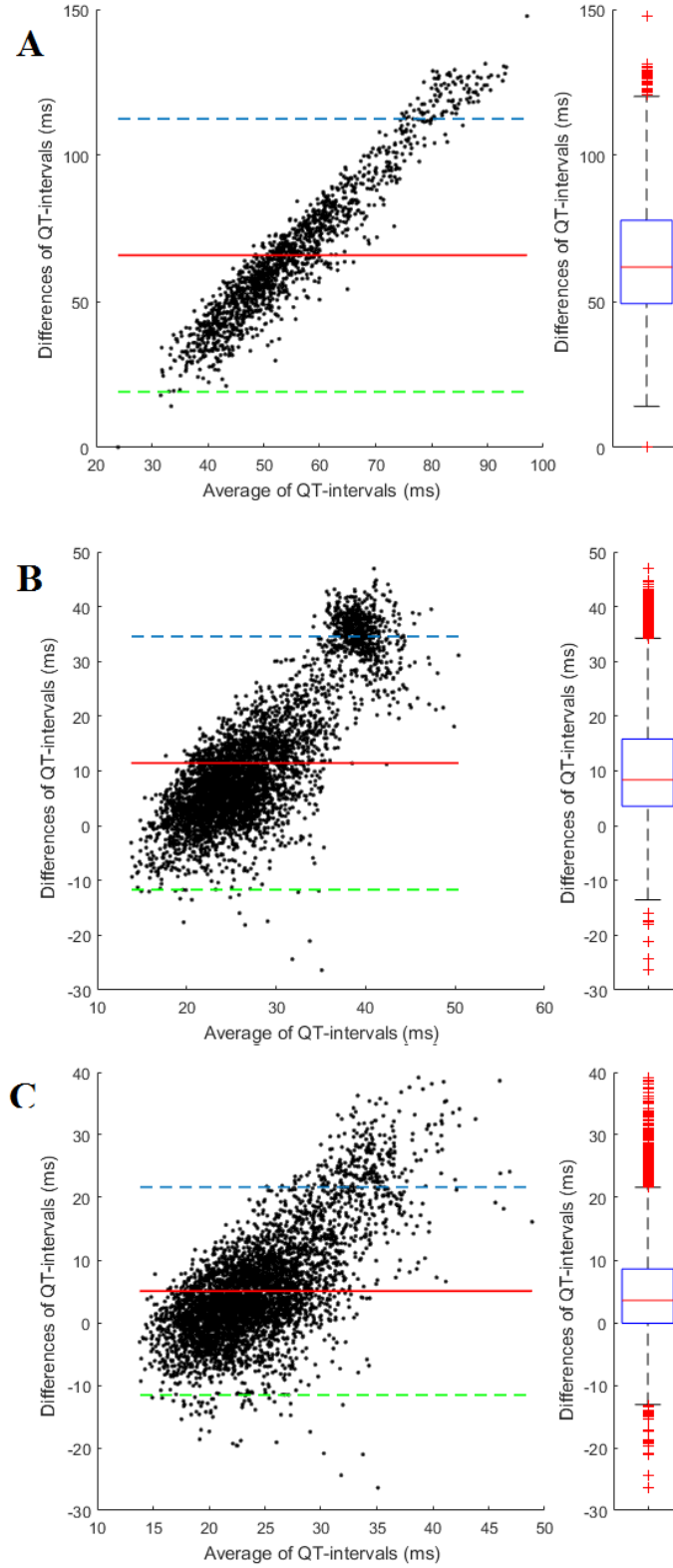
Figure 5.9.: Bland-Altman plot and boxplot of the QT-interval differences (ms) for the algorithm versions human (A), 110 (B) and 111 (C).

5.2. Comparison development and reference subset

The dataset for the evaluation has been divided into a development subset of 14 recordings and a reference subset of 12 recordings. The differences between automatic and manual annotations are calculated for both subsets separately. The values for the versions 100 and 101 are shown in the Tables 5.7 and 5.8 in form of median and IQR in ms.

There are no great differences between the development and the reference subset. The differences for the RR-interval are very similar with a median difference of 0 ms for the development and -0.002 ms for the reference subset. The same is true for the PQ and the QT-interval, although they are in some cases even a bit better for the reference subset, e.g. the QT-interval median difference for version 101 is 5.75 ms for the development and 5.59 ms for the reference subset. The difference between automatic and manual QRS- and the QT_C-interval is always higher for the reference subset, but not so much. For example, the QRS-interval median difference for version 100 and 101 is 3.55 ms and 5.22 ms for the development and the reference subset, respectively.

Interval	development (ms)	reference (ms)
RR	0 [-0.0571,0.00144]	-0.00242 [-0.015,0]
QRS	3.55 [2.15,5.99]	5.22 [3.68,5.51]
PQ	0.514 [-1.63,3.27]	-0.915 [-1.18,1.03]
QT	12.3 [9.09,15.9]	12.8 [7.16,15.7]
QT_C	8.73 [6.4,12.5]	10.2 [5.83,12.3]

Table 5.7.: Comparison of the ECG interval durations (ms) between the development and the reference subset for version 100.

Interval	development (ms)	reference (ms)
RR	0 [-0.0571,0.00144]	-0.00242 [-0.015,0]
QRS	3.55 [2.15,5.99]	5.22 [3.68,5.51]
PQ	0.925 [-1.47,4.62]	-0.522 [-1.18,1.73]
QT	5.75 [3.89,8.33]	5.59 [1.91,7.53]
QT_C	3.79 [2.68,5.33]	4.47 [1.54,5.8]

Table 5.8.: Comparison of the ECG interval durations (ms) between the development and the reference subset for version 101.

5.3. Comparison before and after medical treatment

The provided dataset was initially used to analyse the changes in the ECG signals due to medical treatment. The first recording of each mouse was taken before, the second one was taken after the medical intervention with Atenolol 5mg/kg. Therefore, the ECG intervals are not only analysed overall, but also in terms of the changes caused by the medical treatment.

The comparison of the ECG intervals before and after the medication for the versions 100 and 101 is shown in Table 5.9 and 5.10, respectively. The mean values $\mu \pm$ their standard deviations are displayed together with the p-value. For both annotations, the duration of the RR-interval afterwards is very significantly increased (p-value <0.001). This corresponds to a decrease in the heart rate. The QT_C-interval for the manual and the automatic annotations is significantly decreases (p-value <0.05). The boxplots of the RR-, the PQ-, the QRS- and the QT-interval durations for version 111 before and after medication are shown in the Figures 5.10 and 5.11.

Interval	manual μ (SD) (ms)			automatic μ (SD) (ms)		
	before	after	P-value	before	after	P-value
RR	158 (21.3)	179 (27.8)	<0.001	158 (21.3)	179 (27.1)	<0.001
QRS	10.9 (1.47)	10.9 (1.72)	0.87	15.1 (2.46)	15.2 (2.92)	0.98
PQ	42.1 (6.01)	42.6 (4.7)	0.47	42.4 (5.76)	42.8 (3.47)	0.70
QT	21.6 (1.92)	21.9 (2.12)	0.49	33.5 (4.69)	33.7 (5.46)	0.87
QT_C	17.3 (1.65)	16.4 (1.45)	0.02	26.4 (3.65)	25.3 (3.28)	0.25

Table 5.9.: Comparison of the ECG interval durations (ms) before and after the medical treatment for version 100.

Interval	manual μ (SD) (ms)			automatic μ (SD) (ms)		
	before	after	P-value	before	after	P-value
RR	158 (21.3)	179 (27.8)	<0.001	158 (21.3)	179 (27.1)	<0.001
QRS	10.9 (1.47)	10.9 (1.72)	0.87	15.1 (2.46)	15.2 (2.92)	0.98
PQ	42.1 (6.01)	42.6 (4.7)	0.47	44.1 (7.38)	43.5 (3.68)	0.73
QT	21.6 (1.92)	21.9 (2.12)	0.49	27 (3.72)	26.9 (3.71)	0.85
QT_C	17.3 (1.65)	16.4 (1.45)	0.02	21.4 (2.9)	20.1 (2.21)	0.08

Table 5.10.: Comparison of the ECG interval durations (ms) before and after the medical treatment for version 101.
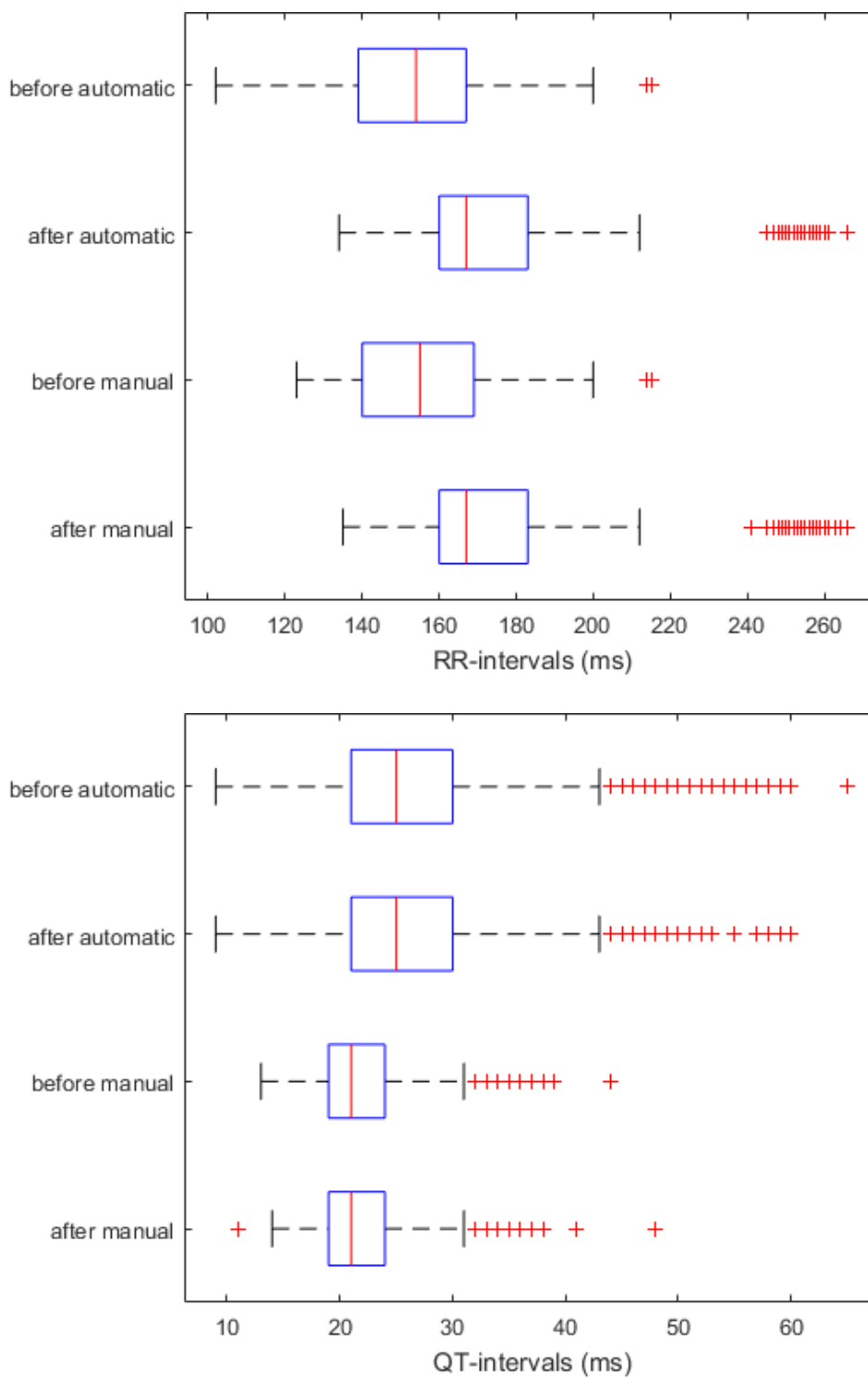
Figure 5.10.: Boxplots of the version 101 and manual RR- and QT-interval durations for the medical treatment.
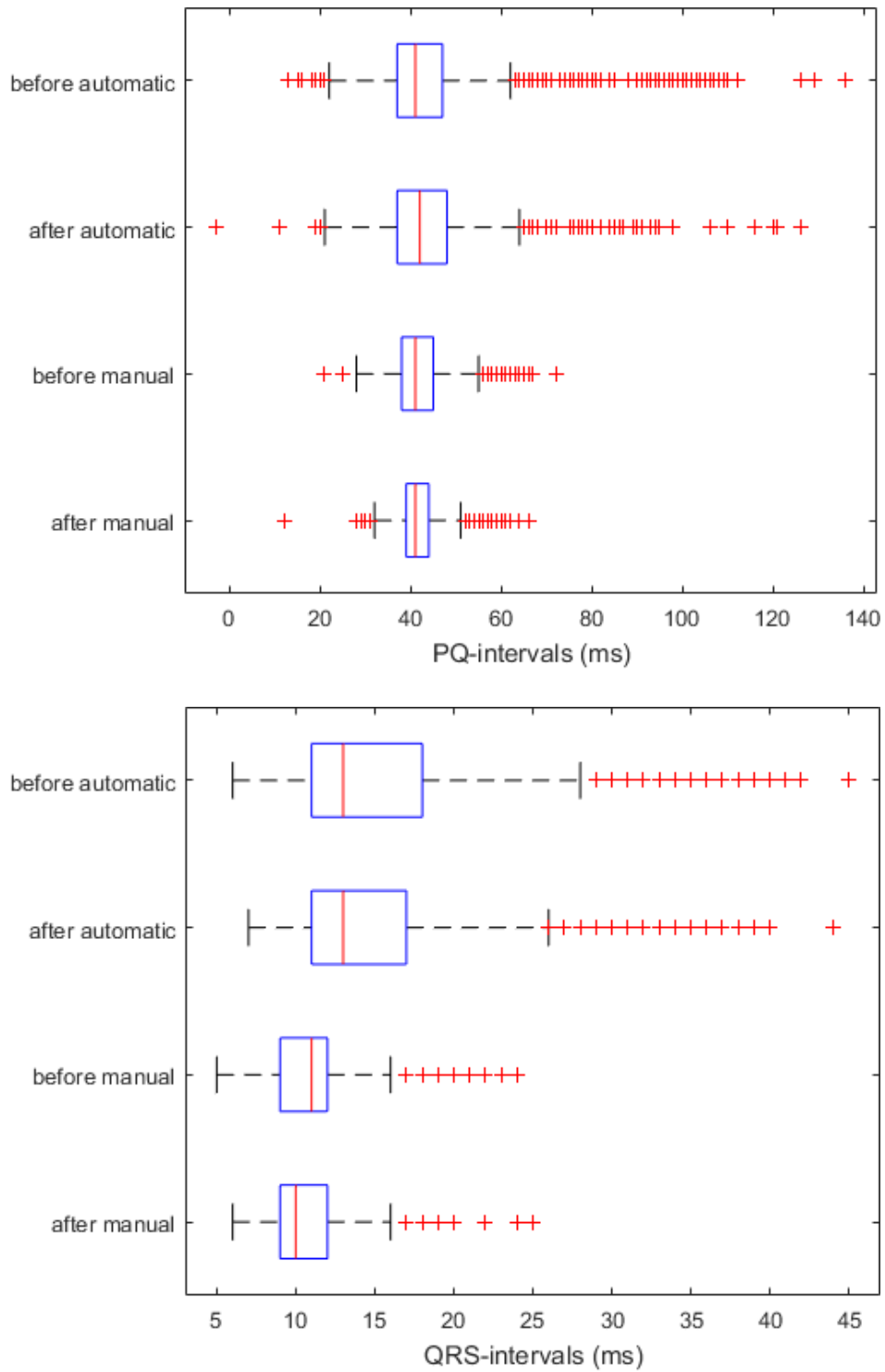
Figure 5.11.: Boxplots of the version 101 and manual PQ- and QRS-interval durations for the medical treatment.

Discussion $\bigg|$ 6

In Chapter 6 the results presented in the previous chapter are interpreted and analysed. First, the differences between automatic and manual results are discussed. Since the interval calculation is based on the feature annotations, they are analysed together. Furthermore, a default setting proposal is provided to chose one of the 8 different implementations. Then, the calculated ECG intervals are compared to data taken from the literature. And finally, the results before and after the medical treatment of the mice are interpreted.

6.1. Automatic vs. manual results

The subjects of discussion in the following subsection are the differences between automatic and manual annotations and their consequences for the ECG interval calculations. The interpretation is based on the tables and figures provided in Section 5.1 and the Appendix A.2. At the end, a suggestion for the default setting of the algorithm is given.

6.1.1. R-peaks and RR-intervals

The results of the human algorithm, which are equal to the automatic results, are very convincing. If the R-peak is detected, the difference of the majority to the manual labelling is less than 1 ms for all versions. It is not perfectly detected, because signal shapes with a double peak such as illustrated in Figure A.3 (top, right) can lead to a detection on either the first or the second peak. The missing 72 R-peaks are all in one lead in one mouse, where the P-wave was wrongly detected as R-peak. This increases not only the FN but also the FP number. The R-peak is the basis for all other feature detections. As a result, the 72 heart beats are not recognised correctly in the other features either. The number of FP is higher than 72 which indicates misclassifications in more than one lead and mouse.
Due to the exact location of the R-waves, the RR-intervals are also well predicted. The average duration between two R-peaks of about 160 ms corresponds to a heart rate of 375 bpm. However, the clusters in the Bland-Altman plot in Figure 5.6 and the boxplot of the interval durations indicate that the 13 mice of the study had different heat rates.

6.1.2. QRS-complex

The QRS-complex duration is based on the QRS-onset and -offset location. The QRS-onset detection of the human algorithm is reused in the murine algorithm. The detection rate is the same as for the R-peaks, but the beginning of the QRS-complex is generally detected too soon. The actual location is closer to the R-peak, often located at the beginning or in a slightly negative deflection before the R-peak. The mouse annotations are rather detected at the preceding edge (see Figure 5.3 B, lead Z). Thus, the IQR is slightly shifted towards negative differences.

The human algorithm detects a "QRS-offset", but the annotation is far too late. In regard to that, the new feature detection of the QRS-offset has been definitely successful. Positioning the index at the middle point of the upward slope is not correct for all ECG morphologies, such as the signal template shown in Figure A.3 (left, top). For these cases, the manual annotations are positioned at the minimum in the negative valley. And in some cases, the QRS-offset and the T-wave are still located too late in the signal. Thus, the location is still a little bit overestimated, but only by a fraction compared to before.

The premature QRS-onset and the late QRS-offset positions lead to an extended QRS-interval. The comparison of the Bland-Altman plots (see Figure 5.8) for the human and the mouse results shows that the shape of the point cloud has changed. Without the new feature detection, the point clouds have a more elongated shape and the range on the y-axis is wider. For the murine algorithm, the points are more accumulated around the median. Thus, the wrong elongation of the interval is weakened by the new QRS-offset detection. Anyway, there is still a strong trend towards overestimation of longer QRS-complexes.

6.1.3. T-wave features and QT-interval

Similar to the QRS-offset, the quality of the T-wave features can be increased by using the new feature detection. In the human algorithm, the median location of many annotations is between 26 and 60 ms too late, if they are detected at all. Many annotations are missing, because the criteria for a successful detection are not fulfilled. This leads to a high number of FN annotations. With the adapted algorithm, the number of TPs can be increased, and at the same time the distance to the target values is reduced. Since the T-onset and the QRS-offset are treated simultaneously, they have the same shift to the right compared to the manual annotations. The reason is explained in Subsection 6.1.2. Their FP and especially the FN numbers differ due to the case when the T-wave features are not annotated, but the slope of the QRS-complex is. Thus, there are more T-onset than QRS-offset annotations missing, which also influences the sensitivity and the positive prediction. At this point, it should be mentioned that the number of FP counts should be the same for all three T-wave features due to their automatic all-or-none annotation. Since this is not the case, it is assumed that single annotations have been forgotten or intentionally not annotated during the manual

labelling.

The T-peak is the first of the two features, for which two detection methods were implemented. Both approaches achieve comparable differences to the actual annotations, but the detection rate differs. For the prominent maximum more T-peaks are detected, resulting in a higher FP value and a lower FN value. For the wings function, less T-peaks are detected and the relationship is vice versa. This suggests, that the wings function criteria are more strict than the condition of a prominent maximum.

The second step, where a choice between two alternatives can be made, is the T-offset detection. The application of either the geometric or the TRA method shows one major change. At constant detection rate, the difference to the actual location is smaller for the TRA method. By using the first local maximum of the trapeziums area instead of the global maximum, the TRA-detected T-offset is closer to the T-peak. This corresponds to the manual annotations. Since the definition of the T-wave endpoint is still a topic of discussion on its own, the results depend on the given target values. For a different dataset with a clearly recognisable negative T-wave deflection, the results would be different. For this reason, the T-offset correction step has been implemented, but not used. Since already the geometric method shows a delay in the T-offset location, the gap between the target values and the predicted locations would diverge even further for an activated T-offset correction.

The intervals from QRS-onset to T-offset for manual and automatic annotations are different. The trend is clearly towards an overestimation of the interval duration, especially for large averages of the two QT-intervals. The statement about the shape of the data point clouds in the Bland-Altman plots of the QRS-intervals is also valid for the QT-intervals. The larger difference to the actual T-offset for the versions with the geometric T-offset annotation is reflected in the Bland-Altman plot by a cluster (see Figure 5.9 B), which is located in the upper right corner. The higher average and the positive differences indicate a wrongly detected QT-interval elongation. The QT_C-interval is not further analysed, since its informative value for murine data is subject to ongoing discussion [3, 12] (see Section 6.2). However, the results can be explained as a consequence of the RR- and the QT-intervals behaviour.

6.1.4. P-wave features and PQ-interval

The determination methods for the P-wave features have remained unchanged for the murine algorithm. Only the input has changed, since the P-wave features depend on the T-offset and the QRS-onset. The different numbers of FP and FN detections compared to the input features are the result of omitted P-waves in the manual labelling. If the P-wave was not clearly recognisable, it was skipped. Especially the high FP value indicates, that many P-waves which are automatically detected are not distinguishable for the user's eyes and should not be annotated. Comparing the results between the versions using the geometric and the TRA-

based method as T-offset determination, a difference in the detection rate for the P-wave features is shown. Overall, the geometric method shows slightly higher TP values than the TRA-method. One possible explanation is that the delayed detected T-offset does not fulfill some criteria in the P-wave analysis. Therefore, the features of the P-wave will not be annotated, which leads to lower FP values. The P-peaks, which are correctly detected, are annotated quite accurately. Both the onset and the offset tend to be located too early on average with many outliers in both directions. The detection method is designed to analyse monophasic P-wave characteristics. However, the P-waves in the murine dataset sometimes show a biphasic characteristic, which leads to premature feature annotations.

Both features for the PQ-interval calculation are generally located too early in the signal. Since the P-onset and the QRS-onset are both shifted in the same direction, the overall influence on the interval duration is minimal. The median of the differences is close to 0 for all versions. The data points in the Bland-Altman plots (see Figure 5.7) are accumulated around an average which corresponds to the median of the interval duration.

6.1.5. Default setting for murine algorithm

The 8 different implemented versions of the algorithm are labelled with a three-digit code, as shown in Table 5.1. Each digit corresponds to a task that can be solved with two approaches. This code is also used to run the murine algorithm and activate the desired methods. After analysing the results of all versions in terms of detection rate and accuracy of ECG feature annotations and the duration of the ECG intervals, the default setting for the algorithm version is proposed. For each digit, the preferred method is chosen. The methods are analysed in the reverse digit order because of their impact on the results.

The T-offset determination is the task symbolised by the 3rd digit. It influences both the T-features, as discussed in the Subsection 6.1.3, and the P-features, as discussed in the Subsection 6.1.4. The optimal method decreases the differences between the target values and increases the TP values at the same time compared to alternative approaches. Unfortunately, both methods fulfill only one of those two requirements. The TRA-method decreases the differences, but results in higher TP numbers. The geometric method decreases the number of TPs, but have higher values for the differences. However, the focus of this thesis was more on the correct detection of the T-wave features and therefore the TRA-method is favoured over the geometric method. That offers an other additional advantage. The basis for further analysis in the T-offset correction is the TRA-detected T-offset, independent of which method is used to determine the initial T-offset. For an activated correction step, only one function needs to be called, since the T-offset detection and correction based on the TRA-method are implemented together. Thus, the 3rd digit of the default setting is 1. This reduces the candidates for the "best" version to 4.

The 2nd digit represents the T-peak determination. The exact location of the T-

peak is not very important, since it is often neglected for further ECG parameter calculations. And the differences to the target values are similar for both methods anyway. However, even though the T-peak location is not of great interest, its existence is. As stated in Section 4.2.1, the T-wave analysis is only continued if a T-peak could be located. Instead of limiting the T-peak search, which would also reduce the possibility to distinguish between correct and incorrect T-wave features, an advanced correction step based on all three T-features is preferable. As discussed in the Subsection 6.1.3, the wings function is more strict in its detection than the prominent maximum approach. Thus, the prominent maximums approach with digit 0 is chosen.

The task expressed by the 1st digit is the clustering. The two different clustering methods have no noticeable influence on neither the detection rate nor the distance to the target values. Hence, the version with the highest number of TP is selected from the last two. The analysis results in a default setting of 101 for the applied version. It should be mentioned that the requirements and therefore the "best" version can vary from dataset to dataset.

6.2. Comparison to literature

Data found in the literature is summarised in Table 2.3. It is used for the comparison with the ECG intervals of the murine algorithm version 101 (see Table 5.6). It was already mentioned in Section 2.2.5 that the different study configurations make it difficult to compare the data. The used anaesthesia influences the heart's electrical activity and therefore the duration of ECG intervals, as stated by Danik et al. [15]. The ECG signals of the used dataset were recorded under the influence of isoflurane. According to Speerschneider and Thomsen [3], isoflurane reduces the heart rate and prolongs the QT-interval. Therefore, the calculated intervals based on the annotations of version 111 are only compared to the last two studies [17, 32] in Table 2.3.

The average heart rate of the two studies is around 442 bpm. The calculation of the average heart rate for all 26 recordings results in a lower heart rate of around 370 bpm. However, the 26 recordings also contain those 13 signals which have a lower heart rate due to the medical treatment. Considering only the 13 recordings before the intervention, the heart rate increases slightly to an average of around 380 bpm. The cluster in the RR-interval Bland-Altman plot indicate higher heart rates for single individuals.

The remaining intervals are not significantly influenced by the medication. Thus, the results of the entire dataset are used for further analysis. The mean QRS-complex of 15 ms ± 6.09 SD and the median of 13 ms with an IQR of [11,17] are exceeding the values from the literature data of 8.4 to 11.3 ms. The opposite is the case for the QT-interval. The median algorithm duration of 19.5 ms with an IQR of [16.3,23.1] and the mean of 26.7 ms ± 8.61 SD is below the 46.3 to 66 ms interval

suggested by the literature. The reason for that could be the default setting of the algorithm, which ignores a negative deflection after the J-wave. Thus, the QT interval is shortened. The median duration of the algorithm determined PR-interval is 41 ms with an IQR of [37,47] and the mean is 43.6 ms $\pm$ 11.7 SD. Thus, the PR-interval is located in the interval of 33.2 to 59.6 ms indicated by the literature.

The QT_C-interval is calculated according to the formula 2.2 by Mitchell et al. [23]. In the studies of Speerschneider and Thomsen [3] and Boukens et al. [12], it is discussed whether the formula is an adequate heart rate correction of the QT-interval. They suggested to not use the formula for anaesthetised mice due to the varying heart rates. Therefore, the QT_C-interval is not further analysed or compared to reference values.

6.3. Comparison development and reference subset

The comparison by means of the differences between automatic and manual results shows no big differences for the two subsets. Since the development subset was used for the algorithm planning, larger values for the reference subset would mean overfitting occurred. For some features, the values for the development subset are lower compared to the reference subset, but not much. There are even some features, for which the differences for the reference subset are lower. Generally, the values for the differences does not show a trend towards overfitting.

6.4. Comparison before and after medical treatment

The betablocker Atenolol binds specific to β_1-receptors and is used for the treatment of hypertension. Its main consequences for the ECG intervals are a reduced heart rate, which corresponds to an increased duration between two R-peaks, and the elongation of the QT-interval [55]. This changes were also observed for animal models. Ruppert et al. [56] analysed the influence of reference compounds such as Atenolol on the cardiac electrophysiology of guinea pigs. Unfortunately, no study could be found on mice. The data in Table 5.9 and 5.10 suggests that the reduction of the heart rate also applies to mice. Both the manual and the automatic results show a highly significant increase in the RR-interval duration. In contrast, an increase in the QT-interval duration is not noticeable in our dataset. The increase for the QT_C-interval is only significant for the manual but not for the murine results. Since the RR-intervals have the same values for the mean and SD, this is a consequence of the QT-interval values.

Conclusion and Outlook | 7

In conclusion, an algorithm for the automatic ECG feature detection specialised for mouse data was implemented and evaluated. The foundation for the murine algorithm was the AIT ECGsolver, which was developed for human ECG signal analysis. The QRS-offset and T-wave feature determination methods are exchanged or adapted to fit the different ECG morphology. After determining the features, the ECG intervals are calculated automatically. Three algorithm steps were solved by two different methods. The resulting versions were compared to each other and to manually labelled feature annotations, which served as target values. Generally, the developed algorithm performed better than the human algorithm. The major weaknesses of the non-specialized analysis regarding the different T-wave shape have been eliminated. There is still room for some improvements, but the tendency of the results is promising.

During the evaluation it turned out that the annotation of the P-wave features still shows potential for improvement. Since the wave shape does not differ so much from human signals, the focus was more on the adaptation for QRS-offset and T-wave features. However, the sensitivity and the positive prediction of the algorithm could be improved, if the detection rate for the last determination step is more adapted to the wave shape in murine ECG signals. This could be a task for future work. Additionally, a lead correction after processing one complete ECG signal with more than two leads could be added. The number of correct annotations could be improved by using the information of all leads. Missing or wrong detected features could be located and rechecked with the additional data.

Furthermore, the algorithm should be tested with murine data showing a clear recognisable negative T-wave. A correction step to detect the T-offset at the end of such a negative deflection is already implemented. Unfortunately, there was no possibility to test the extension due to the ECG morphology of the used dataset and the manual annotations, which did not distinguish between J- and T-wave.

It would also be interesting to implement an algorithm, which is capable of deciding the best methods to apply for the currently analysed dataset on its own. A possibility could be to use a semi-automatic approach. By manually labelling a few features at the start of the signal, the users enter some reference points and the algorithm learns from them. Then, the further analysis is applied automatically, which can be extended to an analysis in real time.

Appendix | A

A.1. ECG morphologies of data set

Different ECG leads produce different shapes of the ECG signal, as already mentioned in section 2.2.4 in connection with the polarity of a distinct T-wave. However, the ECG morphology in the used data set also varies within the leads. Examples for different characteristics in the three leads X, Y, and Z are shown in the Figures A.1, A.2 and A.3, respectively.
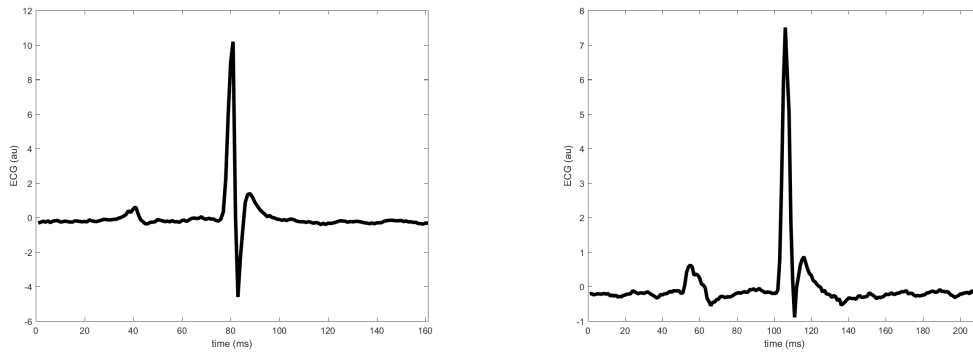
Figure A.1.: Two examples for the different ECG morphology in lead X.
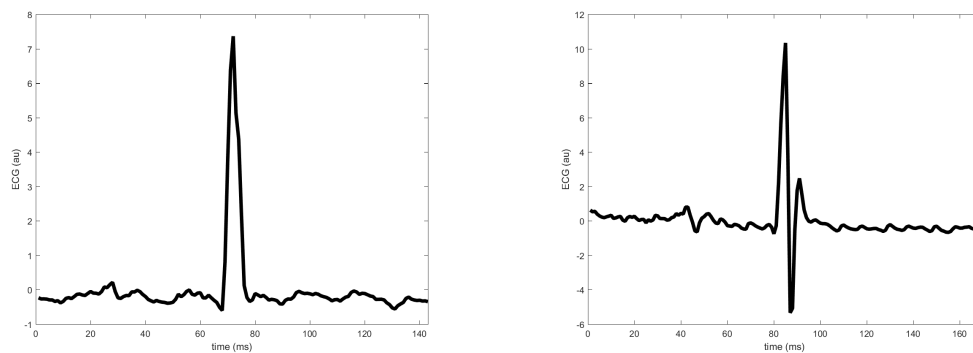
Figure A.2.: Two examples for the different ECG morphology in lead Y.
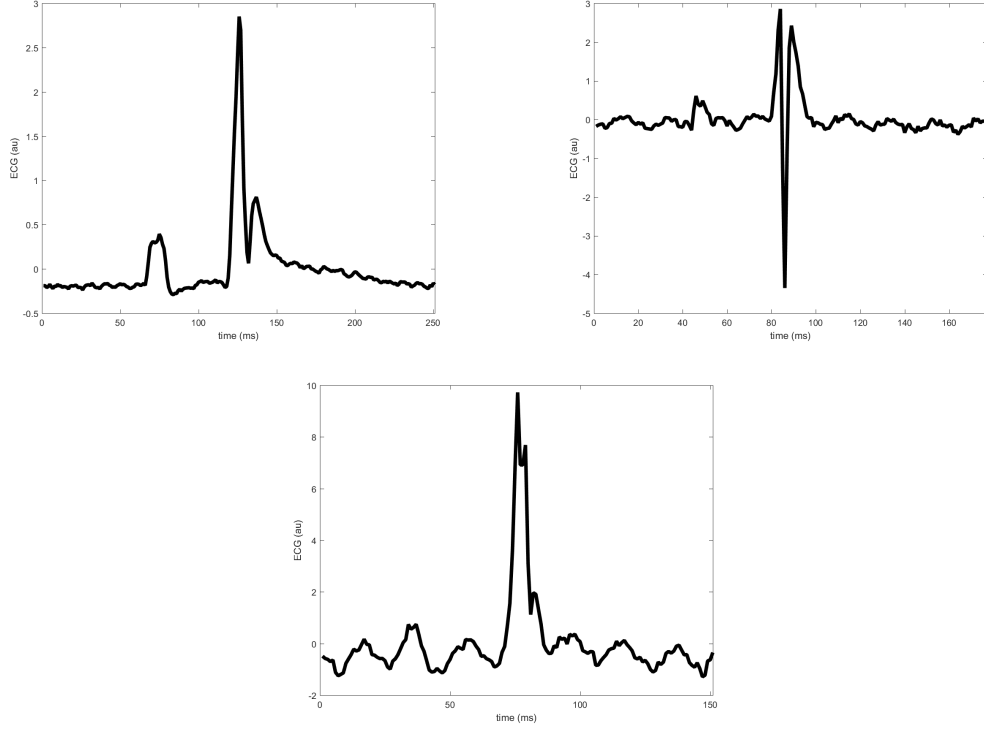
Figure A.3.: Three examples for the different ECG morphology in lead Z.

A.2. Comparison automatic and manual results

In this section, additional data for the comparison of the manual and the automatic results is provided. The main results of the comparison are shown in Section 5.1 and discussed in Section 6.1.

A.2.1. ECG feature annotations

The values for TP, FP, FN, sensitivity and positive prediction for 6 of the 8 algorithm versions are displayed in the Tables A.1 to A.6 together with the median and the IQR of the differences to the target values. The tables for version 110 and 111 are shown in Section 5.1 (in the Tables)A.7 and A.8). The corresponding boxplots for all 8 versions illustrating the differences in ms for all ECG features to their target values are given in the Figures A.4 to A.11.

Features	TP	FP	FN	Se [%]	Pp [%]	Differences (ms)
QRS-offset	4784	108	81	98.34	97.79	0 [0,1]
T-peak	4478	138	332	93.1	97.01	0 [0,0]
T-onset	4477	139	332	93.1	96.99	0 [-1,1]
T-offset	4479	137	332	93.1	97.03	6 [2,12]
P-peak	3908	570	251	93.96	87.27	0 [0,0]
P-onset	3908	570	251	93.96	87.27	0 [-3,1]
P-offset	3908	570	251	93.96	87.27	-1 [-4,0]

Table A.1.: Performance values of all ECG features detected by the murine algorithm version 000 compared to the manual annotations.
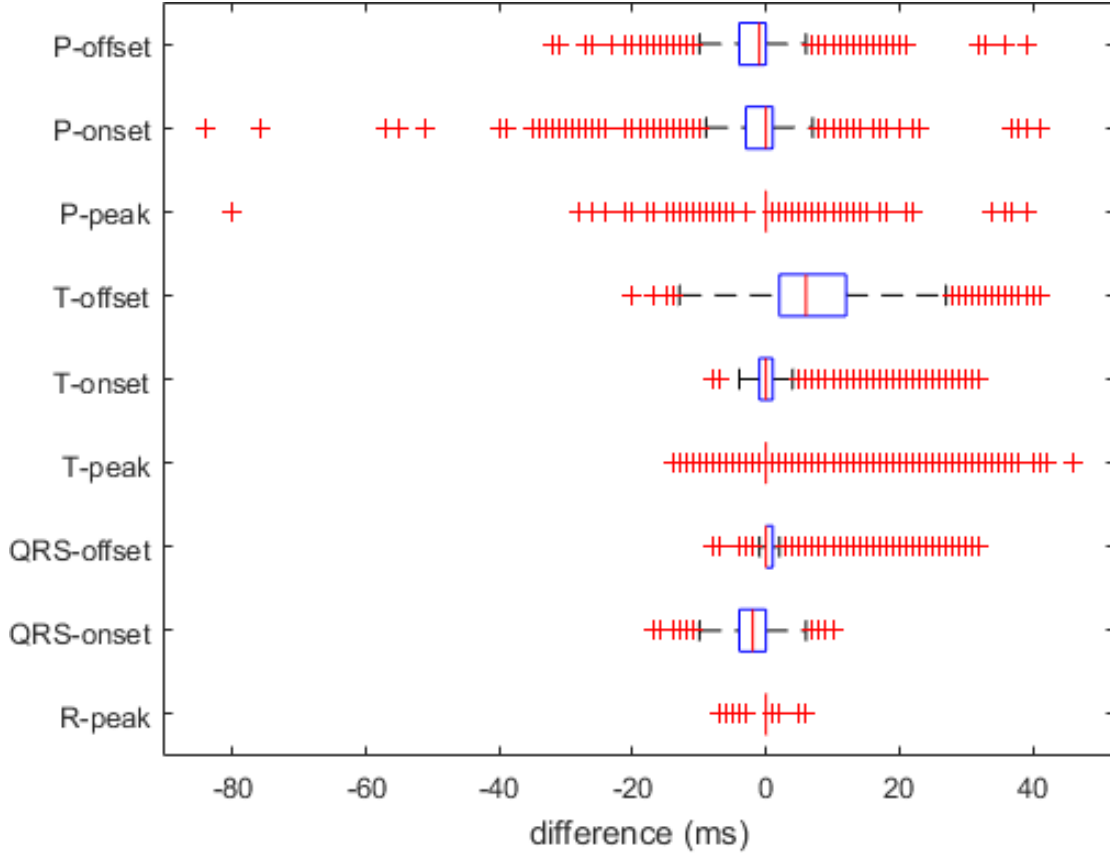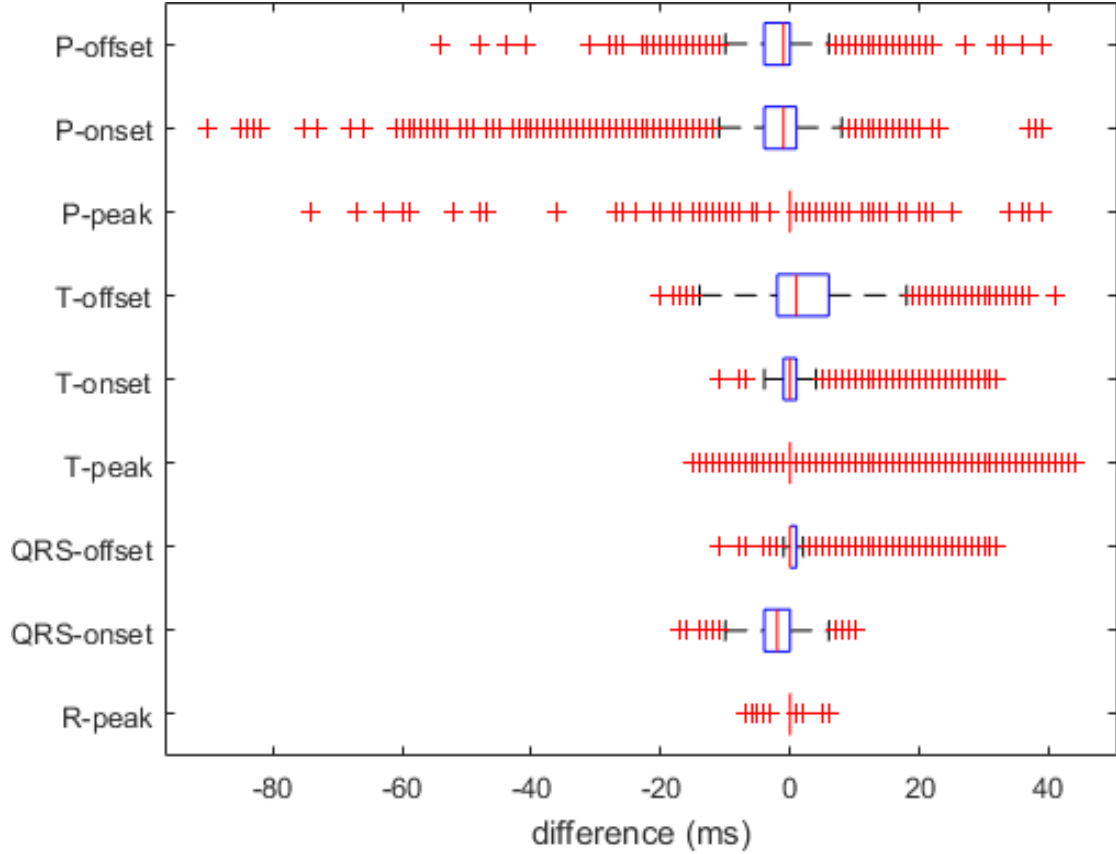

Figure A.4.: Boxplots of the differences (ms) between the annotations determined by the murine algorithm version 000 and the manual annotations for all ECG features.

Features	TP	FP	FN	Se [%]	Pp [%]	Differences (ms)
QRS-offset	4784	108	81	98.34	97.79	0 [0,1]
T-peak	4478	138	332	93.1	97.01	0 [0,0]
T-onset	4477	139	332	93.1	96.99	0 [-1,1]
T-offset	4479	137	332	93.1	97.03	1 [-2,6]
P-peak	3892	719	267	93.58	84.41	0 [0,0]
P-onset	3892	719	267	93.58	84.41	-1 [-4,1]
P-offset	3892	718	267	93.58	84.43	-1 [-4,0]

Table A.2.: Performance values of all ECG features detected by the murine algorithm version 001 compared to the manual annotations.
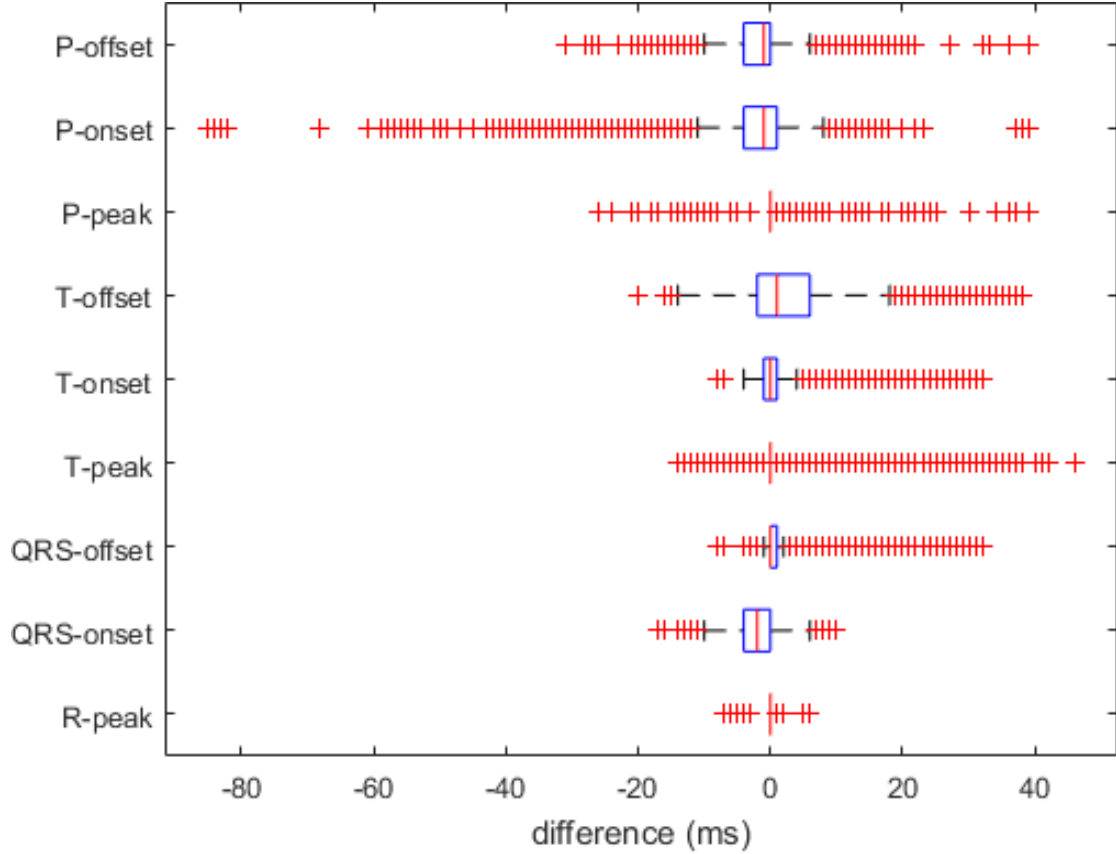
Figure A.5.: Boxplots of the differences (ms) between the annotations determined by the murine algorithm version 001 and the manual annotations for all ECG features.

Features	TP	FP	FN	Se [%]	Pp [%]	Differences (ms)
QRS-offset	4783	108	82	98.31	97.79	0 [0,1]
T-peak	4538	158	272	94.35	96.64	0 [0,0]
T-onset	4537	159	272	94.34	96.61	0 [-1,1]
T-offset	4539	157	272	94.35	96.66	6 [2,12]
P-peak	3905	570	254	93.89	87.26	0 [0,0]
P-onset	3905	570	254	93.89	87.26	0 [-3,1]
P-offset	3905	570	254	93.89	87.26	-1 [-4,0]

Table A.3.: Performance values of all ECG features detected by the murine algorithm version 010 compared to the manual annotations.
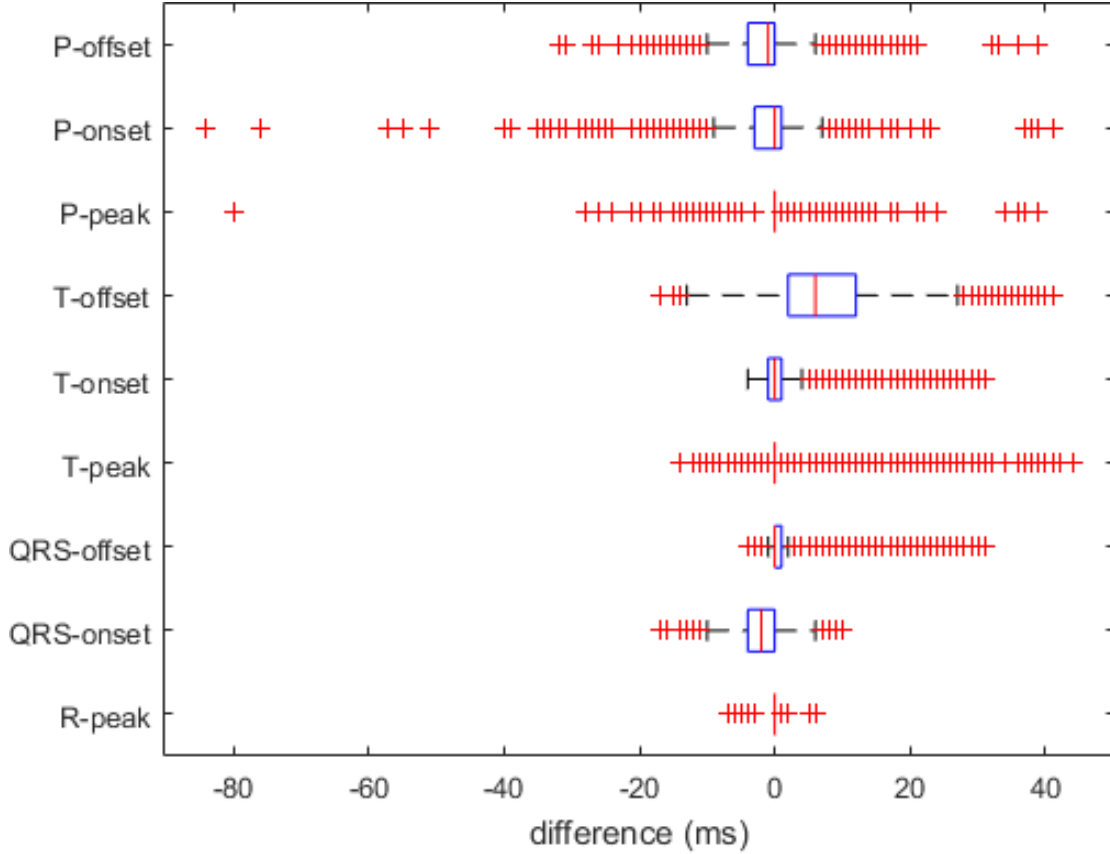
Figure A.6.: Boxplots of the differences (ms) between the annotations determined by the murine algorithm version 010 and the manual annotations for all ECG features.

Features	TP	FP	FN	Se [%]	Pp [%]	Differences (ms)
QRS-offset	4783	108	82	98.31	97.79	0 [0,1]
T-peak	4538	158	272	94.35	96.64	0 [0,0]
T-onset	4537	159	272	94.34	96.61	0 [-1,1]
T-offset	4539	157	272	94.35	96.66	1 [-2,6]
P-peak	3899	727	260	93.75	84.28	0 [0,0]
P-onset	3899	727	260	93.75	84.28	-1 [-4,1]
P-offset	3899	726	260	93.75	84.3	-1 [-4,0]

Table A.4.: Performance values of all ECG features detected by the murine algorithm version 011 compared to the manual annotations.
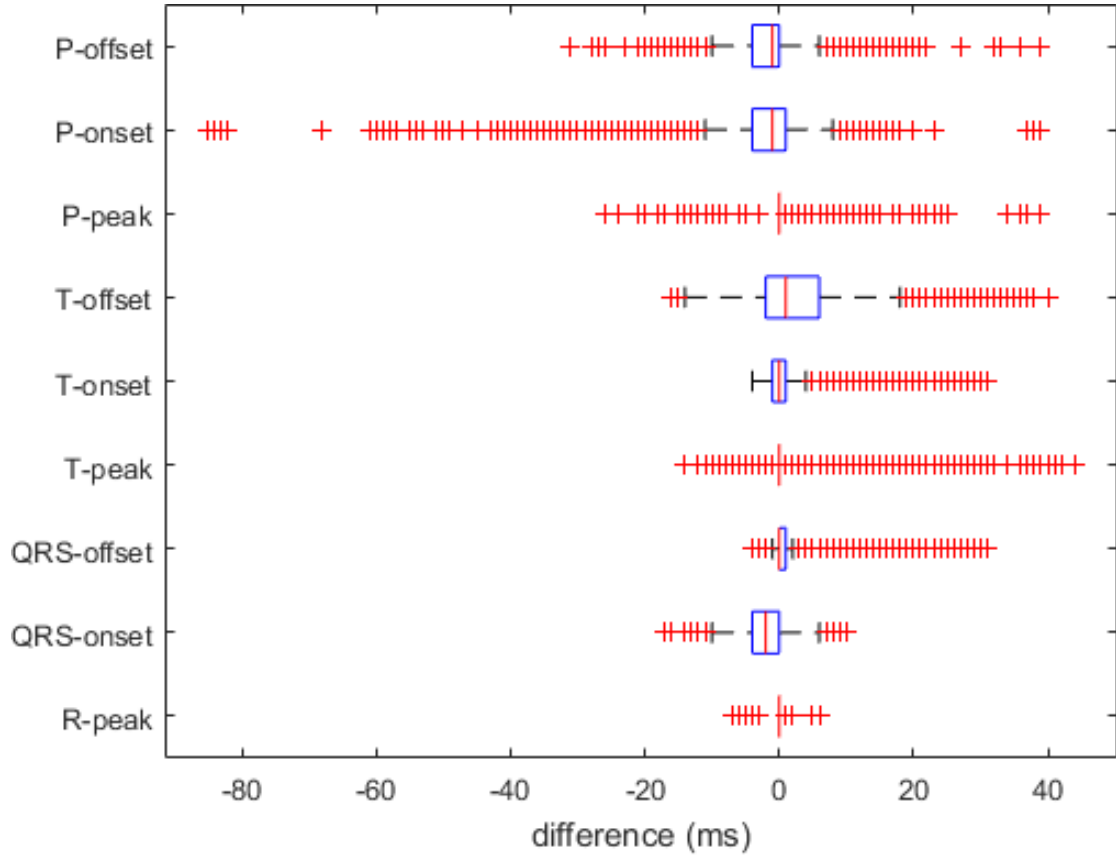
Figure A.7.: Boxplots of the differences (ms) between the annotations determined by the murine algorithm version 011 and the manual annotations for all ECG features.

Features	TP	FP	FN	Se [%]	Pp [%]	Differences (ms)
QRS-offset	4793	108	72	98.52	97.8	0 [0,1]
T-peak	4485	127	325	93.24	97.25	0 [0,0]
T-onset	4484	128	325	93.24	97.22	0 [-1,1]
T-offset	4486	126	325	93.24	97.27	6 [2,12]
P-peak	3912	597	247	94.06	86.76	0 [0,0]
P-onset	3911	597	248	94.04	86.76	0 [-3,1]
P-offset	3912	597	247	94.06	86.76	-1 [-4,0]

Table A.5.: Performance values of all ECG features detected by the murine algorithm version 100 compared to the manual annotations.
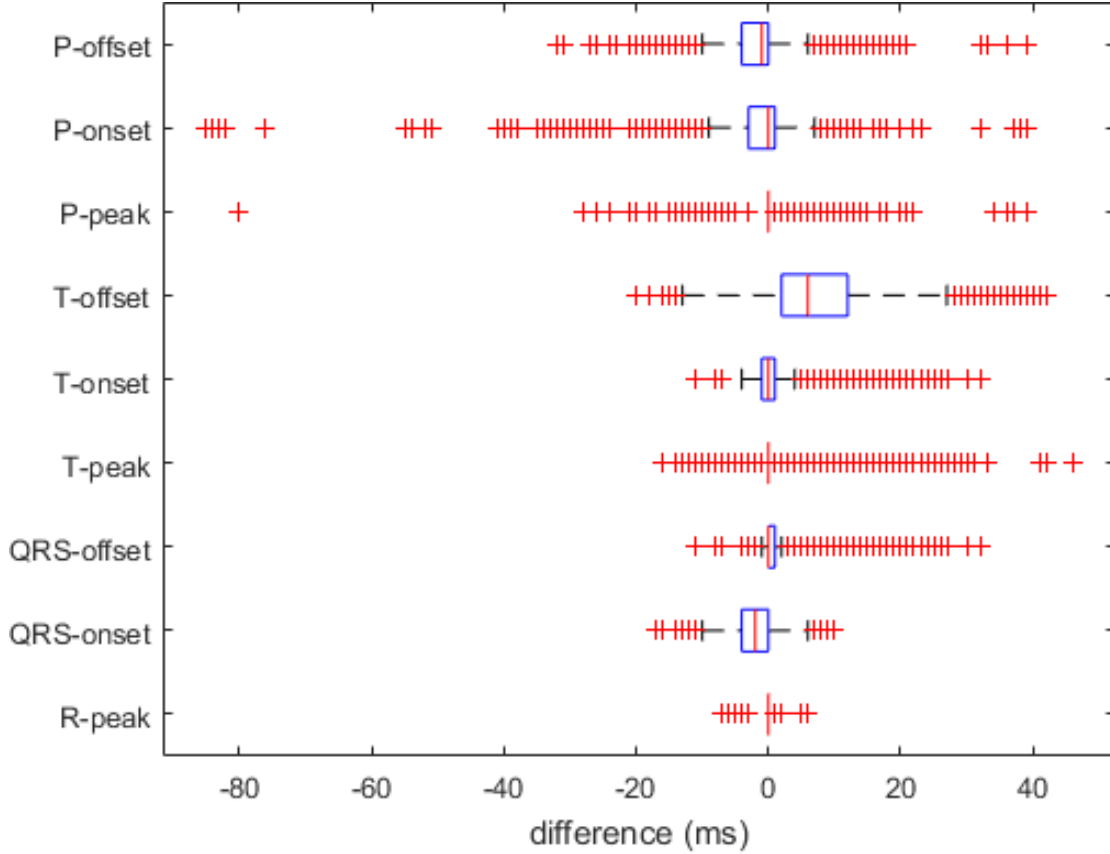
Figure A.8.: Boxplots of the differences (ms) between the annotations determined by the murine algorithm version 100 and the manual annotations for all ECG features.

Features	TP	FP	FN	Se [%]	Pp [%]	Differences (ms)
QRS-offset	4793	108	72	98.52	97.8	0 [0,1]
T-peak	4485	127	325	93.24	97.25	0 [0,0]
T-onset	4484	128	325	93.24	97.22	0 [-1,1]
T-offset	4486	126	325	93.24	97.27	1 [-2,6]
P-peak	3925	734	234	94.37	84.25	0 [0,0]
P-onset	3924	734	235	94.35	84.24	-1 [-4,1]
P-offset	3925	734	234	94.37	84.25	-1 [-4,0]

Table A.6.: Performance values of all ECG features detected by the murine algorithm version 101 compared to the manual annotations.
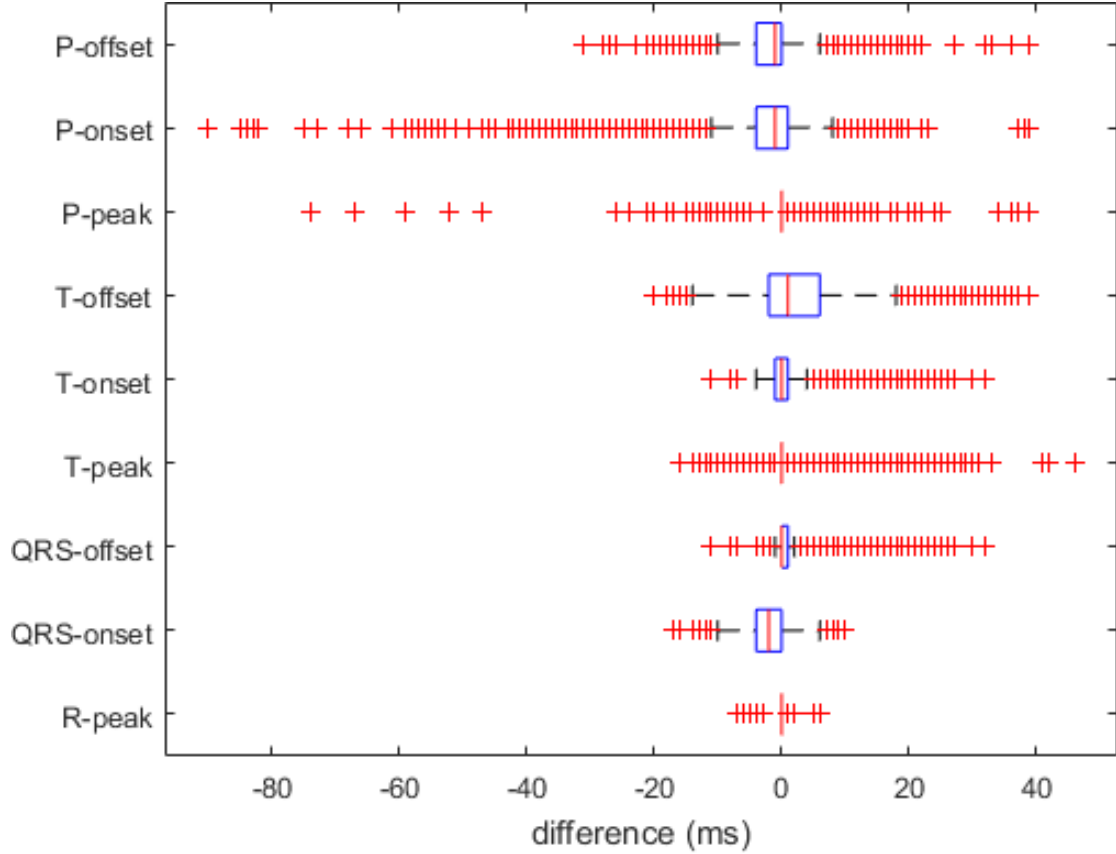
Figure A.9.: Boxplots of the differences (ms) between the annotations determined by the murine algorithm version 101 and the manual annotations for all ECG features.

Features	TP	FP	FN	Se [%]	Pp [%]	Differences (ms)
QRS-offset	4792	108	73	98.5	97.8	0 [0,1]
T-peak	4566	153	244	94.93	96.76	0 [0,0]
T-onset	4565	154	244	94.93	96.74	0 [-1,1]
T-offset	4567	152	244	94.93	96.78	6 [2,13]
P-peak	3936	619	223	94.64	86.41	0 [0,0]
P-onset	3935	619	224	94.61	86.41	0 [-3,1]
P-offset	3936	619	223	94.64	86.41	-1 [-4,0]

Table A.7.: Performance values of all ECG features detected by the murine algorithm version 110 compared to the manual annotations.
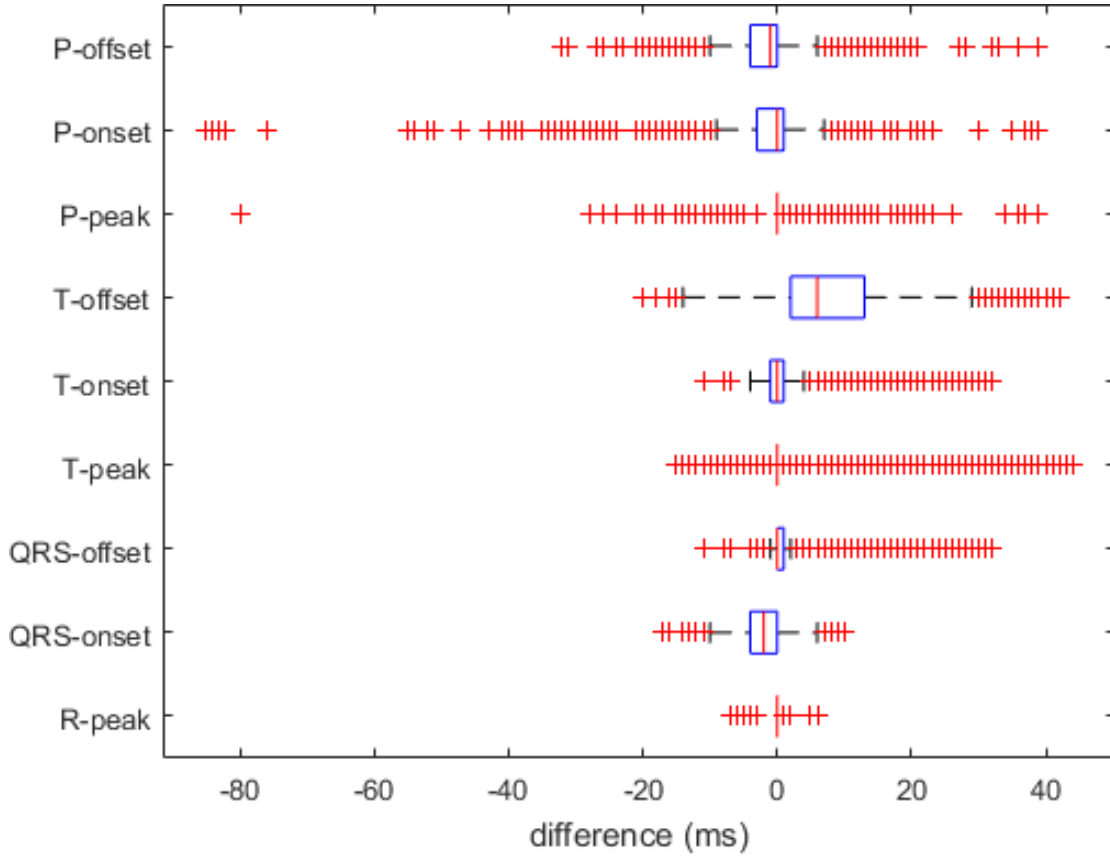
Figure A.10.: Boxplots of the differences (ms) between the annotations determined by the murine algorithm version 110 and the manual annotations for all ECG features.

Features	TP	FP	FN	Se [%]	Pp [%]	Differences (ms)
QRS-offset	4792	108	73	98.5	97.8	0 [0,1]
T-peak	4566	153	244	94.93	96.76	0 [0,0]
T-onset	4565	154	244	94.93	96.74	0 [-1,1]
T-offset	4567	152	244	94.93	96.78	1 [-2,6]
P-peak	3913	739	246	94.09	84.11	0 [0,0]
P-onset	3912	739	247	94.06	84.11	-1 [-4,1]
P-offset	3913	739	246	94.09	84.11	-1 [-4,0]

Table A.8.: Performance values of all ECG features detected by the murine algorithm version 111 compared to the manual annotations.

Figure A.11.: Boxplots of the differences (ms) between the annotations determined by the murine algorithm version 111 and the manual annotations for all ECG features.

A.2.2. ECG intervals

The QRS-, the PQ-, and the QT-interval duration based on the annotations produced by all automatic algorithm versions and the manual labelling are shown in the boxplots in the Figures A.12 - A.14. Since the RR-intervals are very similar for all the annotation methods, the corresponding boxplot is not shown.
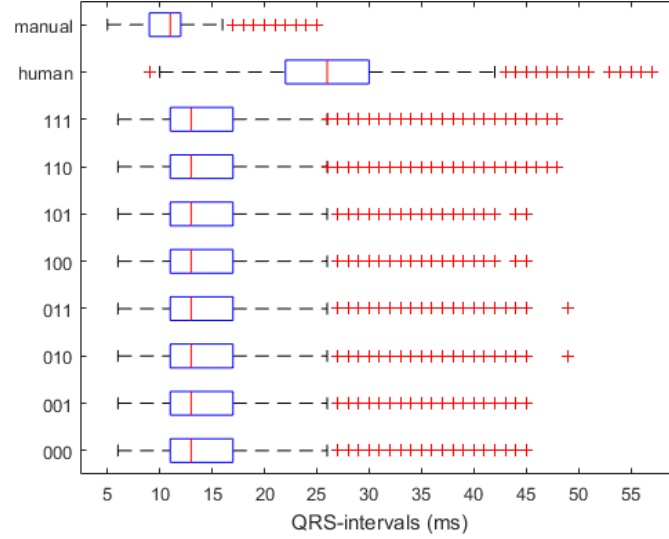
Figure A.12.: Boxplots of the QRS-interval durations (ms) based on the annotations produced by the manual labelling and all the automatic algorithm versions.
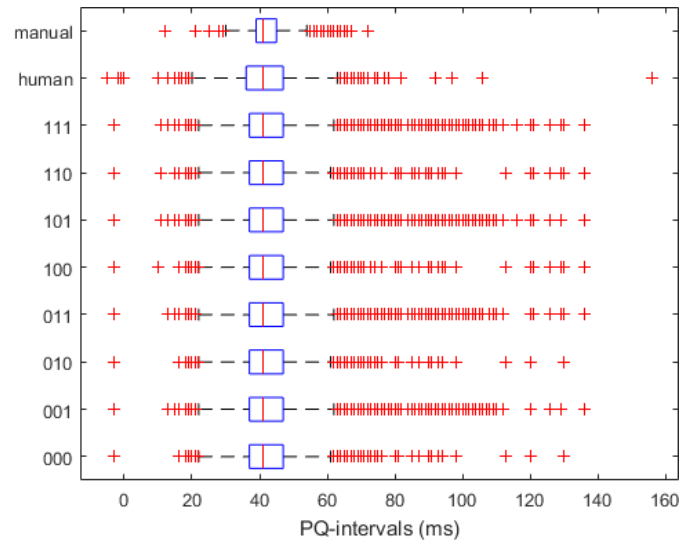
Figure A.13.: Boxplots of the PQ-interval durations (ms) based on the annotations produced by the manual labelling and all the automatic algorithm versions.
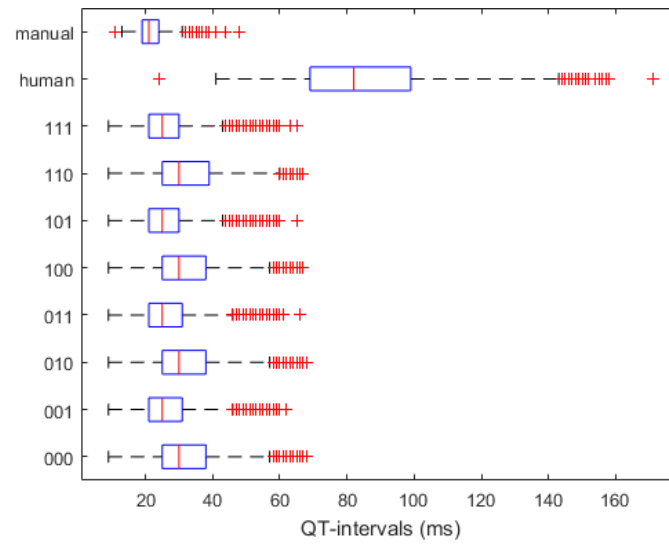
Figure A.14.: Boxplots of the QT-interval durations (ms) based on the annotations produced by the manual labelling and all the automatic algorithm versions.

List of Figures

List of Tables

List of Tables

Bibliography

[1] X. H. Wehrens, S. Kirchhoff, and P. A. Doevendans, "Mouse electrocardiography: An interval of thirty years," *Cardiovascular Research*, vol. 45, pp. 231–237, 2000.

[2] S. Kaese and S. Verheule, "Cardiac electrophysiology in mice: a matter of size," *Frontiers in Physiology*, vol. 3, no. 345, 2012.

[3] T. Speerschneider and M. B. Thomsen, "Physiology and analysis of the elctrocardiographic t wave in mice," *Acta Physiol*, vol. 209, pp. 262–271, 2013.

[4] M. Bachler, C. Mayer, B. Hametner, S. Wassertheurer, and A. Holzinger, *Online and Offline Determination of QT and PR Interval and QRS Duration in Electrocardiography*, pp. 1–15. Springer Berlin Heidelberg, 2013.

[5] P. A. Doevendans, M. J. Daemen, E. D. de Muinck, and J. F. Smits, "Cardiovascular phenotyping in mice," *Cardiovascular Research*, vol. 39, no. 1, pp. 34–49, 1998.

[6] E. Kaniusas, *Biomedical Signals and Sensors I: Linking Physiological Phenomena and Biosignals.* Springer-Verlag Berlin Heidelberg, 2012.

[7] Zoofar, "Heart diagram." `https://commons.wikimedia.org/w/index.php?curid=9841860`, accessed February 26, 2018.

[8] M. J. Cook, "The anatomy of the laboratory mouse," 1965. online available at `http://www.informatics.jax.org/cookbook/figures/figure91.shtml`, accessed February 26, 2018.

[9] H. Pfützner, *Angewandte Biophysik.* Springer-Verlag WienNewYork, 2003.

[10] Chris 73, "Action potential," 2007. `https://commons.wikimedia.org/w/index.php?curid=2241513`, accessed February 26, 2018.

[11] J. Malmivuo and R. Plonsey, *Bioelectromagnetism - Principles and Applications of Bioelectric and Biomagnetic Fields.* 01 1995.

[12] B. J. Boukens, M. R. Rivaud, S. Rentschler, and R. Coronel, "Misinterpretation of the mouse ecg: 'musing the waves of mus musculus'," *The Journal of Physiology*, vol. 592, pp. 4613–4626, 2014.

[13] Jmarchn, "Precordial leads 2," 2010. `https://commons.wikimedia.org/w/index.php?curid=9426668`, accessed April 4, 2018.

[14] E. Frank, "An accurate, clinically practical system for spatial vectorcardiography," *Circulation*, vol. 13, no. 5, pp. 737–749, 1956.

[15] S. Danik, C. Cabo, C. Chiello, S. Kang, A. L. Wit, and J. Coromilas, "Correlation of repolarization of ventricular monophasic action potential with ecg in the murine heart," *American Journal of Physiology - Heart and Circulatory Physiology*, vol. 283, no. 1, pp. H372–H381, 2002.

[16] G. Liu, J. B. Iden, K. Kovithavongs, R. Gulamhusein, H. J. Duff, and K. M. Kavanagh, "In vivo temporal and spatial distribution of depolarization and repolarization and the illusive murine t wave," *The Journal of Physiologie*, vol. 555, pp. 267–279, 2004.

[17] B. J. Boukens, M. G. Hoogendijk, A. O. Verkerk, A. Linnenbank, P. van Dam, C.-A. Remme, J. W. Fiolet, T. Opthof, V. M. Christoffels, and R. Coronell, "Misinterpretation of the mouse ecg: 'musing the waves of mus musculus'," *Cardiovascular Research*, vol. 97, pp. 182–191, 2013.

[18] D. Durrer, R. T. van Dam, G. E. Feud, M. J. Janse, F. L. Meijler, and R. C. Arzbaecher, "Total excitation of the isolated human heart," *Circulation*, vol. 41, no. 6, pp. 899–912, 1970.

[19] Anthony Atkielski, "Sinus rhythm labels," 2007. `https://commons.wikimedia.org/w/index.php?curid=1560893`, accessed February 27, 2018.

[20] A. N. Goldbarg, H. K. Hellerstein, J. H. Bruell, and A. F. Darocz, "Electrocardiogram of the normal mouse, mus musculus: General considerations and genetic aspects," *Cardiovascular Research*, vol. 2, pp. 93–99, 1968.

[21] H. Bazett, "An analysis of the time-relations of electrocardiograms," *Heart*, vol. 7, pp. 353–370, 1920.

[22] S. Luo, K. Michler, P. Johnston, and P. W. Macfarlane, "A comparison of commonly used qt correction formulae: The effect of heart rate on the qtc of normal ecgs," *Journal of Electrocardiology*, vol. 37, pp. 81–90, 2004.

[23] G. F. Mitchell, A. Jeron, and G. Koren, "Measurement of heart rate and q-t interval in the conscious mouse," *American Journal of Physiology - Heart and Circulatory Physiology*, vol. 274, no. 3, pp. H747–H751, 1998.

[24] The Jackson Laboratory, "`https://www.jax.org/strain/000664`." accessed February 27, 2018.

[25] The Jackson Laboratory, "`https://www.jax.org/strain/000665`." accessed February 27, 2018.

[26] The Jackson Laboratory, "`https://www.jax.org/strain/001800`." accessed February 27, 2018.

[27] Charles River Laboratories, "`https://www.criver.com/products-services/find-model/swiss-webster-cfw-mouse?region=23`." accessed February 27, 2018.

[28] J. W. O'Bryant, A. Pachchanian, G. Reimer, and R. Vadheim, "An apparatus for studying electrocardiographic changes in small animals," *Texas reports on biology and medicine*, vol. 7, no. 4, p. 661—70, 1949.

[29] E. A. Lombard, "Electrocardiograms of small mammals," *American Journal of Physiology-Legacy Content*, vol. 171, no. 1, pp. 189–193, 1952.

[30] A. G. Richards, E. Simonson, and M. B. Visscher, "Electrocardiogram and phonogram of adult and newborn mice in normal conditions and under the effect of cooling, hypoxia and potassium," *American Journal of Physiology-Legacy Content*, vol. 174, no. 2, pp. 293–298, 1953.

[31] G. Giordano and G. Nigro, "Caratteristiche dell' elettrocardiogramma normale del mus musculus albus," *Sperimentale*, vol. 107, pp. 63–68, 1957.

[32] M. Merentie, J. A. Lipponen, M. Hedman, A. Hedman, J. Hartikainen, J. Huusko, L. Lottonen-Raikaslehto, V. Parviainen, S. Laidinen, P. A. Karjalainen, and S. Ylä-Herttuala, "Mouse ecg findings in aging, with conduction system affecting drugs and in cardiac pathologies: Development and validation of ecg analysis algorithm in mice," *Physiological Reports*, vol. 3, no. 12, 2015.

[33] B. U. Köhler, C. Hennig, and R. Orglmeister, "The principles of software qrs detection," *IEEE Engineering in Medicine and Biology Magazine*, vol. 21, no. 1, pp. 42–57, 2002.

[34] P. Laguna, N. Thakor, P. Caminal, R. Jane, H. Yoon, and A. Bayes de Luna, "New algorithm for qt interval analysis in 24-hour holter ecg: performance and applications," *Med. Biol. Eng. Comput.*, vol. 28, pp. 67–73, 1990.

[35] N. B. McLaughlin, R. W. Campbell, and A. Murray, "Comparison of automatic qt measurement techniques in the normal 12 lead electrocardiogram.," *Heart*, vol. 74, no. 1, pp. 84–89, 1995.

[36] C. R. Vázquez-Seisdedos, J. E. Neto, E. J. Marañón Reyes, A. Klautau, and R. C. Limão de Oliveira, "New approach for t-wave end detection on electrocardiogram: Performance in noisy conditions," *BioMedical Engineering OnLine*, vol. 10, p. 77, Sep 2011.

[37] I. I. Christov and I. I. Simova, "Fully automated method for qt interval measurement in ecg," in *2006 Computers in Cardiology*, pp. 321–324, Sept 2006.

[38] V. Chu, J. M. Otero, O. Lopez, J. P. Morgan, I. Amende, and T. G. Hampton, "Method for non-invasively recording electrocardiograms in conscious mice," *BMC Physiology*, vol. 1, no. 6, 2001.

[39] Mouse Specifics, Inc., "`https://mousespecifics.com/heart-monitoring/ecgenie/`." accessed April 10, 2018.

[40] T. Galetin, M. Weiergräber, J. Hescheler, and T. Schneider, "Analyzing murine electrocardiogram with physiotoolkit," *Journal of Electrocardiology*, vol. 43, no. 6, pp. 701 – 705, 2010.

[41] M. P. Tarvainen, J.-P. Niskanen, J. A. Lipponen, P. O. Ranta-aho, and P. A. Karjalainen, "Kubios hrv – heart rate variability analysis software," *Computer Methods and Programs in Biomedicine*, vol. 113, no. 1, pp. 210 – 220, 2014.

[42] N. Naumenko, J. Huusko, T. Tuomainen, J. T. Koivumäki, M. Merentie, E. Gurzeler, K. Alitalo, R. Kivelä, S. Ylä-Herttuala, and P. Tavi, "Vascular endothelial growth factor-b induces a distinct electrophysiological phenotype in mouse heart," *Frontiers in Physiology*, vol. 8, p. 373, 2017.

[43] S. Xing, S.-W. Tsaih, R. Yuan, K. L. Svenson, L. M. Jorgenson, M. So, B. J. Paigen, and R. Korstanje, "Genetic influence on electrocardiogram time intervals and heart rate in aging mice," *American Journal of Physiology-Heart and Circulatory Physiology*, vol. 296, no. 6, pp. H1907–H1913, 2009.

[44] L. A. Gottlieb, A. Lubberding, A. P. Larsen, and M. B. Thomsen, "Circadian rhythm in qt interval is preserved in mice deficient of potassium channel interacting protein 2," *Chronobiology International*, vol. 34, no. 1, pp. 45–56, 2017.

[45] N. Bakeer, J. James, S. Roy, J. Wansapura, S. K. Shanmukhappa, J. N. Lorenz, H. Osinska, K. Backer, A.-C. Huby, A. Shrestha, O. Niss, R. Fleck, C. T. Quinn, M. D. Taylor, E. Purevjav, B. J. Aronow, J. A. Towbin, and P. Malik, "Sickle cell anemia mice develop a unique cardiomyopathy with restrictive physiology," vol. 113, no. 35, pp. E5182–E5191, 2016.

[46] ADInstruments, "`https://www.adinstruments.com/products/labchart`." accessed March 29, 2018.

[47] MathWorks, "`https://de.mathworks.com/help/stats/pdist.html#d119e554335`." accessed March 13, 2018.

[48] S. Lloyd, "Least squares quantization in pcm," *IEEE Transactions on Information Theory*, vol. 28, no. 2, pp. 129–137, 1982.

[49] MathWorks, "`https://de.mathworks.com/help/stats/k-means-clustering.html`." accessed March 13, 2018.

[50] D. Arthur and S. Vassilvitskii, "K-means++: The advantages of careful seeding," in *Proceedings of the Eighteenth Annual ACM-SIAM Symposium on Discrete Algorithms*, SODA '07, pp. 1027–1035, Society for Industrial and Applied Mathematics, 2007.

[51] MathWorks, "`https://de.mathworks.com/help/stats/hierarchical-clustering.html`." accessed May 2, 2018.

[52] R. O. Duda, P. E. Hart, and D. G. Stork, *Pattern Classification*. Wiley-Interscience, 2000.

[53] C. T. Zahn, "Graph-theoretical methods for detecting and describing gestalt clusters," *IEEE Transactions on Computers*, vol. C-20, no. 1, pp. 68–86, 1971.

[54] J. M. Bland and D. Altman, "Statistical methods for assessing agreement between two methods of clinical measurement," *The Lancet*, vol. 327, no. 8476, pp. 307 – 310, 1986. Originally published as Volume 1, Issue 8476.

[55] M. Viitasalo and J. Karjalainen, "Qt intervals at heart rates from 50 to 120 beats per minute during 24-hour electrocardiographic recordings in 100 healthy men. effects of atenolol.," *Circulation*, vol. 86, no. 5, pp. 1439–1442, 1992.

[56] S. Ruppert, T. Vormberge, B.-W. Igl, and M. Hoffmann, "Ecg telemetry in conscious guinea pigs," *Journal of Pharmacological and Toxicological Methods*, vol. 81, pp. 88 – 98, 2016.